

Final Report on Contract NAS 8-24585

July 1, 1972

A Preliminary Design Study
for a Cosmic X-Ray Spectrometer

Center for Space Research
Massachusetts Institute of Technology

(NASA-CR-123910) A PRELIMINARY DESIGN
STUDY FOR A COSMIC X-RAY SPECTROMETER
Final Report (Massachusetts Inst. of Tech.)
1 Jul. 1972 127 p

155

CSCL 14B

N72-33378

Unclas

G3/14 16319

Details of illustrations in
this document are available
separately in microfiche

Distribution: George C. Marshall Space Flight Center

<u>Code</u>	<u>Copies</u>
A&TS-PR-M	11
A&TS-MS-IL	1
A&TS-TU	1
A&TS-MS-I	1
S&E-SSL-T	50
S&E-SSL-C	1

CONTENTS

- 1.0 Introduction
 - 1.1 Contract History
 - 1.2 Summary of activities
- 2.0 Summary of research objectives and results
 - 2.1 Statements of work
 - 2.1.1 Contract NAS 8-24585
 - 2.1.2 Modification #1
 - 2.1.3 Modification #2
 - 2.2 Summary of results keyed to the statements of work
- 3.0 Theoretical and experimental studies of the curved crystal spectrometer and related matters
 - Part I. Laboratory and development program
 - 1. Facilities developed for use in this program
 - 2. Electronics software
 - 3. Electronics systems
 - 4. Channeltron test setup
 - Part II. Related instrumentation and investigations
 - 1. Related facilities developed in conjunction with other programs or ongoing research projects
 - 2. Crystal testing program
 - 3. X-rays from heavy ion collisions
 - 4. X-rays from hot-thin plasma
 - Part III. Curved crystal spectrometer
 - 1. General properties of a curved crystal spectrometer
 - 2. Application to the present experiment
 - 3. Plane crystal spectrometer for the iron lines

Part IV. Engineering descriptions

1. Focal-plane crystal spectrometer
2. Flat crystal spectrometer

4.0 Further theoretical and experimental studies of curved crystal spectrometers

4.1 Spectrometer geometrical optics

4.2 Detector resolution requirements

4.3 Breadboard system design and construction

4.3.1 Curved crystal spectrometer

4.3.2 Spectrometer vacuum system

4.3.3 Control and data acquisition system

4.3.4 Proportional counter

4.4 Lead stearate crystal preparation facility

4.5 Measurement of Bragg reflection of 44 \AA carbon K X-rays by a lead stearate crystal with the breadboard spectrometer

4.6 Test of Bragg reflection from a spherically curved mica crystal

4.7 Tests of windowless photoelectric detectors

1.0 Introduction

This document is the final report on work performed at the Massachusetts Institute of Technology under contract NAS 8-24585 to the Marshall Space Flight Center of the National Aeronautics and Space Administration. It describes the results of theoretical and experimental investigations aimed at the development of a curved crystal cosmic X-ray spectrometer to be used at the focal plane of the Large Orbiting X-Ray Telescope (LOXT) on the Third High-Energy Astronomical Observatory (HEAO-C).

1.1 Contract History

The work described herein was proposed to MSFC in a document dated 1 February 1969 and entitled "Proposal... for a Preliminary Design Study for a Cosmic X-Ray Spectrometer", with G. Clark as Principal Investigator and H. Schnopper as Co-Investigator. This work was funded at a level of \$50,000 for the 8-month period from 18 June 1969 to 18 February 1970. Near the end of this period MIT submitted a proposal for "Continuation of Support for Development of a Cosmic X-Ray Spectrometer..." with H. Schnopper as Principal Investigator and G. Clark as Co-Investigator. The contract was accordingly extended to 15 May 1971 under Modification #1 at an increased cost of \$79,581. Further support for "Continuation of a Preliminary Design Study for a Cosmic X-Ray Spectrometer" was requested by MIT in a proposal dated 1 May 1971 with G. Clark as Principal Investigator

/

and H. Schnopper as Co-Investigator. This final phase of the research was funded at \$50,027 for the period ending 18 February 1972. A no-cost extension until 31 August 1972 was granted to allow for completion of certain measurements and for the preparation of this final report.

1.2 Summary of Activities

At the inception of the program it was recognized by NASA and by the MIT X-ray astronomy group that high resolution Bragg X-ray spectrometry would eventually play a key role in the elucidation of the nature of X-ray sources and the composition of the interstellar medium when space vehicles of sufficient capacity to carry the necessary large effective-area instruments became available. Recent developments in concepts for cosmic X-ray spectrometry at MIT, in particular the unfocused Bragg reflection spectrometer invented by H. Schnopper and K. Kalata, had provided a basis for planning a high-resolution spectrometer to be used at the focus of a grazing incidence X-ray reflection telescope. However, a variety of questions regarding the properties of crystals and detectors, and design problems related to the methods of detection and the optimization of the throughput and resolution of the instrument required theoretical and experimental investigations which were undertaken under this contract.

In the course of this work, the MIT group participated

in a study with scientists and engineers from American Science and Engineering, Inc., Columbia University, Goddard Space Flight Center and MIT, who met during 1969 and 1970 with representatives of MSFC and NASA Headquarters to define the scientific requirements for a "X-Ray Telescope Facility". The report of the study which was submitted in September 1970 formed the basis for planning the HEAO-C mission for which a flight opportunity was released on 1970.

In response to the flight opportunity announcement, MIT joined in a consortium with AS&E, Columbia University and GSFC to propose the "Large Orbiting X-Ray Telescope". Among the instruments proposed for use at the focal plane of the high resolution telescope was the curved crystal spectrometer, the design of which was based on the studies reported herein. Following review and recommendation by the Astronomy Subcommittee of NASA in November 1970, two telescopes proposed by the consortium and certain of the auxiliary instruments, including the MIT curved crystal spectrometer, were approved for phase B funding.

During the earlier part of the work reported herein, the MIT effort was concentrated on the development of spectrometer concepts and their evaluation by theoretical analysis, computer simulation, and laboratory testing with bread-board arrangements of crystals and detectors. In addition, a computer-controlled facility for precision testing and evaluation of crystals in air and vacuum was constructed.

Most of this work was carried out under the supervision of Professor Schnopper and is described in Section 3.0 of this paper. In addition, Section 3.0 reports research on the X-ray emission of multiply ionized atoms which was undertaken to elucidate the properties of line spectra that may be discovered in the study of cosmic X-ray sources.

Following the approval of the MIT proposal for the focal plane spectrometer in late 1970, the major portion of the effort supported under this contract was devoted to the construction of a laboratory breadboard curved crystal vacuum spectrometer for testing the performance of spectrometer systems with various crystals and detectors in configurations closely approximating those that will be used in the flight instrument. In addition, a facility for fabricating lead stearate multilayer diffractors was completed and put into operation, and tests were conducted of several prototype detectors for soft (10 \AA) X-rays including polypropylene film window flow counters, channel-tron detectors and a chevron channel plate intensifier. This work, which was carried out under the direct supervision of Professor Clark, is described in Section 4.0 of this report.

Section 2.0 of this report is a review of the research objectives as contained in the statements of work in the original contract and its two modifications, and a summary

of results, keyed to the statements of work, and referenced to the appropriate parts of the subsequent Sections 3.0 and 4.0.

2.0 Summary of Research Objectives and Results

2.1 Statements of Work

2.1.1 Contract NAS 8-24585

1. A functioning "breadboard" model of a cosmic X-ray spectrometer is to be prepared incorporating the Schnopper technique of Bragg reflection mapping. The model will include the means for producing an X-ray beam with geometrical properties like that expected from a grazing incidence telescope, a suitable bent crystal, and a detector capable of demonstrating the dispersion and resolution capabilities of the system.
2. A vacuum system for testing the spectrometer with soft X-ray ($\lambda = 20 \text{ \AA}$ approximately) is to be constructed.
3. The breadboard model is to be evaluated in the soft X-ray facility.
4. Various crystals such as mica, potassium acid phthalate and others are to be tested and evaluated for use in the spectrometer.
5. Theoretical studies of the optical properties of the Schnopper spectrometer are to be conducted.
6. Theoretical studies of alternative detector systems are to be conducted for the purpose of evaluating their relative merits for use in the satellite X-ray spectrometer.

7. Provide X-ray collector definition, i.e., design and performance requirements, by generating related developmental scientific experiment requirements.

2.1.2 Modification #1

8. The spectrometer design shall be adapted to the requirements of an orbiting instrument. The instrument design shall also be studied for compatibility with vacuum operation and launch survival. Where possible, tests will be made with already existing equipment except as indicated in Task D.

9. The properties of Johansson and Johann optics shall be further investigated and compared. Bragg reflection studies (crystal resolution and perfection) will be continued.

10. A breadboard detector system will be constructed and tested for compatibility with the astrophysical objectives and environmental requirements.

11. A mechanical evaluation system will be constructed and tested.

2.1.3 Modification #2

The present effort on the development of Bragg reflection X-ray spectrometry is to be extended according to the following statement of work:

12. Breadboard tests of the curved crystal

Bragg spectrometer for soft X-rays ($>10 \text{ \AA}$) will be carried out.

13. Crystal testing: For the variety of crystals which appear to be useful over the energy range of interest (approximately 0.2 to 10 keV), a study of reflecting properties vs. X-ray energy will be made.

14. Detector evaluation:

a. Proportional counters of various types, including a multi-chambered design and, if possible, a position-sensitive design, will be tested.

b. A channelplate image intensifier will be tested.

2.2 Summary of Results Keyed to the Statements of Work

2.2.1 Three functioning breadboard curved crystal spectrometers were constructed and used in tests of various crystal and detector configurations including the Schnopper technique of Bragg reflection mapping. The first of these was a relatively crude setup with which the potentialities of the reflection mapping technique were demonstrated with a conically diverging beam of CuK radiation reflected in 8th order from a cylindrically bent mica crystal on the Rowland circle, and a Polaroid film detector. (Section 3, pages 13, 14 and Figures 2, 9.) The second model is a precision spectrometer arranged for operation in air or vacuum. Tests of various crystals in the Johann and Johansson configuration were conducted (Section 3, page 20, Figures 24, 25) The third model is a moderate precision instrument for air or vacuum operation

which provides a test bed for crystals and detectors in configurations which are close approximations to those of the expected flight instrument. (Section 4, pp 7ff and Figures 4.3.2-4).

2.2.2 Two vacuum systems were set up for testing the spectrometer components with soft ($\lambda > 10\text{\AA}$) X-rays. The first is a 36"-diameter high-vacuum chamber that provides a clean high vacuum capable of accommodating the precision single or double crystal spectrometers and various other instruments for testing crystals and detectors (Section 3, page 6). The second system is a 24" stainless steel high vacuum chamber which accommodates the flight configuration breadboard spectrometer (Section 4, page 9 and Figure 4.3.1).

2.2.3 Preliminary tests of the flight configuration breadboard model have been conducted with Copper L radiation ($\lambda \sim 13\text{\AA}$) (Section 4, page 17 and Figure 4.6.1).

2.2.4 The rocking curves and reflection efficiencies of the crystals EDDT, PET and KAP have been measured with a double crystal spectrometer at wavelengths of 6.07 and 8.34 \AA , and their measured properties have been evaluated for use in the LOXT spectrometer (Section 3, Table 4 and Figures 18, 19).

2.2.5 Theoretical studies of various spectrometer configurations including the Schnopper unfocussed configuration have been conducted (Section 3, pp. 10-15, Section 4, pp 1ff).

2.2.6 Theoretical studies of alternative detector systems have been conducted (Section 3, pp. 16-22).

2.2.7 Studies were conducted to define the design of the grazing incidence telescopes. This work was carried out in cooperation with other participants in the study for the X-ray telescope facility and the results appear in the report of that joint effort.

2.2.8 The spectrometer design was adapted to the requirements of an orbiting instrument, and preliminary evaluations were made as to its compatibility with vacuum operation and launch survival (Section 3, pp. 26-32).

2.2.9 The properties of Johansson and Johann optics were further studied, and Bragg reflection studies were continued (Section 3, page 20, Figures 24, 25).

2.2.10 Breadboard evaluation models of several detector systems were set up and tested. (Section 3, page 18; Section 4, pp. 11, 19ff, Figures 4.3.2, 4.7.1).

2.2.11 Several mechanical features that may be used in the flight instrument were incorporated in the flight configuration breadboard model. These include provision for adjusting the Rowland circle radius and for moving the components into the focussed or unfocussed configurations (Section 4, pp. 7, 8).

2.2.12 Vacuum tests of the flight configuration breadboard spectrometer were carried out with Copper L radiation ($\lambda=13.5 \text{ \AA}$) and a spherically bent mica crystal (Section 4, pp. 17, 18).

2.2.13 See Task 4

2.2.14 See Task 10

In addition to the work summarized above, which was carried out in fulfillment of the specific items in the statements of work, three additional efforts were undertaken to supplement the spectrometry development program. One of these is the study of the X-ray spectra of highly ionized atoms produced by bombarding thin foils with high-energy beams of ions (Section 3, pp. 7-10). The second supplementary effort was the design development of a flat crystal spectrometer for wavelengths shorter than the effective cutoff wavelength of the reflection telescopes (Section 3, pp. 31-33). The third effort is the construction of a facility for the production of lead stearate multilayers for Bragg diffraction at wavelengths beyond those for which natural crystals with large enough second spacings are available (Section 4, pp 13ff, Figure 4.4.1).

During the last phase of this study, a difference of opinion developed between the two co-investigators regarding the relative merits in the context of the HEAO-C mission, of

the approved focal plane instrument and of a new approach developed independently by Professor Schnopper. This latter approach employs a separate one-dimensional grazing incidence reflection concentrator and a flat crystal analyzer. In the light of this development, Professor Schnopper modified his evaluations of the technical feasibility of the focal plane spectrometer as expressed in reports of the earlier work and in the LOXT proposal, and included some of these new evaluations in Section 3 which constitutes his contribution to this final report. Some of the issues raised by these new evaluations are discussed in Section 4 which is devoted to the work of the last phase.

It was anticipated that the precision facilities developed earlier in the program for testing crystals in air and vacuum would be employed in accordance with Task 13 during the last phase of this study in a comprehensive evaluation of the crystals that are candidates for use in the focal plane instrument. During the last phase results were, in fact, obtained on EDDT, PET and KAP, and some of the results are reported in section 3.0. The recently completed bread-board spectrometer, with certain additional instrumentation now under construction in the Phase B study, will be capable of providing the additional crystal measurements needed for the definition of the focal plane instrument design. Among the first results from the new facility which are included in this report are a measurement of Bragg reflection of 44 \AA

Carbon K radiation from a 100-layer lead stearate crystal prepared in the newly completed dipping tank, and a preliminary test of a spherically bent mica diffractor in the Rowland configuration.

3.0 Theoretical and Experimental Studies of the Curved Crystal Spectrometer and Related Matters

This section describes work carried out under the direction of Professor Schnopper. The scientific personnel engaged in these studies were:

Dr. H. Schnopper	Associate Professor
Mr. K. Kalata	Staff Scientist
Dr. J. Delvaille	Staff Scientist
Mr. R. Sohval	Research Assistant
Mr. A. Epstein	Research Assistant

Part I Laboratory and Development Program

1. Facilities developed for use in this program

- I. Curved crystal X-ray spectrometer with a detector holder which can raster the detector across the reflection pattern and position it on or off of the Rowland circle.
- II. Two independent separately pumped 0-60 keV 0-10 mA X-ray tubes with interchangeable anodes.
- III. Experimental Set-ups
 - A. Air - a station consisting of a three-part X-ray tube and associated vacuum system, and a table which will accommodate one of our spectrometers.
 - B. Vacuum - a similar station inside of a large vacuum system so that the spectrometer can be evacuated and the X-ray tube window removed for investigations involving low-energy X-rays.
 - C. A 0-60 keV 0-10 mA power supply and a filament supply with a current regulator which provides a highly stable X-ray tube current.
- IV. Analog data acquisition circuitry - two independent data channels each consisting of a charge-sensitive preamplifier, an amplifier, single-channel analyzer, and a digital ratemeter or a scaler and a timer.

V. Experiment Control - a mini-computer (NOVA) is in control of all operations of a given experiment which include:

- A. Data input
- B. Scanning operations
- C. Data output
 - 1. Hard copy
 - 2. Magnetic tape
 - 3. Spectrum plots
- D. Data reduction

2. Electronics Software

Basic software consists of a supervisor program which controls any or all of the subordinate functions simultaneously. Each subordinate function can request the supervisor to type out messages and/or take data from the teletype and/or notify the subordinate function at specific time intervals.

The following subordinate functions exist presently:

a) Spectrometer Control: This routine can count detector output pulses at rates of up to 8KHz and store the data in a specified area.

b) Stepping Motor Control: This routine will control changes in crystal angle and detector angle by activating stepping motors at specified intervals through specified angles. Both interval and angle of transit are communicated by teletype. The crystal angle and detector position can also be controlled by a set of switches near the spectrometer which are connected up as an input device to the computer.

c) Strip Chart Control: Allows graphing of data from spectrometer or any other source. Proper scaling of data may be specified by teletype or done automatically.

d) X-Y Display Control: Allows display of all or any part of data on CRT X-Y display. Scaling of data on the screen may be done dynamically with switches on the computer.

e) Data Input Routines: Punches out data onto paper tape for later analysis or convolution with other data, and reads in data from previous runs, or data taken elsewhere, and then transfers control to one of the data analysis and fitting programs.

3. Electronics Systems

We have automated the control and data processing of the X-ray spectrometer. This is accomplished through the use of a Nova computer and a library of computer programs that have been written for this system. Through the use of this type of control and data handling, a high degree of flexibility is obtained.

The mechanical motions of the spectrometer are under computer control. By appropriately stepping the three stepping motors, the computer can slew the tangent arm until the Bragg angle is reached, and then scan the detector in the x and z directions until it is correctly aligned. The computer can then scan the crystal through a range of Bragg angles and take data obtained from two proportional counters, one of which

detects the radiation reflected from the crystal, and the other which monitors the X-ray flux incident on the crystal. The X-ray spectra obtained through such scans can be displayed on a large display screen or recorded on a dual pen strip chart recorder. Information relevant to the operating conditions of the spectrometer system, such as range of Bragg angles to be scanned and integration time per resolution element, are requested by the computer through a teletype, and during alignment the operator can control the positioning of the instrument through a set of switches placed near the spectrometer and connected to the computer. Additional interfaces are now being built to allow a second spectrometer to be independently controlled, and for more input/output devices to be operated by the computer.

4. Channeltron Test Setup

In order to measure the X-ray detection efficiency of channeltrons and spiraltrons and to investigate other properties such as electron gain as a function of voltage, we have put together a channeltron test station. It consists of a channeltron or operatron mounted in the beam of the X-ray tube inside of the large vacuum tank. A thin window flow proportional counter next to the channeltron is used to determine the incident X-ray flux. There is a complete set of detection electronics and a gas flow system for the proportional counter, and another set, including a specially designed preamplifier that we built for the channeltron,

measures the total change in each pulse out of the channeltron. For low energies the window on the X-ray tube can be removed, and for very low energies, both the channeltron and monitor flow proportional counter can be placed after a Bragg crystal which serves as an X-ray monochrometer.

Part II Related Instrumentation and Investigations

1. Related facilities developed in conjunction with other programs or ongoing research projects.

I. Spectrometers

- A. Two-Crystal (high resolution)
- B. Curved crystal or single crystal
- C. Non-dispersive
 1. LN_2 cooled Si (Li) high resolution detector
 2. Sealed window proportional counters
 3. Replaceable window, flow proportional counters 0.25-1.0 keV

- II. Crystals - A complete range of crystals from OHM $92d=64\text{\AA}$ to quartz ($2d=4.9\text{\AA}$)

We have the following crystals undergoing testing and evaluation (flat crystals $1 \times 1 \times 1/8$):

- 1) EDDT
- 2) ADP
- 3) PET
- 4) KAP

- 5) RAP
- 6) SHA

In addition, we have on hand:

- 1) Calcium Fluoride
- 2) Calcite flat
- 3) Quartz flat also thin (for bending)
- 4) Silicon flat and asymmetrically cut for CrK β
- 5) Topaz thin
- 6) Mica thin
- 7) KAP thin
- 8) OHM bent

III. Experimental Setup

- A. Low-Energy Multi-Purpose X-ray System - a large, clean high vacuum (few x 10⁻⁸ torr) vacuum system with a windowless, replaceable anode X-ray tube, capable of accommodating the two-crystal spectrometer, the curved crystal spectrometer, the channeltron test setup, and the Si(Li) detector. The vacuum system may be used with an extension which places the X-ray tube 15 feet from the main portion of the vacuum system, in order to obtain a very nearly parallel beam of X-rays.
- B. Broad focus, high power (several kilowatt) X-ray tube which may be used with any of our X-ray systems.

- C. A number of high voltage supplies (0-800 V, 0-200 mA; 0-k kV, 0-500 mA; 0-15 kV, 0-4 mA; 0-22 kV, 0-1.5 mA; 0-50 kV, 0-10 mA; 0-25 kV, 0-500 mA) which can be used with any of our high voltage supplies.
- D. A complete detection system for use with channel-trons, proportional counters, and the Si(Li) detector.
- E. A Nova 1200 computer system used for data analysis and experiment control, including a computer-based multi-channel analyzer system.

2. Crystal Testing Program

We are engaged in determining reflection properties of a number of crystals which show promise for use on satellite-based spectrometer systems. With the use of the two-crystal spectrometer, we have determined the rocking curve widths and shapes, and peak reflectivities, of EDDT, and two forms of PET, and are presently measuring the properties of KAP and RAP.

3. X-Rays from Heavy Ion Collisions

The present X-ray research facilities have been acquired with NASA support and have been directed towards hardware development for various mission-oriented programs. In the course of these programs, a program to study the X-rays from heavy ion impact phenomena was begun initially using the

tandem van de Graaf at High Voltage Engineering and presently the dual tandem van de Graaf at Brookhaven. A brief outline of our early results follows.

In stellar processes, high temperatures produce highly energetic atomic collisions. Multiple electronic excitation and stripping occurs which induces a re-arrangement of the electronic configuration and energy levels. Inner shell vacancies caused by these collisions will be filled by electron transitions. The resulting X-ray spectra from these multiply ionized atoms will differ both in characteristic energies and relative intensities from the spectra generated by conventional laboratory apparatuses. In our experiments, high-energy atomic collisions were produced and the resulting X-ray spectra were studied. Very highly ionized and excited states are produced in these interactions. The study of these states will give us a much better understanding of the type of spectra that will be observed from X-ray sources, and the energy regions that should be investigated. In order to be able to do high-resolution studies of the spectra of cosmic X-ray sources, a detailed observational program must be produced in advance. Because of the very limited energy band that the spectrometer can accept at any one setting, it is necessary to know the exact energies and approximate intensities of the X-ray lines to be observed. These studies will serve to provide much of this information, and also to provide models on the basis of which satellite results can be analyzed.

The data that we have were obtained by using a single-stage or two-stage tandem van de Graaf to produce beams of Cl, Br, and I at energies between 10 and 150 meV. The ion beam was incident on thin and thick foils of a large number of different materials. The spectra were obtained with a Si(Li) solid state detector and, for most of our data, computer-based multi-channel analyzer system. The beam ions initially have a charge between +9 and +13, further stripped in passing through the foil, and in the interactions which produce X-rays, both the beam ion and target atom are even more highly stripped, usually leaving only a few electrons.

We have just begun detailed analysis of the data, but many interesting results have already been obtained. Those of great astrophysical interest include line energy shifts frequently of several hundred electron volts, and in a number of cases, over one keV; significantly broadened lines, indicating unresolved lines from many excited states contributing to the spectra; large differences in relative production of a number of L and M lines as the interaction energy is changed, and electron capture from the continuum, leading to energies greatly different from the usual X-ray line energies. In order to study some of these effects in more detail, and to obtain data similar to that from the orbiting spectrometer, we have built a small, high-resolution curved crystal spectrometer and a vacuum system which can be taken to the van de Graaf at Brookhaven. We plan to use the spectrometer to do high-resolution studies of a number of

lines from highly stripped to excited states.

4. X-Rays from a Hot-Thin Plasma

We are engaged in setting up an experiment to measure X-rays produced in a hot ($5 \times 10^6 \text{ }^\circ\text{K}$), thin (10^{14} - 10^{16} ions/cm³) plasma to be produced in the Alcator device at the National Magnet Laboratory at MIT. These temperature and density parameters correspond nicely with models of many X-ray sources. We will investigate the X-ray spectra and production cross-sections with our Si(Li) detector and the high-resolution curved crystal spectrometer.

Part III. Curved Crystal Spectrometer

1. General Properties of a Curved Crystal Spectrometer

All X-ray crystal spectrometers are based on the fact that crystals efficiently reflect X-rays only if the Bragg angle and the wavelength approximately satisfy the Bragg Condition $n\lambda = 2d \sin \theta_n$ where d is the crystal lattice spacing, θ is the Bragg Angle for the n th order reflection and λ is the wavelength. Figure 1 illustrates the geometrical arrangement of the curved crystal spectrometer⁽¹⁾. The point source and the center of the crystal are located on the Rowland circle of radius $R/2$, and the normal to the crystal at its center is a diameter of the Rowland circle. Each ray \vec{r} from the point source is defined by the angles of its horizontal divergence, α , and vertical divergence ϕ from the ray that strikes the center of the crystal. The ray $\vec{r}(\alpha, \phi)$

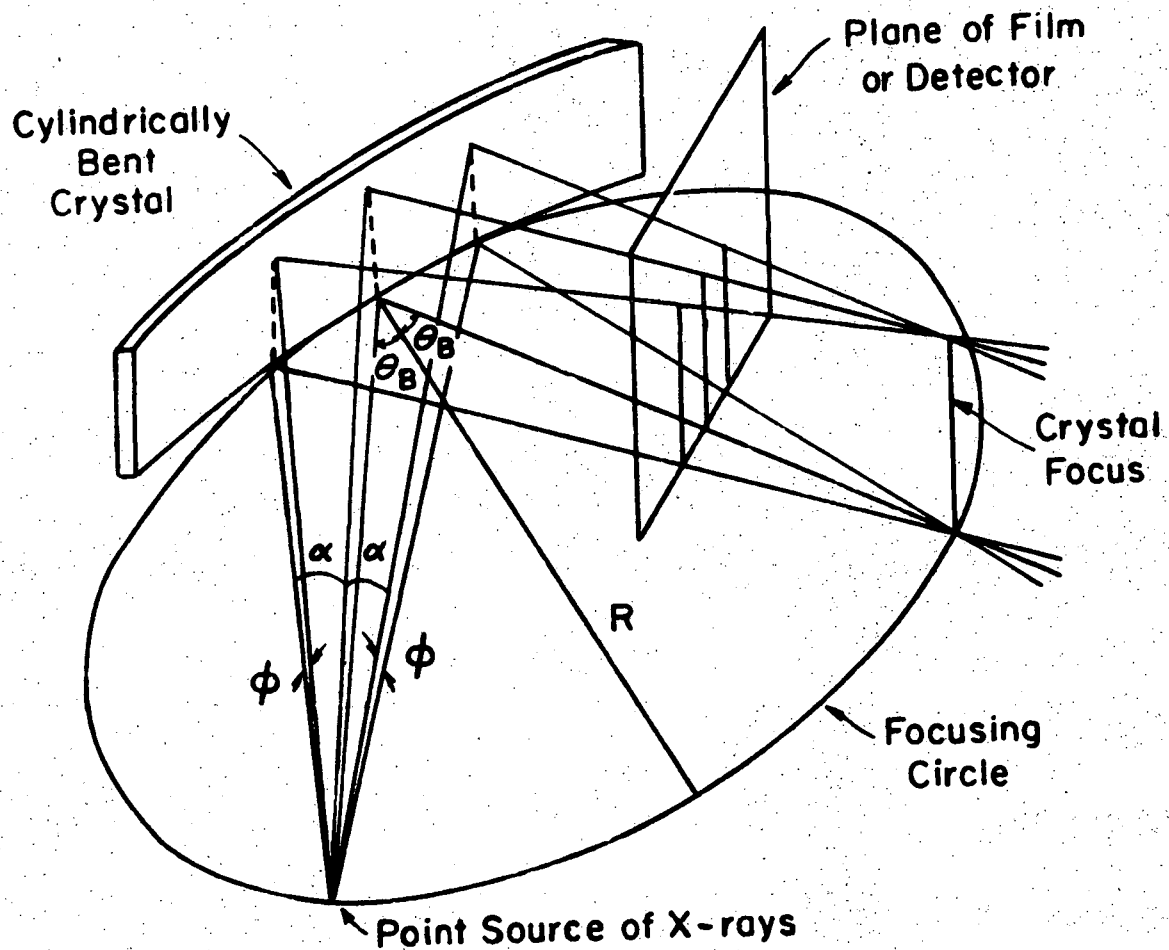


Figure 1. A schematic diagram of the X-ray spectrometer

strikes the crystal at a Bragg angle that differs slightly from that of the central ray by an amount, Δ , which depends on the particular configuration of the bent crystal. Three crystal configurations are of special interest, viz. cylindrically bent to radius R (Johann); spherically bent to radius R; and cylindrically bent to radius R and then cylindrically ground to radius R/2 (Johansson). For these three configurations one can show that the deviation is given by the relations

$$\sin (\theta_B + \Delta) = \sin (\theta_B + \delta) \cos \phi \quad (\text{Johann}) \quad (\text{Eq. 1})$$

$$\cos (\theta_B + \delta) = \cos \theta_B \cos \alpha$$

$$\cos (\theta_B + \Delta) = \cos \theta_B \cos \alpha \quad (\text{Spherical}) \quad (\text{Eq. 2})$$

$$\sin (\theta_B + \Delta) = \sin \theta_B \cos \phi \quad (\text{Johansson}) \quad (\text{Eq. 3})$$

Since α and ϕ are in general small,

$$\Delta \approx \frac{2}{2} \cot \theta_B - \frac{\phi^2}{2} \tan \theta_B \quad (\text{Johann}) \quad (\text{Eq. 4})$$

$$\Delta \approx \frac{\alpha^2}{2} \cot \theta_B \quad (\text{Spherical}) \quad (\text{Eq. 5})$$

$$\Delta \approx -\frac{\phi^2}{2} \tan \theta_B \quad (\text{Johansson}) \quad (\text{Eq. 6})$$

Note that with spherical or Johannson optics, one of the aberrations is eliminated so that the contours of equal Bragg angle deviation on the crystal are approximately straight lines.

In the case of a high-resolution crystal, the focusing defect caused by the angular spread of the radiation coming from the telescope focus causes a significant degradation of resolution at the conventional focus on the Rowland circle. If, however, the detector is between the crystal and the conventional focus as shown in Figure 1, then each point in the detector plane receives reflected radiation from a unique spot on the crystal corresponding to a unique value of (2θ) and therefore to a unique value of Δ given by one of the Equations 1-3. Figure 2 shows the effects of focusing on the dispersion at the detector plane as the film is moved successively further from the crystal. It is evident that the spectrum can be measured by integrating the intensity in the detector plane along lines corresponding to contours of equal Δ on the crystal. A two-dimensional detector array is required for Johann optics, but only one-dimensional arrays are required for Johannson and spherical optics. For Johannson optics, it is possible to place the detector at the crystal focus. If the detector is at the focus with Johann or spherical optics, different wavelengths reflected from portions of the crystal with different values of the horizontal divergence focus to the same point on the Rowland circle, thereby degrading the resolution. For long wavelengths, however, crystal resolutions become poorer

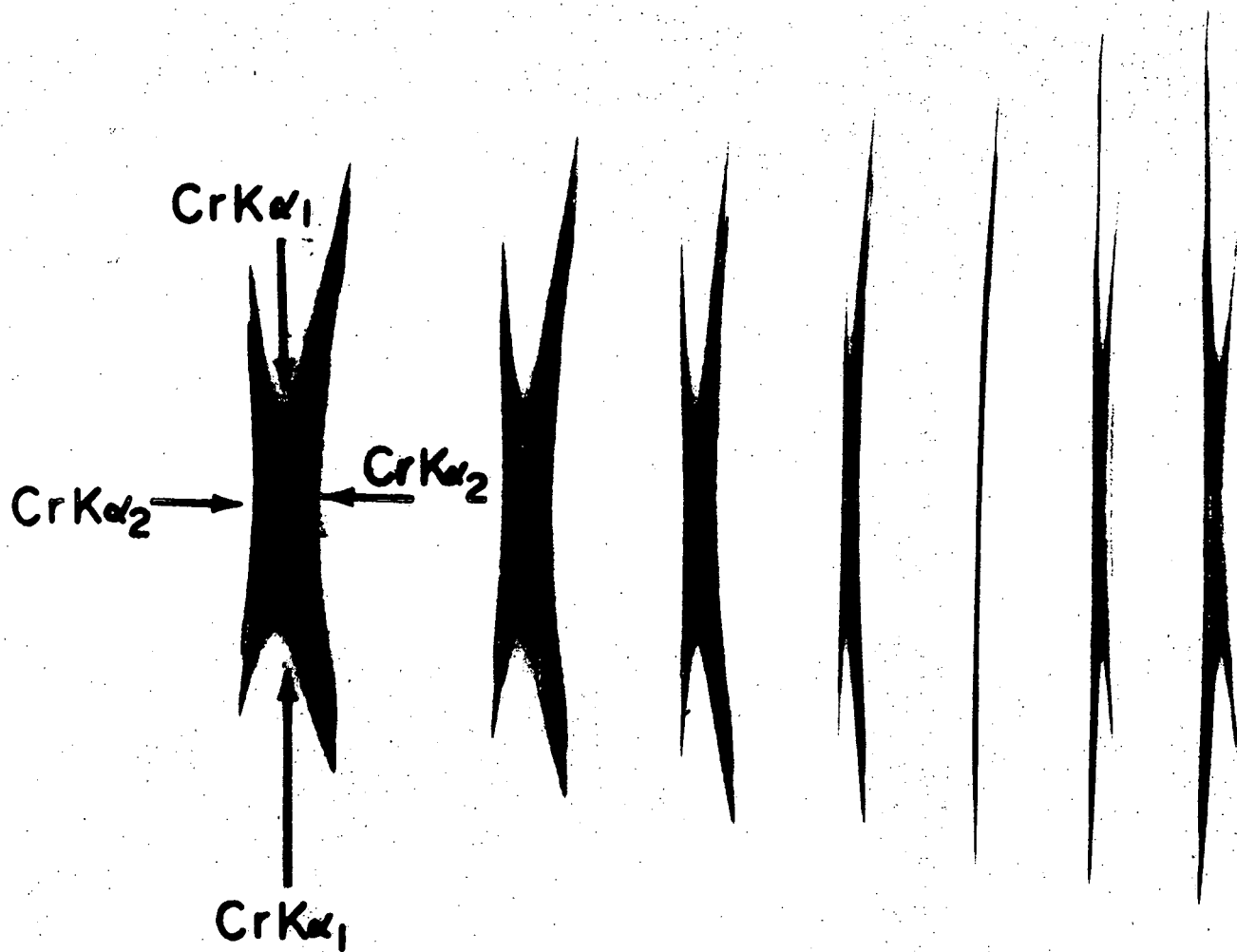


Figure 2. X-ray pictures of the $Cr K\alpha, \alpha_2$ doublet in fifth order after reflection from a cylindrically bent mica crystal with a radius of 13.5". The distance between the crystal center and the film is, from left to right, 3.75", 4.75", 5.75", 6.75", 7.75", 8.75", and 9.75".

than the degraded instrumental resolution, and it becomes practical to use a smaller detector by placing it at the focus. The geometry for focusing optics is shown in Figure 3.

A ray tracing program was developed in order to demonstrate the properties of the instrument. To date, Johann and spherical optics have been studied for cases of solid and hollow cones of radiation. The hollow cone is typical of the distribution to be expected from the X-ray telescope.

Figures 4 and 5 show the distributions of reflected intensity at the focus at two different Bragg angles. In Figures 4 and 5, the crystal is set exactly to the Bragg angle which corresponds to the centroid of the incident wavelength distribution. In Figures 3b and 4b, the Bragg angle is shifted by a small increment and the bulk of the focused distribution is shifted toward the top and bottom. With this setting, a hollow cone distribution can be used efficiently and modest resolution can be maintained. Similar effects are illustrated for the case of an intermediate detector position in Figures 6 and 7. In these distributions, a hypothetical $K\alpha_1$, $K\alpha_2$ doublet is assumed and several different central Bragg angles are chosen. Solid and hollow beams are contrasted. It is clear that if a suitable offset Bragg angle is chosen, the hollow beam geometry presents no problem. These cases are summarized in Table 1.

Some of these effects have been tested in the laboratory with Cu K radiation reflected in 8th order from a cylindrically bent mica crystal. Figure 8 shows the effect on the focused

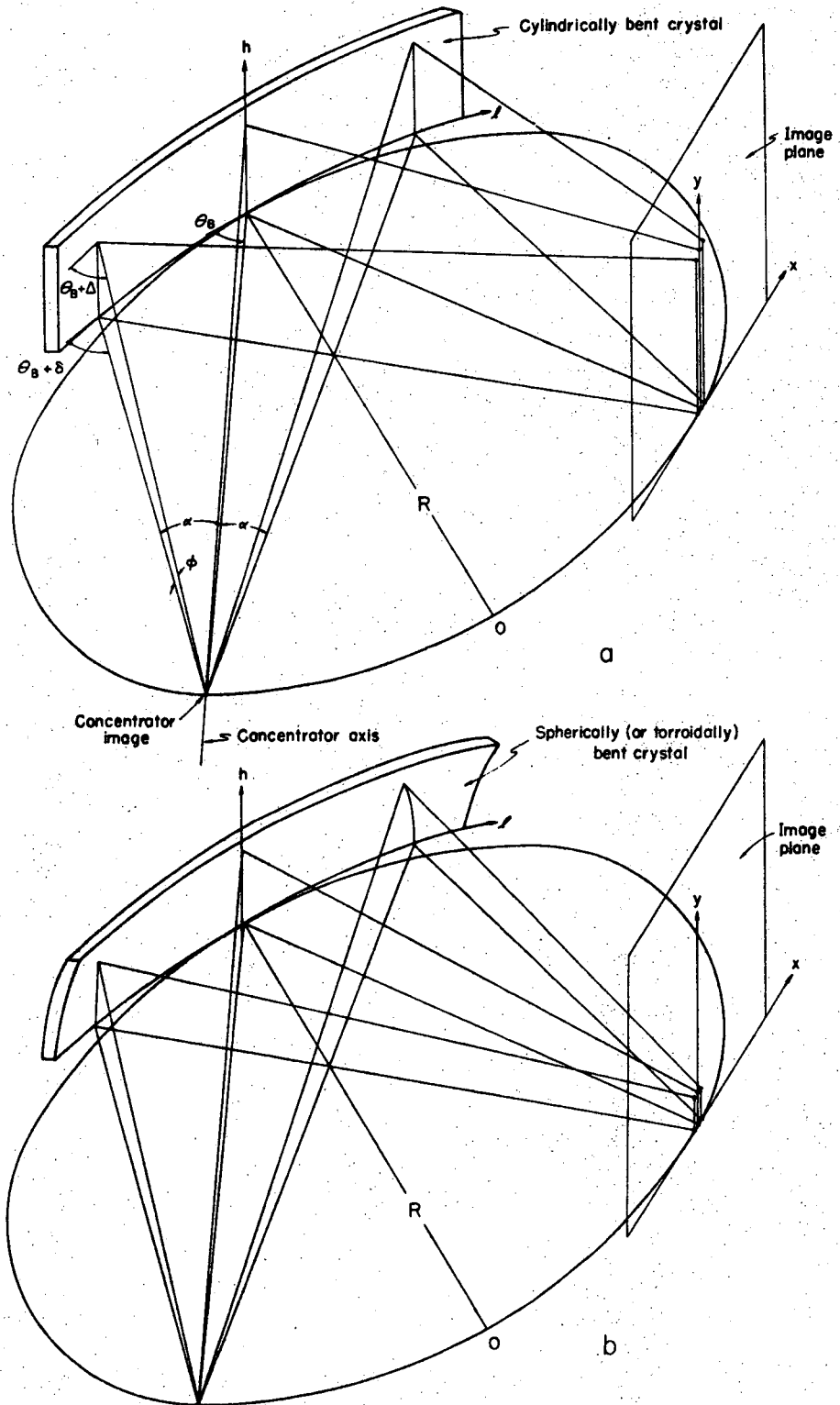


Figure 3. Focusing optics geometry

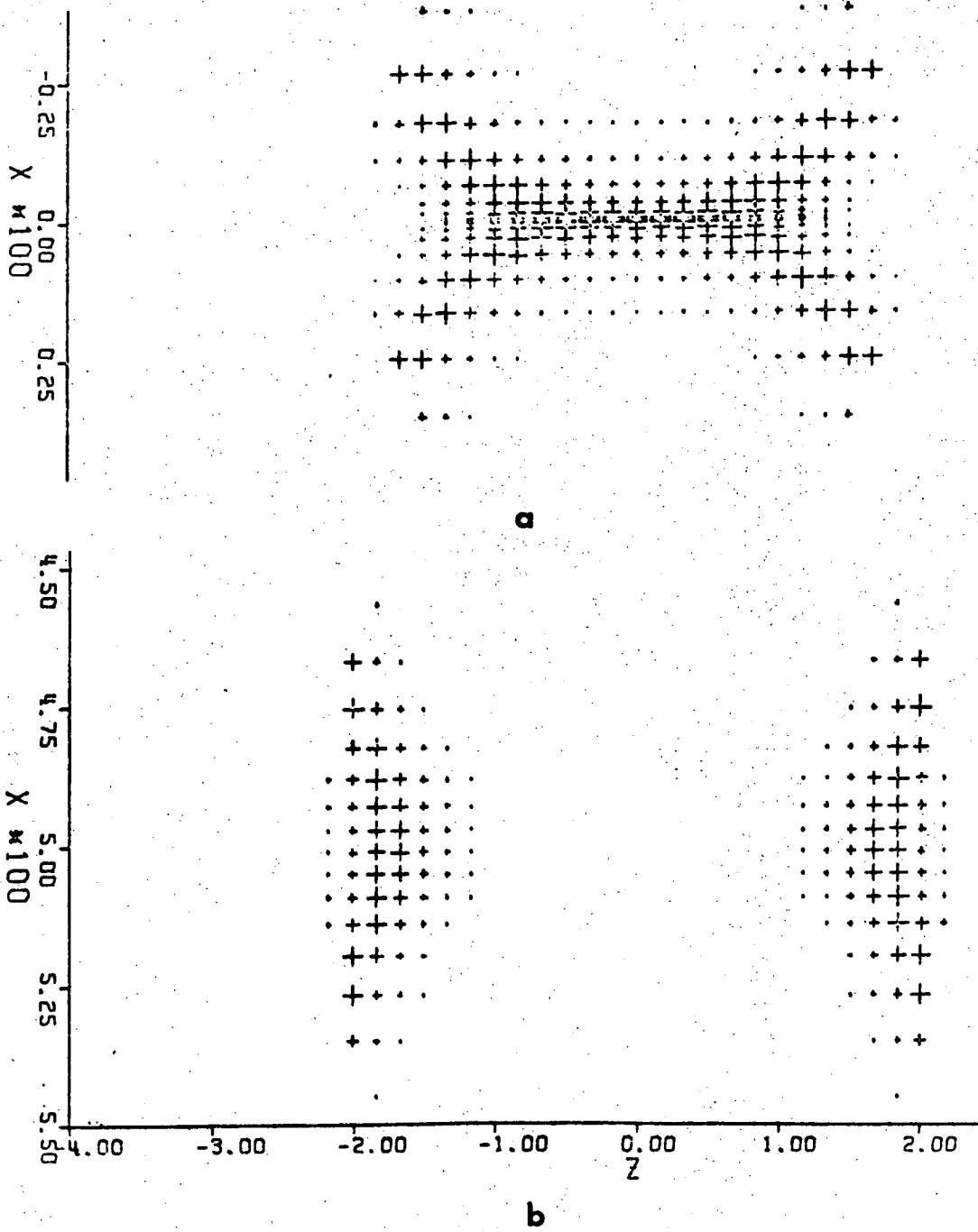


Figure 4. Computer simulations of the distribution of reflected intensity over the crystal image for $\theta_p=40^\circ$ and two settings of the crystal angle. X and Z are in inches.

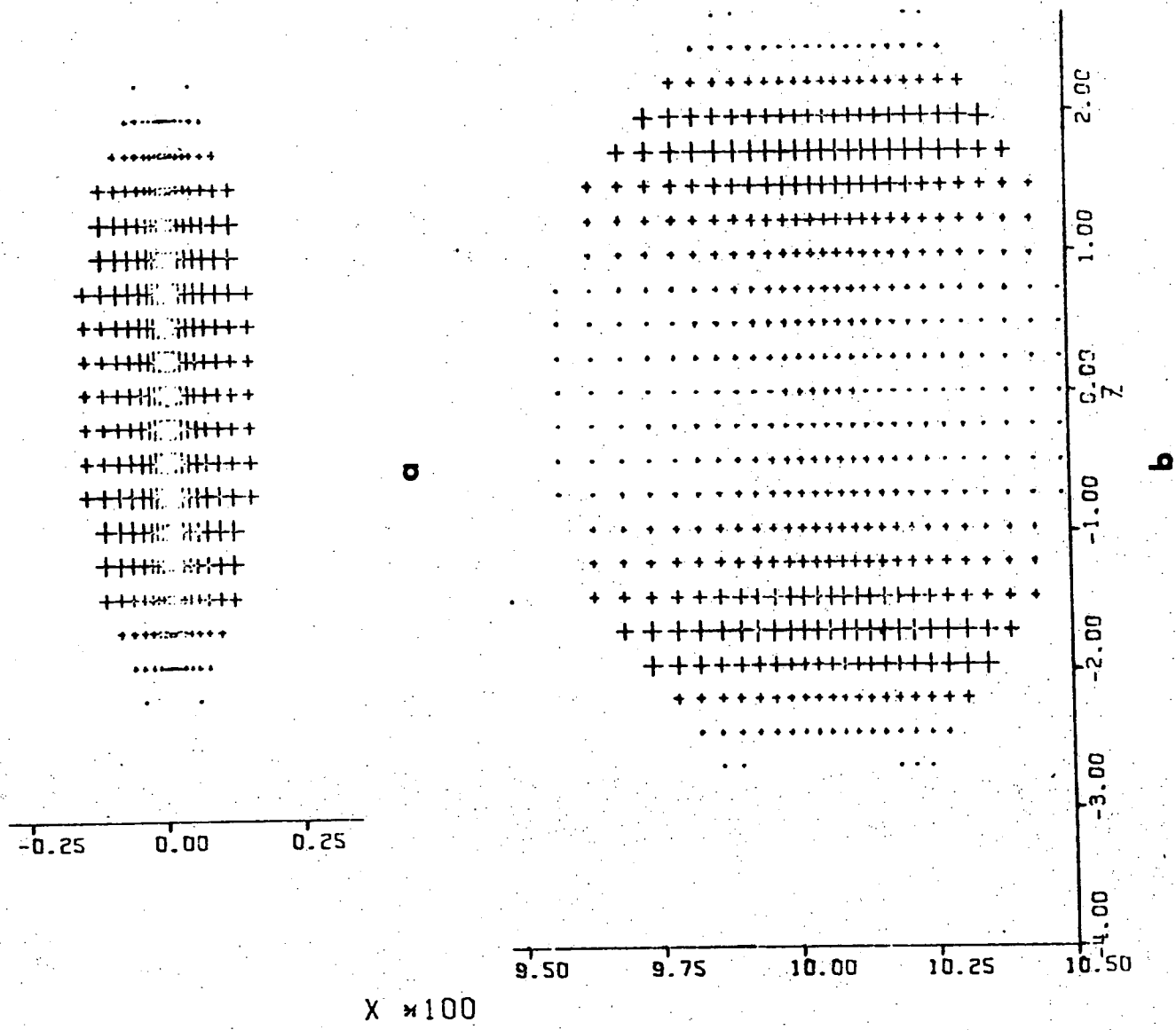


Figure 5. Computer simulations for $\theta_B = 70^\circ$.

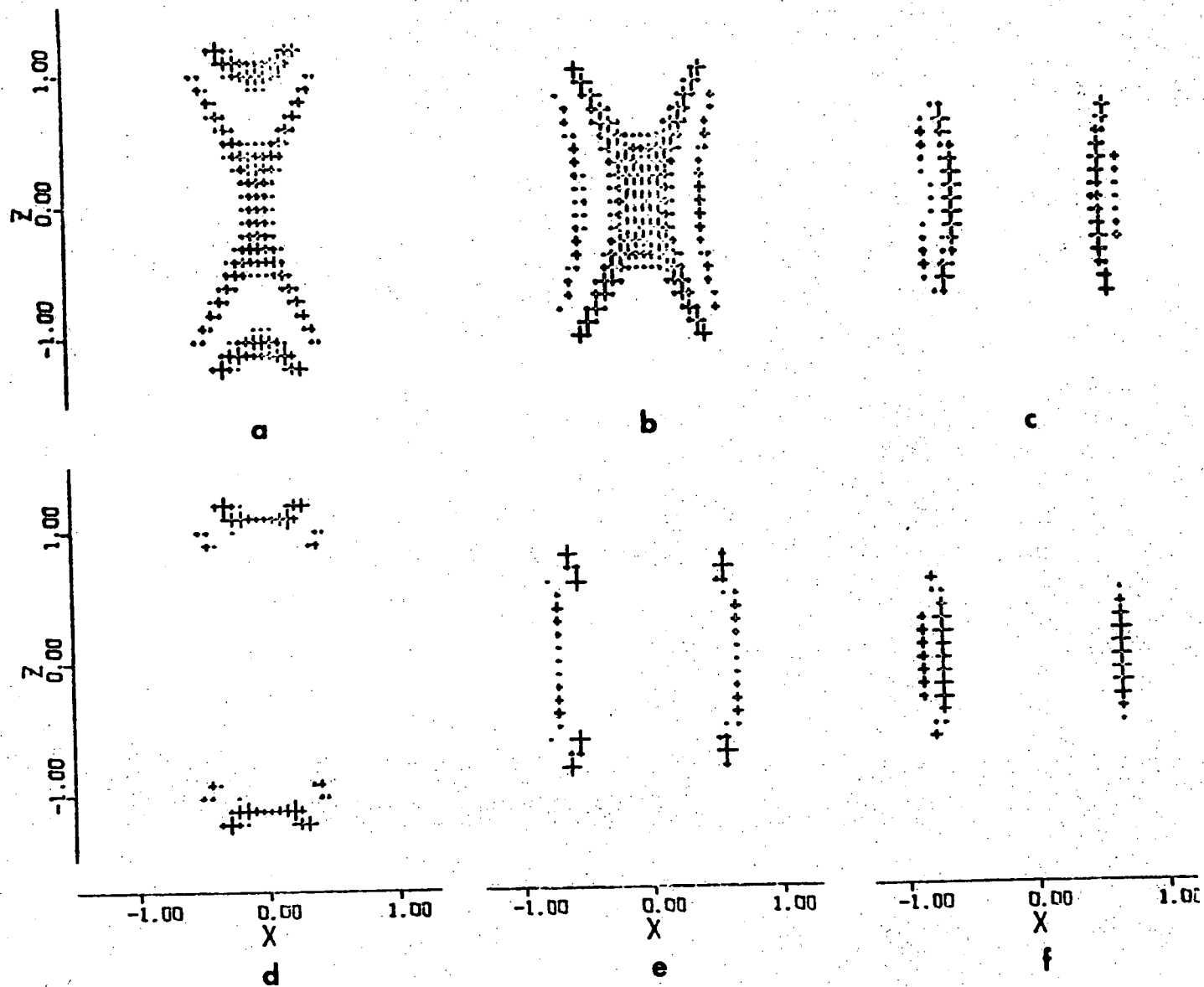


Figure 6. Computer simulation of the reflection pattern of $\text{CuK } \alpha_1 \alpha_2$ radiation from a cylindrically bent crystal at several crystal settings. The Bragg angle is 38° , the crystal is 10 inches from the source, the detector plane is 3 inches from the crystal, and a 10° cone of incident radiation is used.

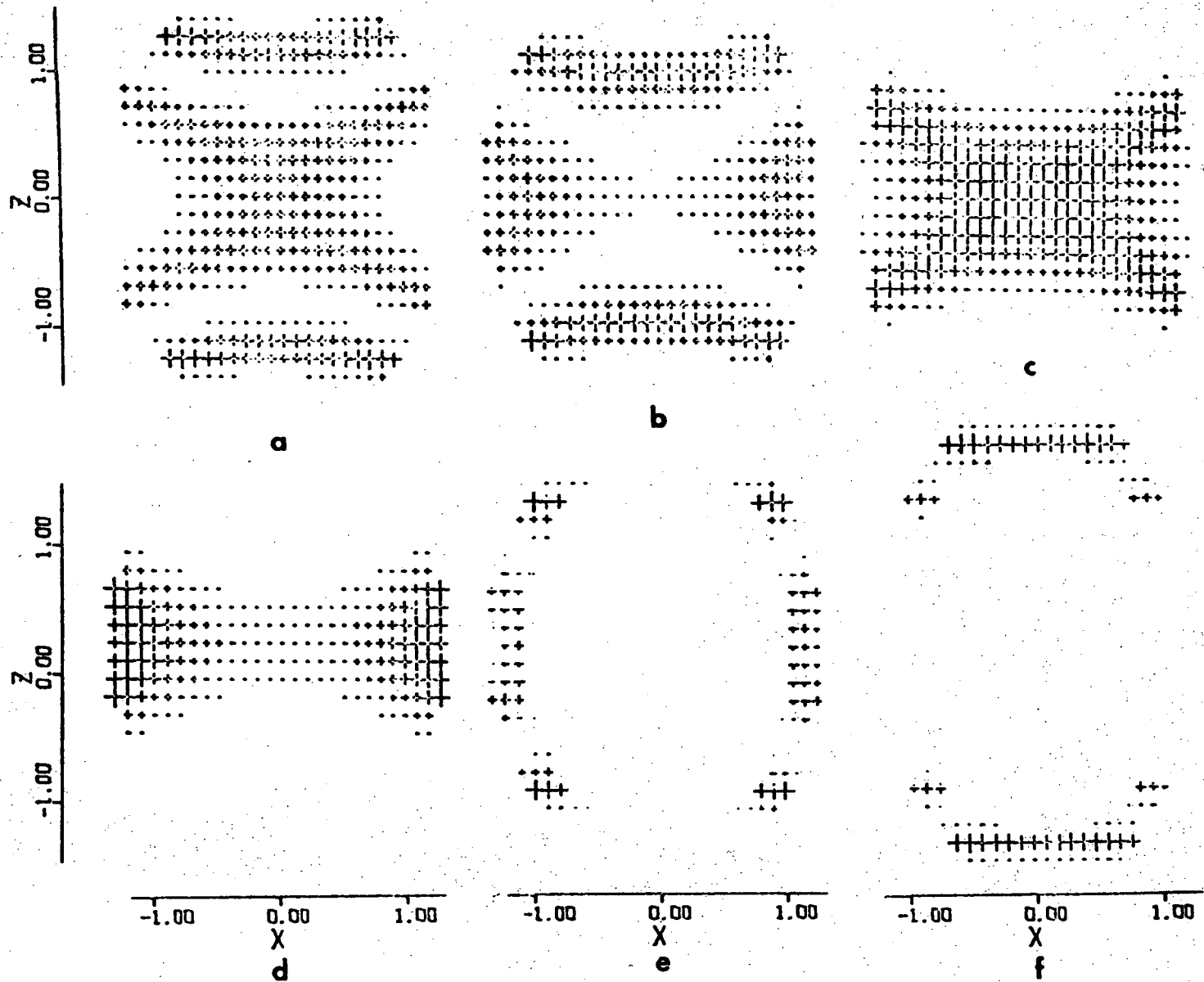


Figure 7. Computer simulations of the reflection pattern of CrK $\alpha_1 \alpha_2$ radiation from a cylincridally bent crystal at several crystal settings. The Bragg angle is 67° , the crystal is 10 inches from the source, the detector plane is 3 inches from the crystal, and a 10° cone of incident radiation is used.

Table 1.

Summary of Ray Tracing Parameters

θB	λ	$\Delta \theta B_1$	$\Delta \theta B_2$	Cone	Optics	Figure
degree		Min.	Min.			
40°		0.0'	---	Solid	Johann	3a
		-6.7'	---			3b
70°		0.0'	---			4a
		-9.2	---			4b
38°	CuK $\alpha_{1,2}$	6.0	0.5	Solid	Johann	5a
		0.0	-5.5			5b
		-8.0	-13.5			5c
		6.0	0.5	Hollow		5d
		-6.0	-11.5			5e
		-12.0	-17.5			5f
67°	CrK $\alpha_{1,2}$	12.0	0.9	Solid		6a
		8.0	-3.1			6b
		0.0	-11.1			6c
		-4.0	-15.1	Hollow		6d
		8.0	-3.1			6e
		20.0	8.9			6f

a. $4 \leq \lambda \leq 12 \text{ \AA}$

b. $12 \leq \lambda \leq 25 \text{ \AA}$

c. $25 \leq \lambda \leq 60 \text{ \AA}$

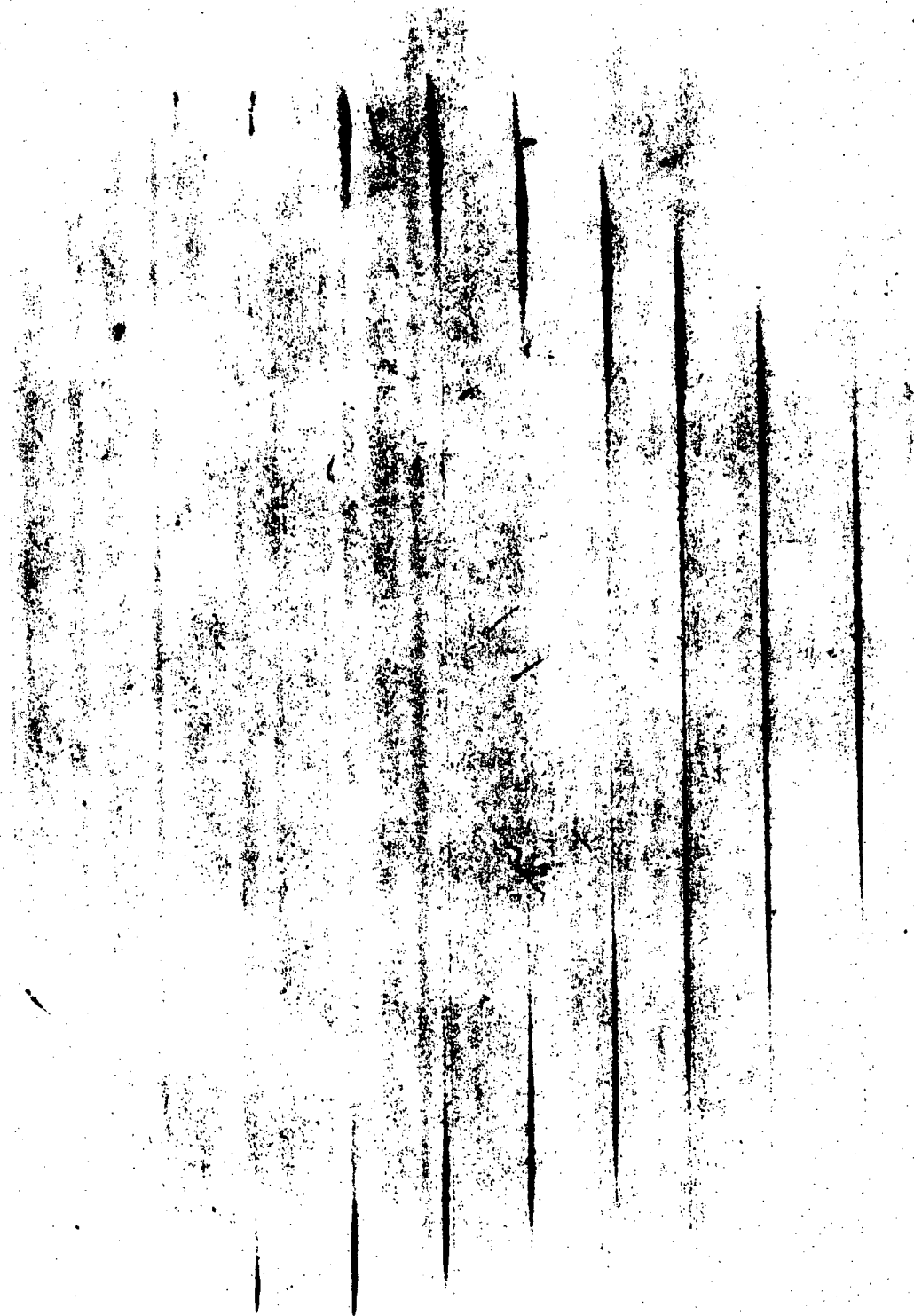


Figure 8. X-ray pictures of the focused reflection pattern of CrK $\alpha_1 \alpha_2$ radiation from a cylindrically bent crystal with a radius of 13.5 inches. In each succeeding picture the central Bragg angle is decreased by 10° .



Figure 9. X-ray pictures of the $\text{CuK } \alpha_1 \alpha_2$ doublet in 8th order after Bragg reflection from a cylindrically bent mica crystal with a radius of 10 inches. The film was placed 3 inches from the crystal and the difference between the Bragg angle and the crystal angle is a) $11'$; b) $6'$; c) $0'$; d) $-8'$.

image of changing the central Bragg angle while Figure 9 shows the intermediate detector case.

Since the Bragg angle varies over the crystal, the fraction of the total incident intensity in a given spectral line which is reflected is always less than the peak reflectivity that would be obtained if $\Delta = 0$. Furthermore, if the crystal width is on the order of or narrower than the line width, only a part of the line is reflected even if all positions of the crystal are at the Bragg angle. If we assume a crystal with a 100% peak reflectivity, then the efficiency factor F is the ratio of the number of reflected X-rays to the number of incident X-rays. For a given cone of incident radiation, F is a function of the central Bragg angle θ_B , and depends on the type of optics used and on the width of the crystal rocking curve and the line width. For a general crystal, the total efficiency is the product of F and the peak reflectivity of the crystal.

The values of F for line widths ($E/\Delta E$) and crystal resolutions of 1500 and 3000, and Bragg angles of between 10° and 80° have been calculated and are shown in Figures 10 and 11. These figures also give the total effective area of the telescope-spectrometer combination. In Figure 11, the telescope efficiency is also included. The values of the efficiency given in Figures 10 and 11 were calculated assuming that the crystal angle was set at the optimal position for the incident radiation.

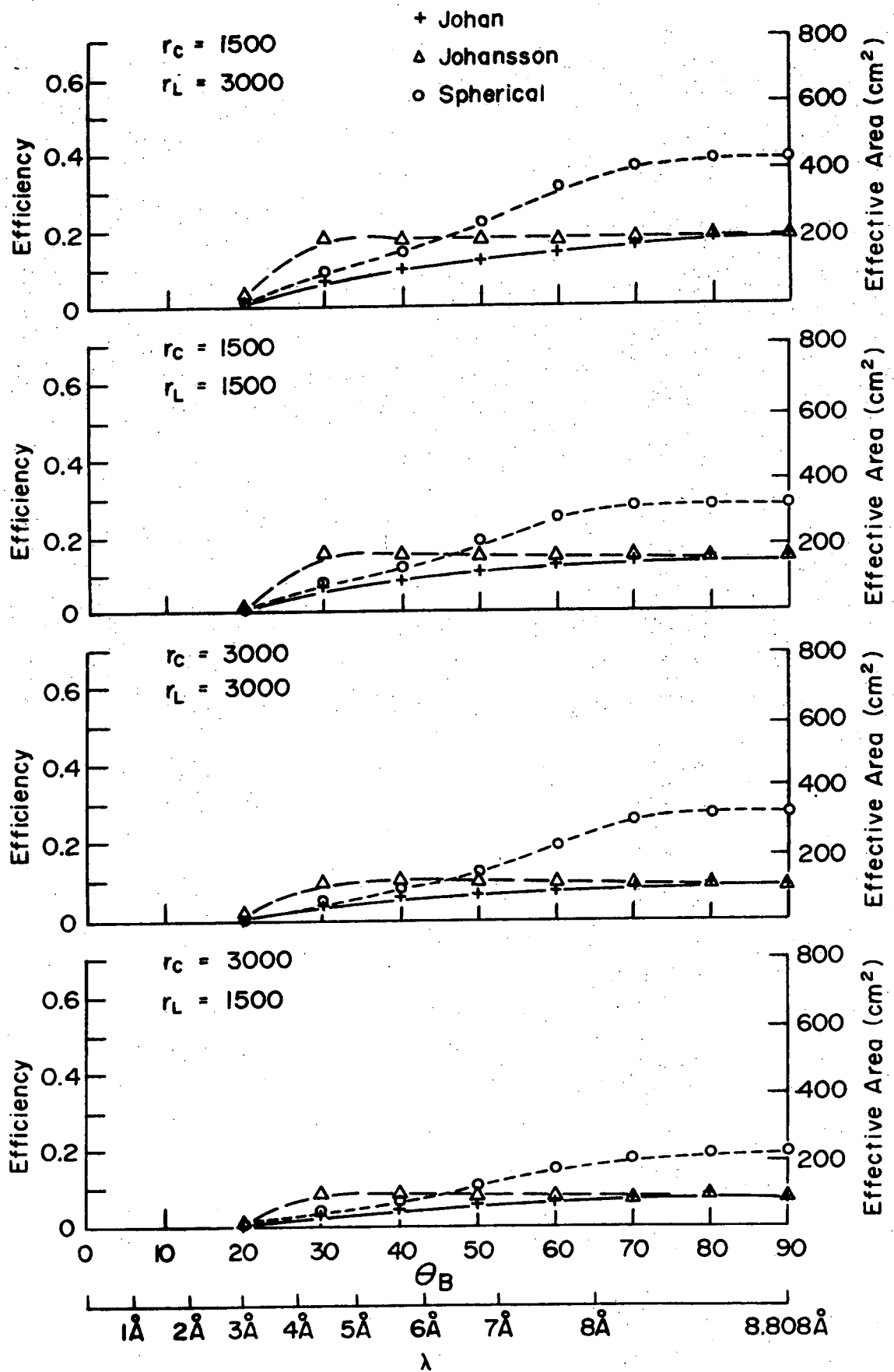


Figure 11.

(LINE REFLECTION EFFICIENCY)*
 (GRAZING INCIDENCE REFLECTION EFFICIENCY)

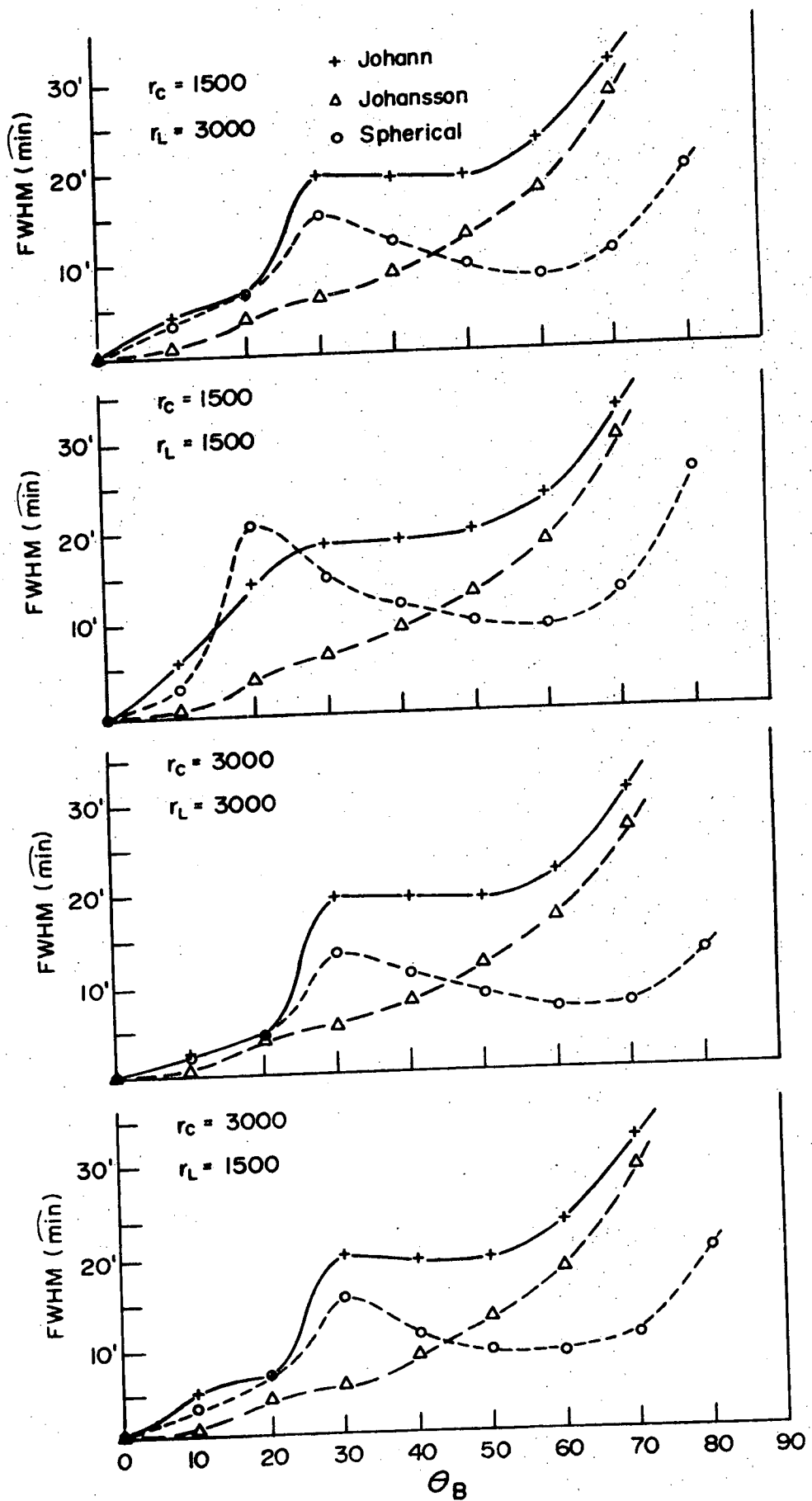


Figure 12.

FWHM OF THE CURVED CRYSTAL REFLECTION PATTERN
(Without Grazing Incidence Efficiency)

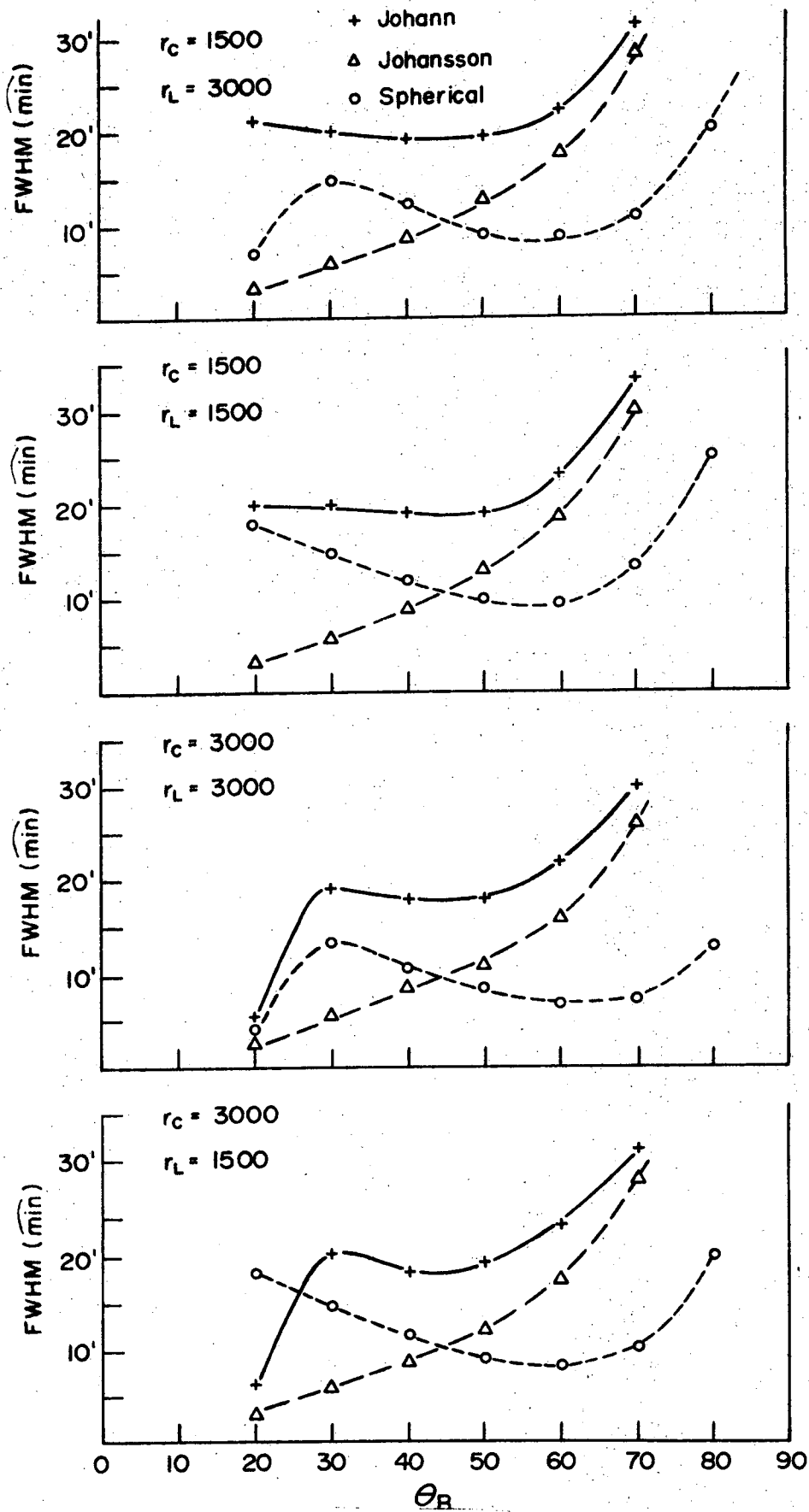


Figure 13.

FWHM OF THE CURVED CRYSTAL REFLECTION PATTERN
(With Grazing Incidence Efficiency)

As can be seen in Figures 6, 7 and 9, if the center of the crystal is set to the Bragg angle, only a small portion of the crystal reflects the line radiation; only if the central angle is offset from the Bragg angle causing the reflection pattern to move to the top or sides is a significant portion of the incident ring of radiation reflected. Figures 12 and 13 give the FWHM of the reflection pattern of the crystal as a whole as the central angle is changed. This value is a measure of how accurately the central angle has to be set relative to the optimal angle in order to still reflect a portion of the line being investigated.

2. Application to the Present Experiment

For practical reasons associated with crystal properties and detector requirements, we shall divide the wavelength range of interest into three broad bands: $\lambda < 4\text{\AA}$, $4\text{\AA} < \lambda < 15\text{\AA}$ and $\lambda > 15\text{\AA}$.

From the results of Tucker⁽²⁾ and others^(3,4,5), there are distinct special features to be observed in each of these wavelength regions. Tables 2, 3 and 4 and Figures 14, 15, 16⁽⁶⁾ and 17⁽⁷⁾ describe a number of crystals and their reflection properties throughout the wavelength region of interest. The results of Table 3 have been obtained in our laboratory with a two-crystal spectrometer. The two-crystal rocking curves obtained in our lab for the cleaved and the etched and treated PET are shown in Figures 18 and 19. Figure 20⁽⁸⁾ shows the properties of a Kanigen coated telescope

Table 2.

Integrated reflectivities, peak reflectivities,
and rocking curve widths for various crystals
at Cu K (1.5 Å)¹

Crystal	(Plane)	2d (Å)	Order	Surface	R _C	R _P	Rocking Curve Full Width at Half Maximum
SiO ₂ ²	(2023)	2.744	1	etched	8.0×10^{-5}	50%	3.2
LiF	(200)	4.026	1	cleaved	8.8×10^{-5}	7.5%	185
LiF	(200)			etched	8.8×10^{-5}	7.5%	185
LiF	(200)			polished	2×10^{-4}	23%	100
LiF	(200)			ground	3.8×10^{-4}	25%	150
LiF ³	(200)			abraded	6×10^{-4}	20%	500
LiF ³	(200)			abraded	4.4×10^{-4}	27%	300
LiF	(220)		1	ground	1.4×10^{-4}	6%	330
PET	(001)	8.742	1	cleaved and polished	1.1×10^{-4}	27%	55
EDDT	(010)	8.808	1	polished	1.2×10^{-4}	31.5%	40
EDDT	(010)			ground	8.6×10^{-5}	32%	29
SHA	(110)	13.98	2	as grown	1.0×10^{-4}		45

Table 2 (continued)

Crystal	(Plane)	2d (Å)	Order	Surface	R_C	R_P	Rocking Curve Full Width at Half Maximum
RAP	(001)	26.12	5	cleaved	8×10^{-5}		13
KAP	(001)	26.63	7	cleaved	4.1×10^{-5}		10

¹From I.W. Ruderman and B. Michelman, President Status of X-ray Analyzer Crystals, Isomet Corp. report, unless otherwise noted.

²O. Adell, G. Brogren, and L.E. Haeggbloom, Ark. F. Fysik 1, 197 (1954).

³F.W. Lytle and R.G. Bingham, Some Diffraction Techniques for X-ray Astronomy, Boeing Scientific Research Laboratories Document D1-82-0875.

Table 3.

Relative peak reflectivities and crystal resolutions for various crystals

Collimation Crystal	2d (Å)	13.3Å		23.6Å		44.6Å	
		I ²	$\Delta\lambda$	I	$\Delta\lambda$	I	$\Delta\lambda$
KAP	26.6	240	.97	42	.33		
OHM	63.5	24	.35	65	.80	449	1.2
Pb-Laurate	70	810	.40	1000	.49	350	1.6
Pb-Myristate	79						
Pb-Stearate	100	1000	.46	1000	.65	1000	1.7

¹BHenke and R. Lent, Some Recent Work in Low Energy X-Ray and Electron Analysis, "Advances in X-Ray Analysis", Vol. 12, pp. 480-495.

²Relative to Pb-Stearate

³Calculated from $\Delta\lambda = d \cos\theta\Delta(2\theta)$, where $\Delta(2\theta)$ is the full width at half maximum of the rocking curve of the crystal, including the .1° collimation.

TABLE 4

A. Measured Properties - Two-Crystal Spectrometer

Crystal	order	λ (Å)	FWHM min	$[I/I_0]_{\max}$	R radians
EDDT	(1, -1)	6.07	0.8	0.13	0.69×10^{-4}
PET					
2 cleaved	(1, -1)	6.07	1.2	0.40	1.81×10^{-4}
1 cleaved			2.55	0.30	3.14×10^{-4}
1 treated					
2 treated			3.90 ^a	0.21 ^{a,b}	3.14×10^{-4} ^a
KAP	(2, -2)	8.34	0.6	0.36	0.89×10^{-6}

B. Derived Single-Crystal Properties^b

Crystal	Order	λ (Å)	ΔE eV	$[I/I_0]_{\max}$	Rc ^a radians	(E/ ΔE)
EDDT	1	6.07	0.25	0.22	0.42×10^{-4}	7.67×10^3
PET						
cleaved	1	6.07	0.37	0.80	1.08×10^{-4}	5.17×10^3
treated			1.2	0.41	1.89×10^{-4}	1.59×10^3
KAP	2	8.34	0.17	0.007	0.67×10^{-6}	8.68×10^3
	1	17.5	0.61	0.05	0.71×10^{-4}	1.15×10^3

a) Inferred

b) Lorentzian line shape assumed

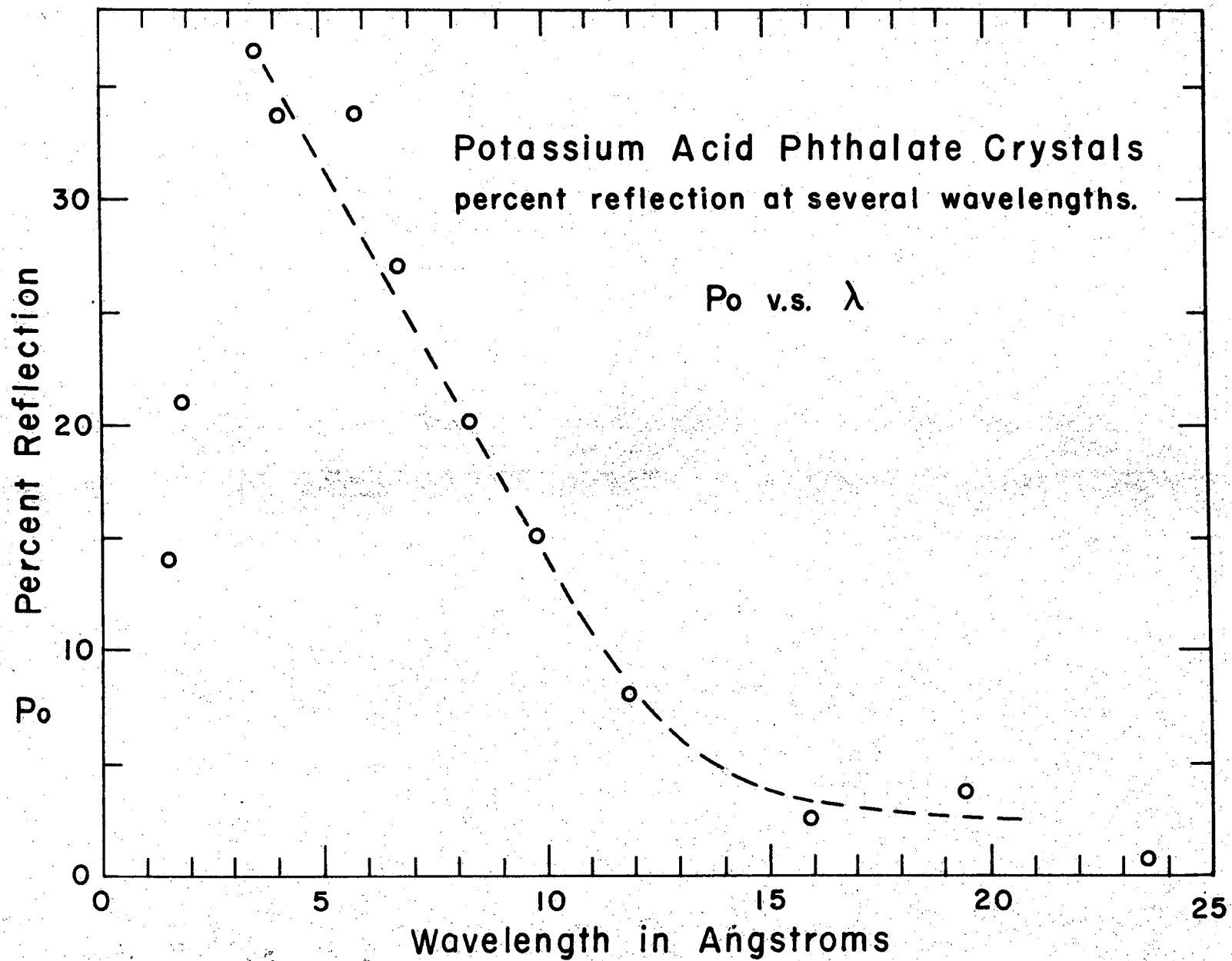


Figure 14. A graph of the peak reflectivity of a KAP crystal versus wavelength of the incident X-rays.

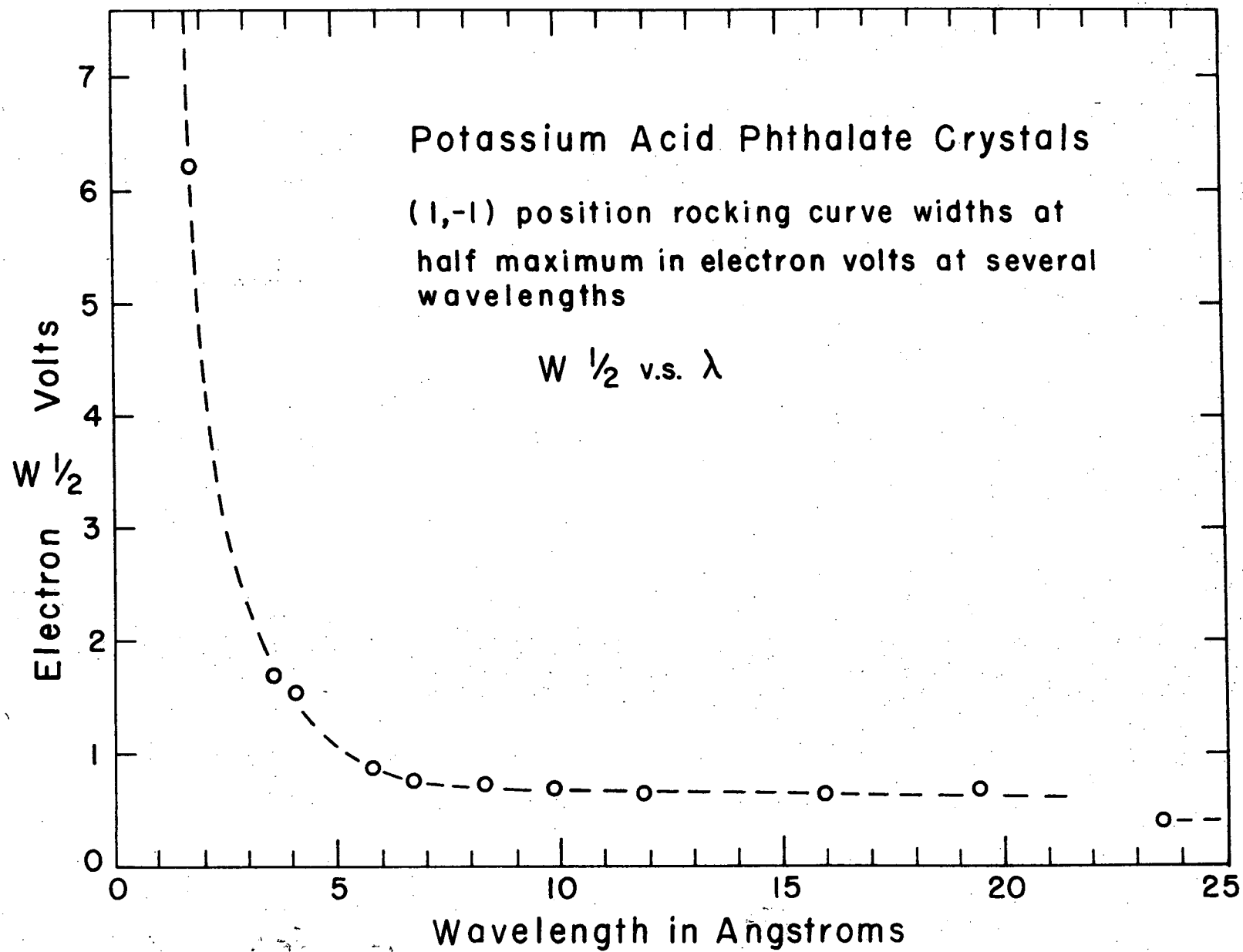


Figure 15. A graph of the rocking curve width at half maximum of a KAP crystal in electron volts versus wavelength.

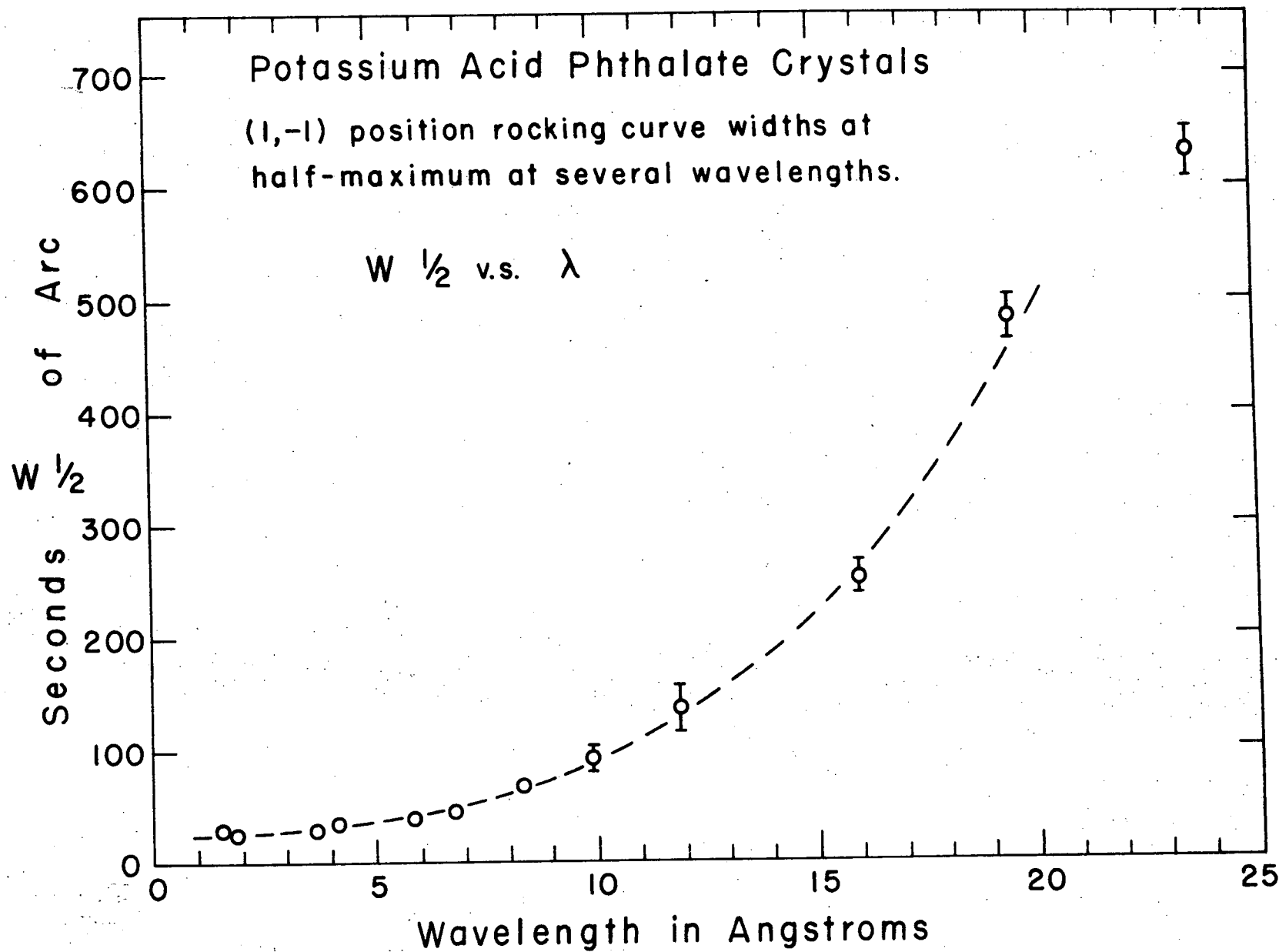


Figure 16. A graph of the rocking curve width at half maximum of a KAP crystal in seconds of arc versus wavelength.

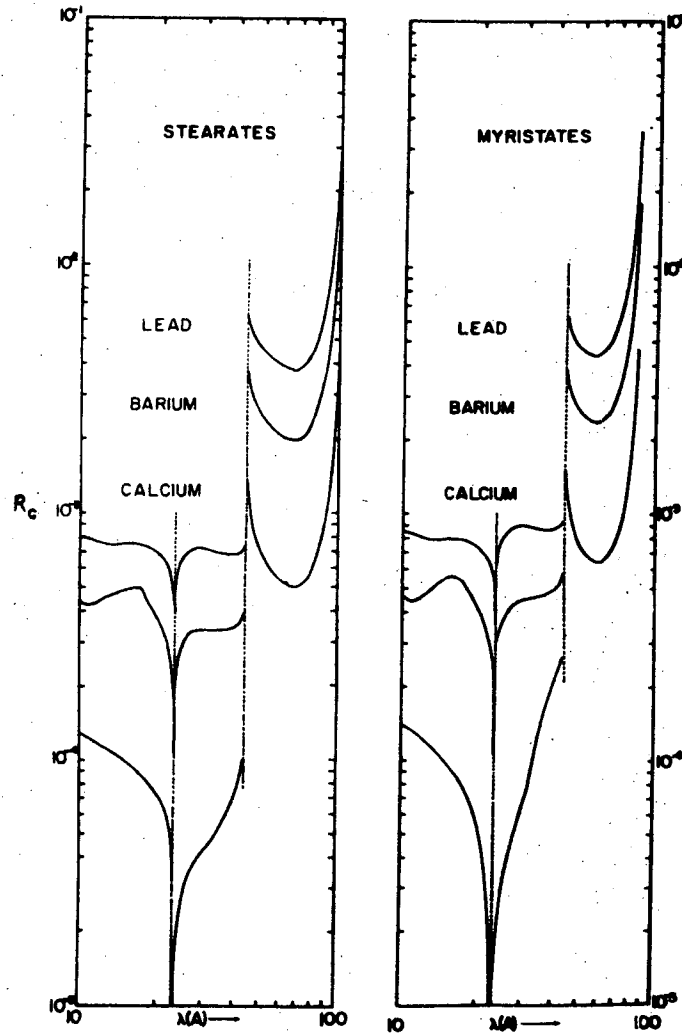


Figure 17. Coefficient of reflection R_c for several stearates and myristates as a function of wavelength.

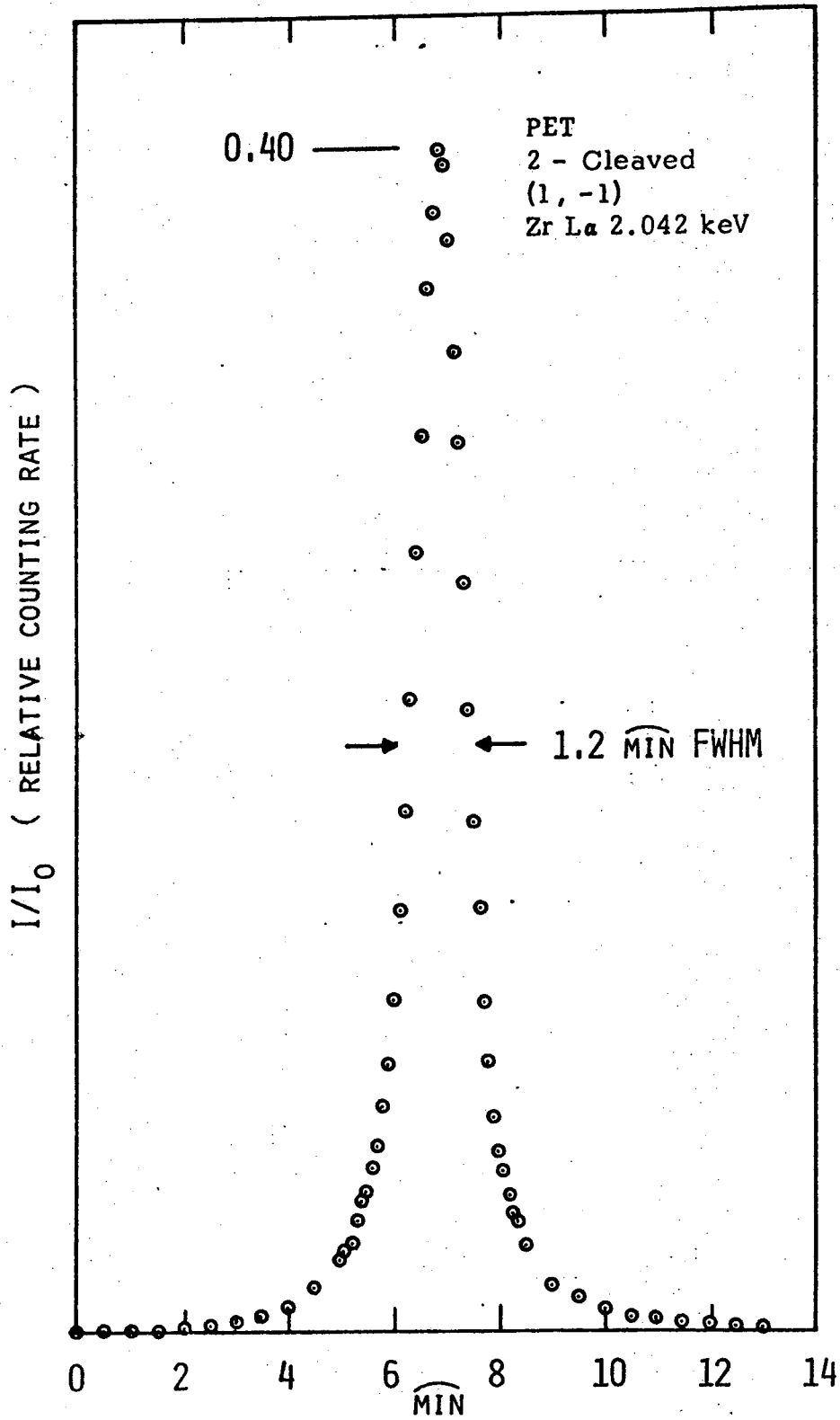


Figure 18. Normalized test results for two cleaved PET crystals.

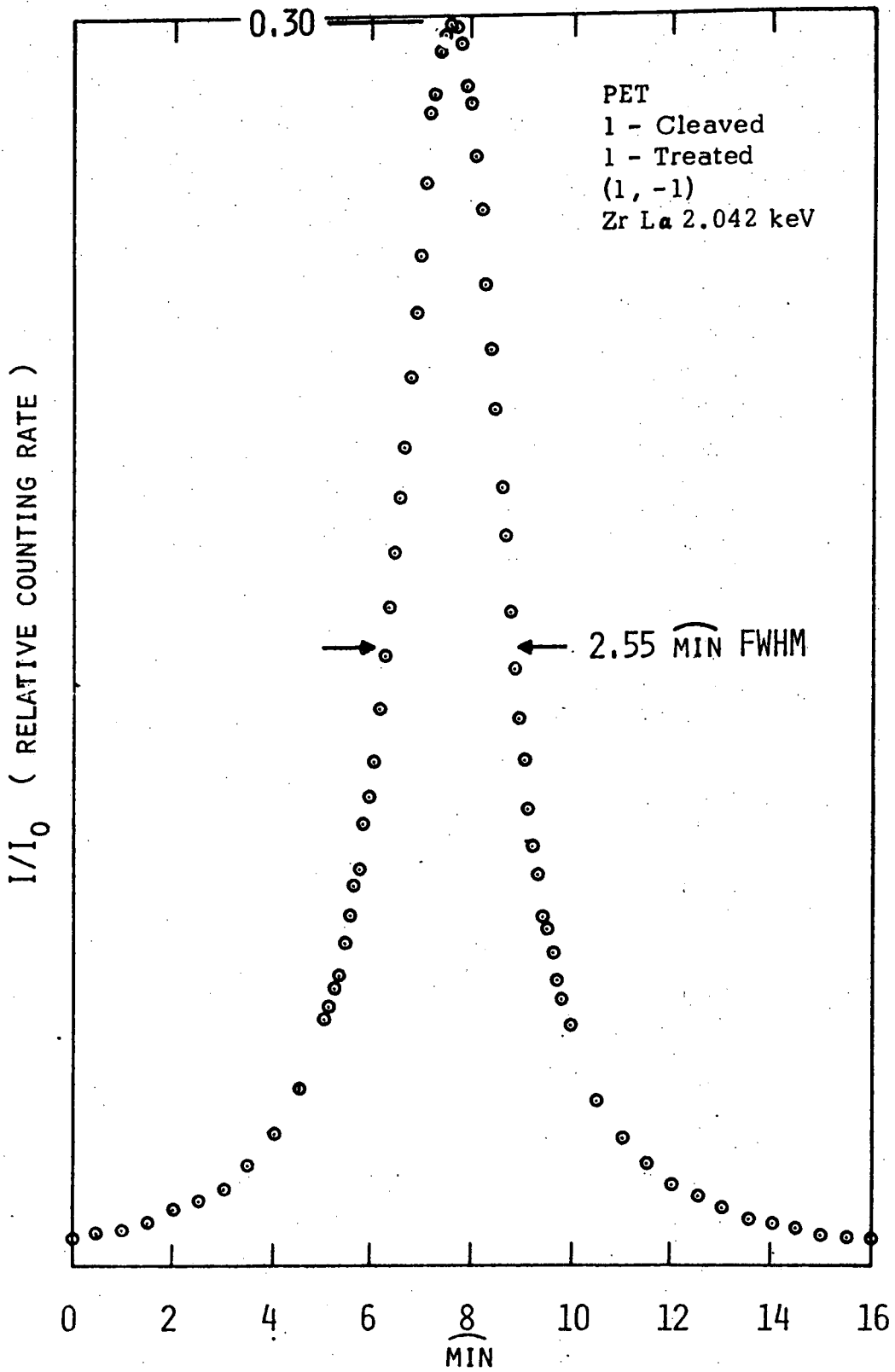


Figure 19. Normalized test results for one cleaved and one treated PET crystal.

mirror. These data yield several important conclusions. The efficiency of the telescope falls rapidly for wavelengths below about 4 \AA and is also low in the region near the Ni L edges. The highest practical crystal resolution and reflectivities are attained at short wavelengths, and both of these parameters decrease with increased wavelength.

A further consideration is the finite spread of the image of the X-ray telescope which for a point object is described by a function of the form e^{-ar^2}/r . This distribution is largely due to scattering from irregularities in the mirror surface and partially destroys the unique assignment of a wavelength to an (α, ϕ) pair. In order to offset as much as possible the adverse effects of a finite source distribution, it is desirable to make the diameter of the focal circle diameter at least 24 inches. Since the telescope focal length is 240 inches, deviations from specular reflection are amplified by a factor of 10 in the plane of dispersion, and it is therefore desirable to minimize the scatter in the beam which is reflected from the telescope.

Source elongation in the horizontal direction (plane of dispersion) directly broadens the spread in the incident Bragg angle and hence reduces the resolution for a detector placed any point between the crystal and the focus. However, source elongation in the vertical direction affects the resolution only slightly. By choosing a suitable central Bragg angle, the reflection pattern can be positioned at the top and bottom of the crystal and a modest resolution can still be retained.

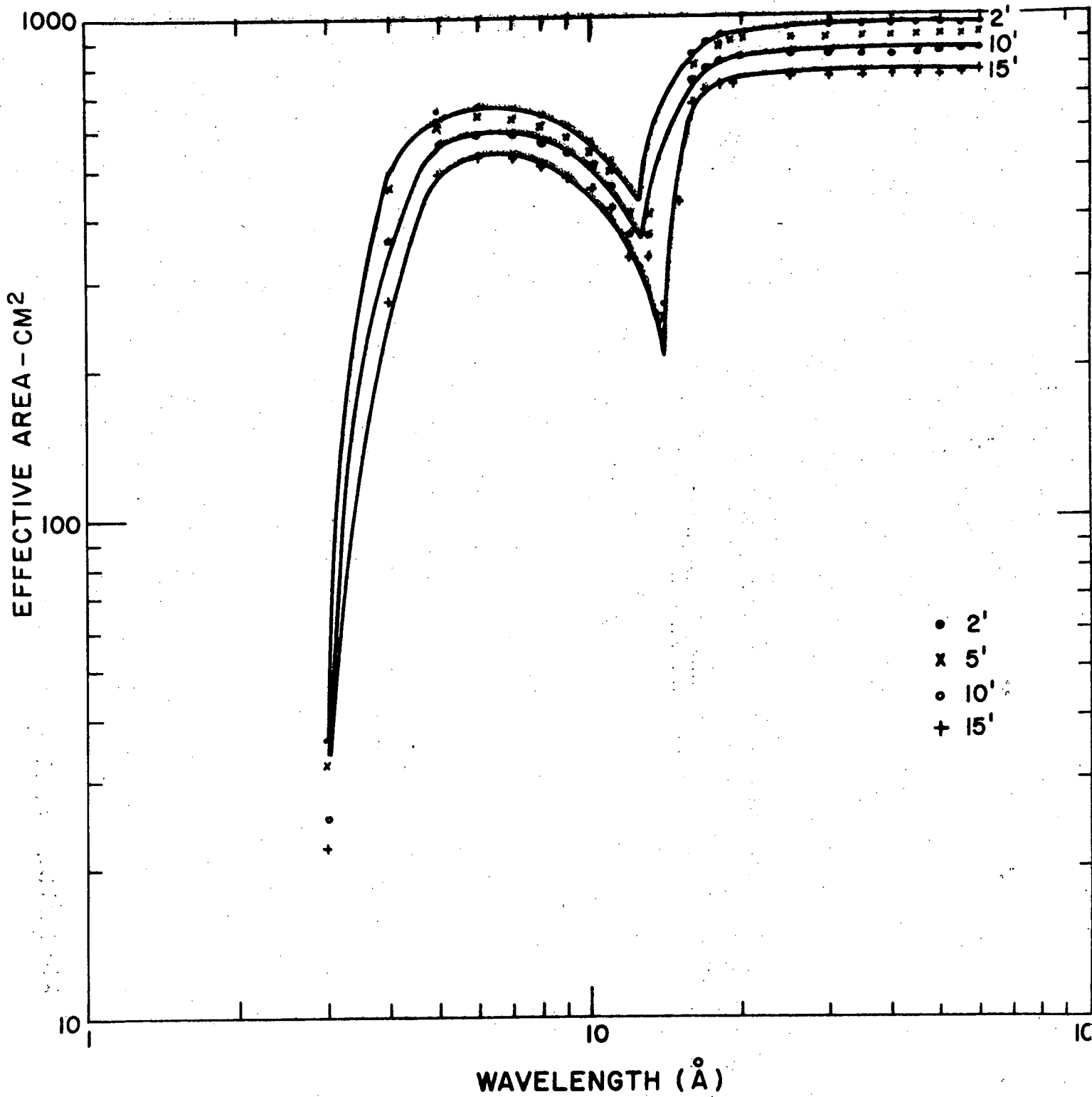


Figure 20. Effective area of the High Resolution Mirror as a function of wavelength for various incident angles.

This requires though, that the spacecraft be pointed on the source to within about $1/2''$ arcmin. Extended sources (greater than a few arc sec in size) pose a problem for the spectrometer since X-rays of the same wavelength can strike the same portion of the crystal at different angles. In order to obtain high resolution, a vertical slit must be used to limit the portion of the source viewed to about a few arc sec by 1 arc min. Because of spacecraft jitter, however, the slit must be moved about to follow the motion of the image. This must be done on board in real time.

Below about $8-10 \text{ \AA}$ highly resolving crystals (resolutions greater than 3000) are available and proportional counters are very efficient (at 8 \AA a 1 mil Be window has a transmission of 45%). For longer wavelengths, crystal resolutions become much poorer (see Figure 16 and Tables 2 and 3), and extremely thin windows are required to obtain good proportional counter efficiencies. To obtain high efficiency and high detector spatial resolution, an imaging proportional counter with wire spacings of $.050''$ will be placed near the crystal approximately $1/3$ of the way from the crystal reflection pattern. It will have a spatial resolution of about $.050''$, so that the detector resolution will be around 6000. A higher signal to noise ratio can be obtained by positioning the detector at the crystal focus, resulting in a poorer resolution (approximately 3000).

For the longer wavelength range, such a high resolution

is not necessary, and it becomes possible to use a small linear array of detectors at the focus in order to obtain the highest sensitivity. The highest detection efficiency in the 10 - 70 Å range will be obtained by using an array of preamplified spiraltron electron multiplier tubes^(8,9) with a high-efficiency photocathode material such as CsI deposited on the inner surface of the collecting cones. We have tested the efficiency of a base Mullard channeltron in our lab, and obtain efficiencies of 1.5% at 6 Å and 1.9% at 14 Å, so that it is necessary to use a photocathode material to increase this efficiency. This means that no visible light or UV must be allowed to enter the detection system. A photograph of a typical preamplified spiraltron is given in Figure 27. For this instrument the cones will have a collecting area of .15" x .20", and there will be two linear arrays of spiraltrons side by side to encompass the wandering of the focus due to spacecraft jitter. This detector array is shown in Figure 28. The .20" spatial resolution of the spiraltron array corresponds to a detector resolution of between 3000 (if the convolution of the line width and crystal width is 3000 or greater) and 1500 (if the convolution is less than 1000). Because the incident X-rays will make an angle of 10° with the photocathode surface, the detection efficiency with CsI will vary from 40 to 80% in the 8 - 70 Å range. Graphs of measured photocathode efficiencies as a function wavelength and incidence angle are shown in Figures 21 - 23.^(9,10,11)

Both of these detector systems will have low background

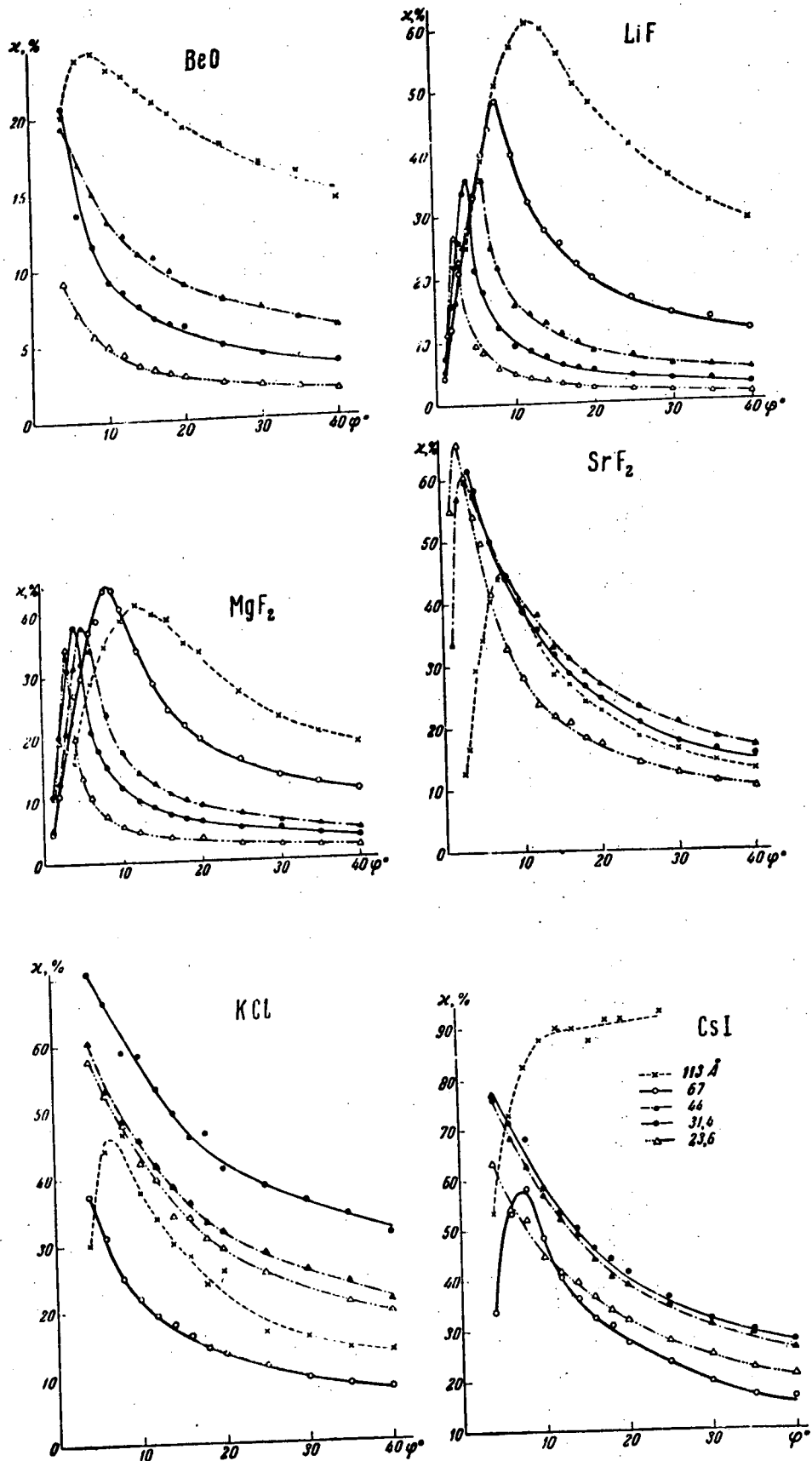


Figure 21. Photocathode efficiencies as a function of the angle of incidence.

C-2

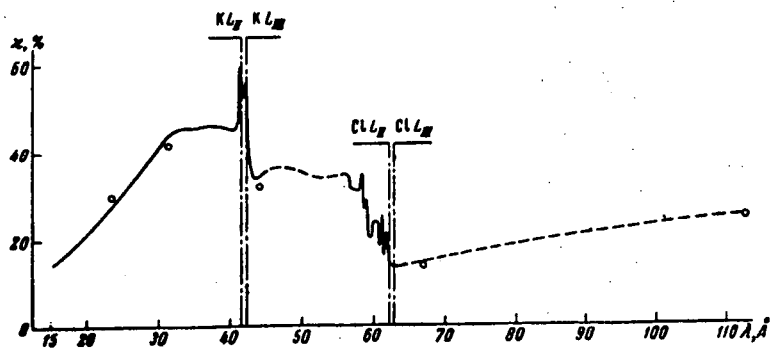
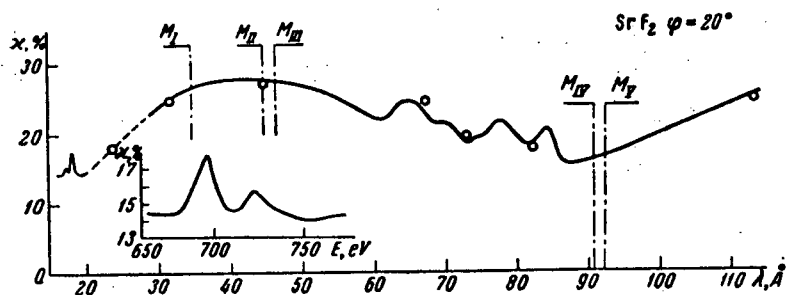
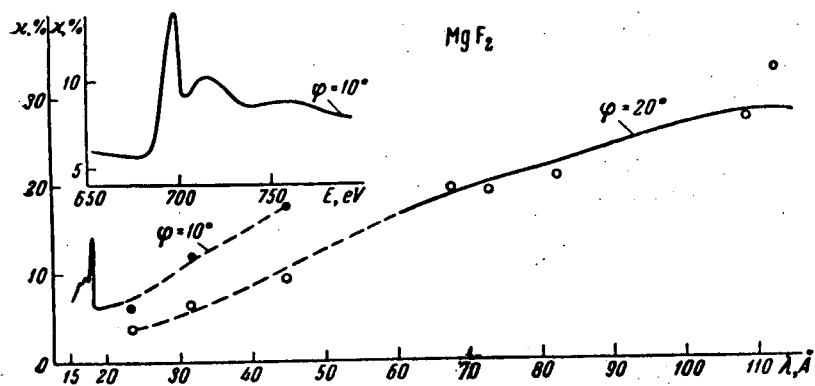
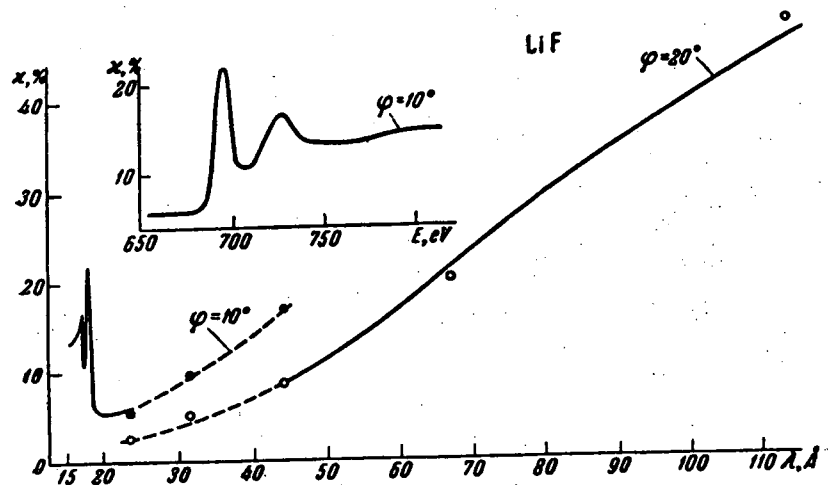


Figure 22. Photocathode efficiencies as a function of wavelength.

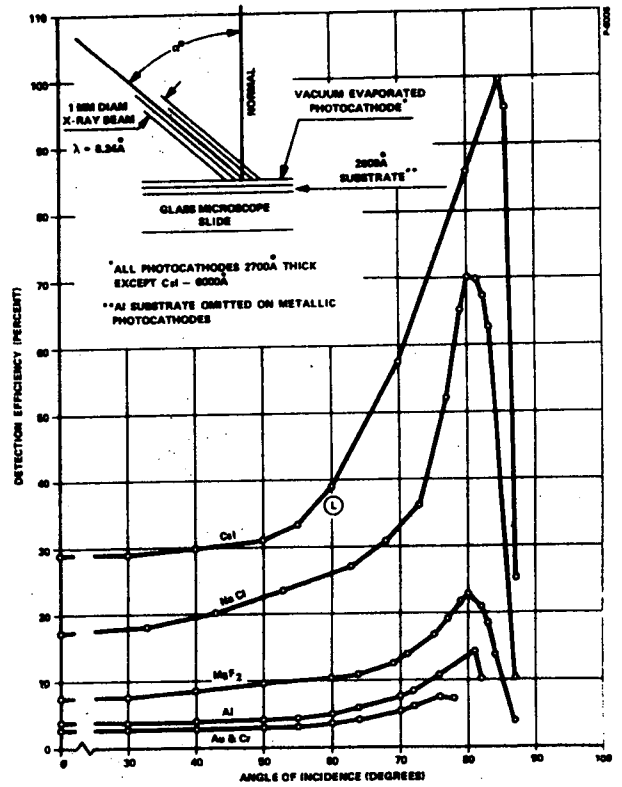
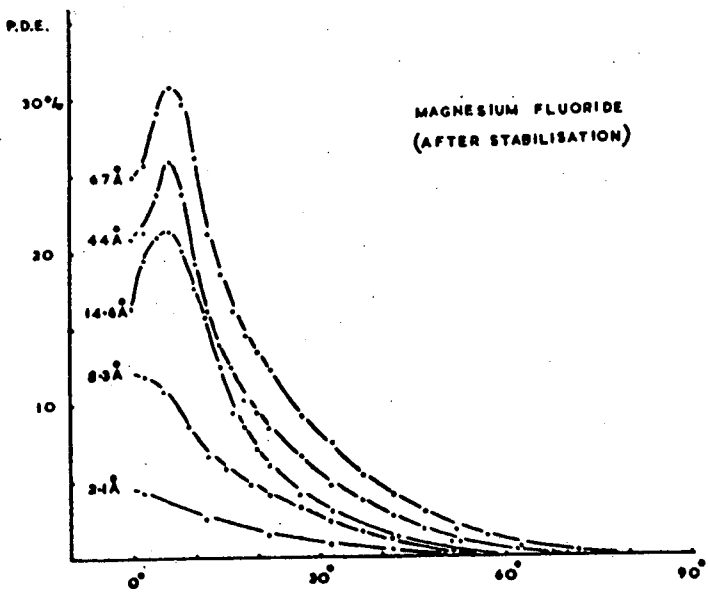
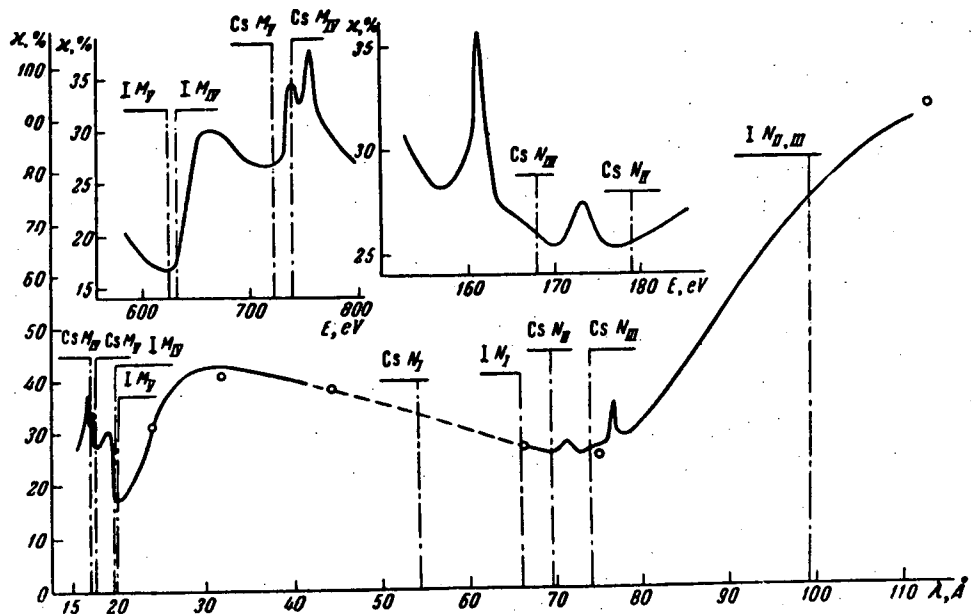


Figure 23. Photocathode efficiencies as a function of wavelength and angle of incidence.

rates and therefore high sensitivity. The imaging proportional counter will have a background count of about $.01 \text{ count/cm}^2 \text{ sec}$ and each spiraltron will have a dark noise of less than $.005/\text{sec}$ ⁽¹²⁾. Because of the nature of the reflection pattern, only a small fraction of the detector will be illuminated by the Bragg reflected radiation at a given setting of the instrument. Thus a total detector background of about $.05 \text{ count/sec}$ should be attained.

We are considering four crystals to cover the three wavelength regions discussed above. Either EDDT or PET in combination with the imaging proportional counter will cover the short wavelength part of the $4\text{-}12 \text{ \AA}$ range while SHA will be used for the long wavelength part if problems related to its extreme fragility can be overcome. RAP in combination with the spiraltron array will be used for $12\text{-}25 \text{ \AA}$ and either OHM, lead laurate or lead myristate for $25\text{-}70 \text{ \AA}$. All of these crystals are vacuum and radiation stable so that their performance will not degrade while in orbit. Both lead myristate and lead laurate have been tested in a vacuum at 40°C for 40 days⁽¹³⁾.

The actual choice of crystals will depend greatly on laboratory tests. The crystal choice is complicated by the fact that there are few crystals that can be bent cylindrically to the accuracy needed for the spectrometer. Quartz, mica, and KAP are the only crystals usually used for high-resolution curved crystal spectrometers. Both Johansson and spherical problems present much more formidable problems. It is very difficult to bend crystals spherically without breaking them or severely distorting the surface. We have

done a little work on attempting to bend mica and KAP spherically, but with little success. There are techniques for bending NaCl and LiF spherically, but not to the accuracy needed, and these processes degrade the already poor resolutions of these crystals. These crystals also have too small a 2d spacing for use with the telescope. Quartz can be bent spherically, but only to long radii (~40"), and only the central portion of the bent crystal is in general used. Quartz also has too short a 2d spacing. Johansson optics also presents great problems because the crystals must be almost 1/8" thick in order to accommodate the grinding. It appears that the only crystals that can be bent without cracking when that thick are LiF and NaCl, and even these crystals develop internal faults. We obtained 2" square Johansson ground LiF, EDDT and KAP crystals and 1" square cylindrically bent OHM from Isomet on a best effort basis. X-ray pictures of the reflection pattern of these crystals are given in Figures 24 and 25. The EDDT and KAP developed visible cracks, and the LiF crystal is not good enough for high resolution studies. Further study must be made into these problems.

We now estimate the minimum detectable integrated signal strength. We assume a background limited case, a telescope with a geometrical area of 1100 cm² and an observation time of 1000 sec. Then in order to be detectable a signal at a given wavelength must be greater than three standard deviations or

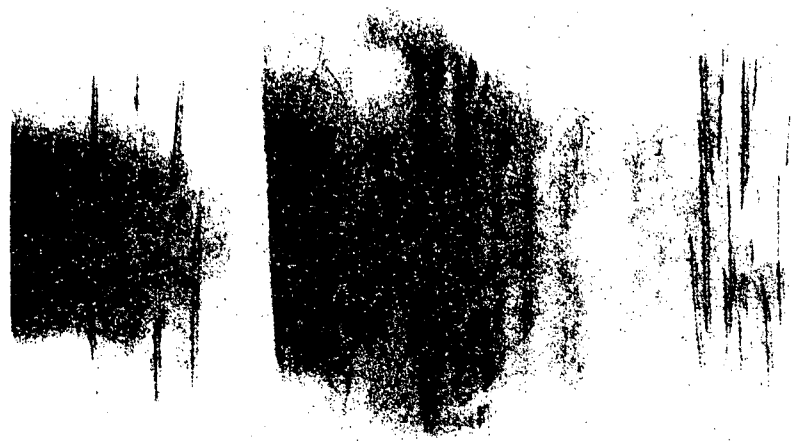
$$I_{\text{MIN}} = \frac{3\sqrt{ab/t}}{AEFR_p \eta}$$



49.9° 50°
LiF, 2nd Order

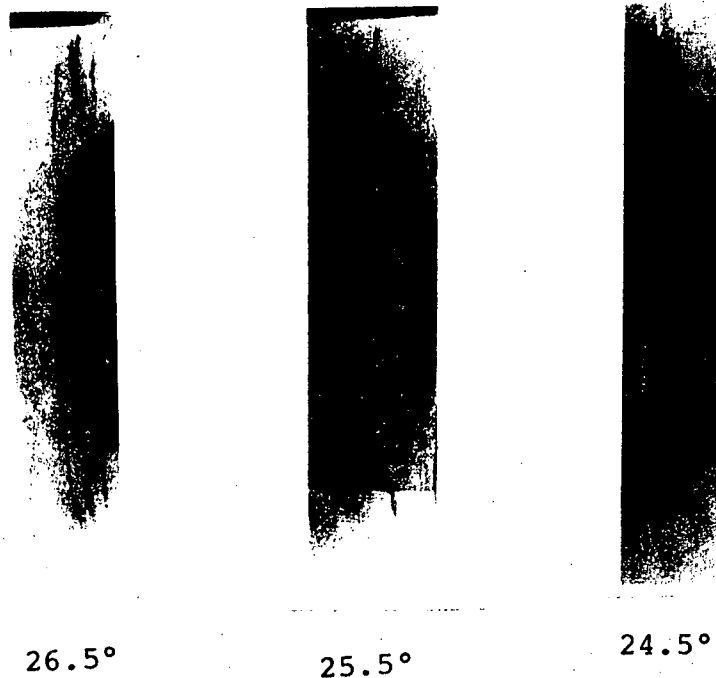


OHM
15th Order
(Johann)



35° 35.5° 36°
ADP, 4th Order

Figure 24. Reflection patterns from Johansson ground crystals.



KAP, 7th Order

Figure 25. Reflection pattern of Johansson ground KAP.

where b is the background counting rate, t is the observation time, A is the geometrical telescope collecting area, E is the telescope efficiency, F is the previously defined efficiency factor, a is the area of the portion of the detector which detects the reflected line radiation, R_p is the peak reflectivity and η is the detector efficiency. With all factors considered, I_{\min} turns out to be approximately 1 to $3 \times 10^{-3} \text{ cm}^{-2} \text{ sec}^{-1}$ throughout the wavelength region. These intensities correspond to 1/500 of the line strengths predicted for Sco X-1⁽²⁾. Higher sensitivities could be attained if spherical or Johansson optics could be used, although this seems unlikely at the moment.

To estimate the minimum detectable absorption edge discontinuity for a given source strength, we again assume a signal limited condition. The minimum detectable fractional change in counting rate at the edge is then given by

$$\frac{\Delta I}{I} = \frac{3\sqrt{2}}{\sqrt{A E R_c F(E) \cot \theta_B t}}$$

and the minimum detectable columnar density of interstellar matter is given by

$$N_H = \frac{\Delta I/I}{(\sigma_1 - \sigma_2)}$$

where R_c is the single crystal coefficient of reflection, $F(E)$ is the incident flux in $\text{keV/cm}^2 \text{ sec keV}$ and σ_1 and σ_2 are the total linear absorption coefficients on either side of the

absorption edge and are determined from specific models of the interstellar medium. (14,15)

If Sco X-1 is taken as the source, and an observing time of 1000 sec is used on either side of the edge, then the following are the minimum detectable $\Delta I/I$

Edge	$(\Delta I/I)_{\min}$	Crystal
Carbon K	.05	Pb Myristate
Oxygen K	.03	KAP
Neon K	.10	KAP
Silicon	.10	PET

3. Plane Crystal Spectrometer for the Iron

The element iron is of special interest in astrophysics. Unfortunately, however, the K lines of the iron ions have wavelengths shorter than the effective wavelength cutoffs of either telescope. Therefore, a separate instrument employing direct Bragg reflection from a plane crystal must be used to search for these potentially important lines and to measure their characteristics.

A plane crystal spectrometer would consist of a narrow honeycomb collimator, a slab of Bragg reflecting crystals and a low background proportional counter. The collimator will be an aluminum honeycomb with a $1/2^\circ$ FWHM field of view and with its axis coaligned with that of the telescopes to within $\pm .05^\circ$.

The slab of crystals will be mounted so that the incident angle can be scanned over a range of several degrees. X-rays transmitted by the collimator will be reflected by the crystals into the proportional counter which will have a 2 mil beryllium window and an internal anti-coincidence jacket. Pulse height and risetime discrimination will be employed to reduce further the background rate.

Two modules will be mounted on one side of the optical bench so as to utilize effectively the two triangular apertures between the heat shield and the telescope objectives. Each of these apertures has a useful area of approximately 350 cm^2 , which we shall take as the effective projected area of the crystals in the subsequent estimate of the performance of the system. One module will employ Li F crystals to achieve high sensitivity for the detection of emission lines at the expense of resolution. The other will employ quartz crystals to achieve high resolution for the purpose of detecting Doppler broadening or shifts at the expense of sensitivity.

We now estimate the sensitivity of the instrument. We assume that in searching for a line the Bragg angle will be set alternately on and just off the value expected for the line, with equal time t being spent on and off. We call $I(E)$ the energy spectrum of the continuum (expressed as $\text{kev}/\text{cm}^2 \text{ sec kev}$), I the intensity of radiation in the line, A the projected area of the crystal, R_p the peak reflectivity, and R_c the integrated reflectivity. Assuming that the rocking

curve is broader than the line width, as is probably the case with Li F, we find for the minimum detectable (3σ) line intensity the expression

$$I_{\min} \sim \frac{3 \sqrt{2I(E)R_c \cot\theta + 2B}}{R_p \sqrt{At}}$$

We now assume that B, the background rate per unit area of the proportional counter (using wall-less anticoincidence, rise time discrimination, and pulse amplitude selection), will be $0.005 \text{ cm}^{-2} \text{ sec}^{-1}$. For the brighter sources we may assume that the intensity integrated from 3 to 10 keV is $1.0 \text{ keV cm}^{-2} \text{ sec}^{-1}$ or less so that $I(E) \sim 0.2 \text{ cm}^{-1} \text{ sec}^{-1} \text{ A}^{-1}$. The quantities R_c and R_p have the approximate values 10^{-4} and .25 respectively for LiF. With these values $I(E) \cot\theta R_c$ is much less than B. The noise will therefore be dominated by the counter background, and the contributions from the continuum and from the line itself can be neglected. We then have

$$I_{\min} \sim \frac{3}{R_p} \sqrt{\frac{2B}{At}}$$

Assuming $t = 10^3 \text{ sec}$ and $A = 300 \text{ cm}^2$, we find

$$I_{\min} \sim 2 \times 10^{-3} \text{ cm}^{-2} \text{ sec}^{-1}$$

This corresponds to an energy flux of $5 \times 10^{-3} \text{ keV cm}^{-2} \text{ sec}^{-1}$ which is about 10^{-3} of the total energy flux from Sco X-1.

In the case of the Crab pulsar, we shall select only the X-ray counts which occur during the optical pulse and thereby

suppresses the background relative to the pulsar signal. Since the pulsar duty cycle is about 25%, the observing time would thereby be reduced by a factor of 4. This would reduce the noise by 2, but leave the signal unaffected. Thus the minimum detectable signal would be reduced by a factor of about 2 to $I_{\min} \sim 10^{-3} \text{ cm}^{-2} \text{ sec}^{-1}$, or about 0.03% of the pulsar average photon intensity.

IV Engineering Descriptions

1. Focal Plane Crystal Spectrometer

The High-Resolution Spectrometer is 75 inches long, 22.50 inches wide, and 37.5 inches high. These dimensions would be subject to change; it is not believed this time, however, that they would need to increase.

Inside this envelope, six different, independent motions would control the relative positions of the crystals and the detectors. Each independent motion would be performed by a stepping motor and monitored by a shaft encoder for verification. Thus the carriage holding crystals and detectors can move back and forth along the X-ray telescope axis. As shown on Figure 26, the carriage would ride on rods, positioned axially by a stepping motor driving Saginaw type ball screw. The crystals, of which there are four shown, would be positioned in or out of the optical axis by a rotational indexing movement; also by a stepping motor and using a shaft encoder to accurately determine its position.

Also riding on the crystal carriage is an elongated arm-slide mechanism which adjusts the detector to crystal spacing as required. One or the other of the two detectors may be positioned in the optical path by a 90° rotation of the assembly.

The crystals, as well as the detectors, may be rotated on an axis normal to the optical path by additional stepping motors.

A wide choice of standard components are available to make up the proposed assembly. - Saginaw type screws, stepping motors and shaft encoders from many vendor sources will easily fulfill the precision positioning requirements.

The instrument utilizes two different detectors for different wavelength observations, a spiraltron array is used for longer wavelengths while an imaging proportional counter is used for harder radiations.

A spiraltron detector is shown in Figure 27, and the array dimensions are shown in Figure 28. The 32 x 2 linear array of spiraltrons are arranged electrically organized in an 8 x 8 array as in Figure 29. Each 8 spiraltrons in a row and a column are connected in parallel to an amplifier/discriminator serving that particular row or column as shown in Figure 30. Each spiraltron is identified with a certain combination consisting of a specific horizontal amplifier and a specific vertical amplifier.

If the signals are above the threshold, the signals are allowed to set an associated binary bint in the vertical column and horizontal row registers. The horizontal address logic decoder/encoder translates the position of the single bit in the vertical column register into a parallel 3-bit binary word identifying the horizontal address and stores this information in a 3-bit buffer. The vertical address information is processed similarly. The four bit levels of the "OR" horizontal and vertical address buffers are compared in an

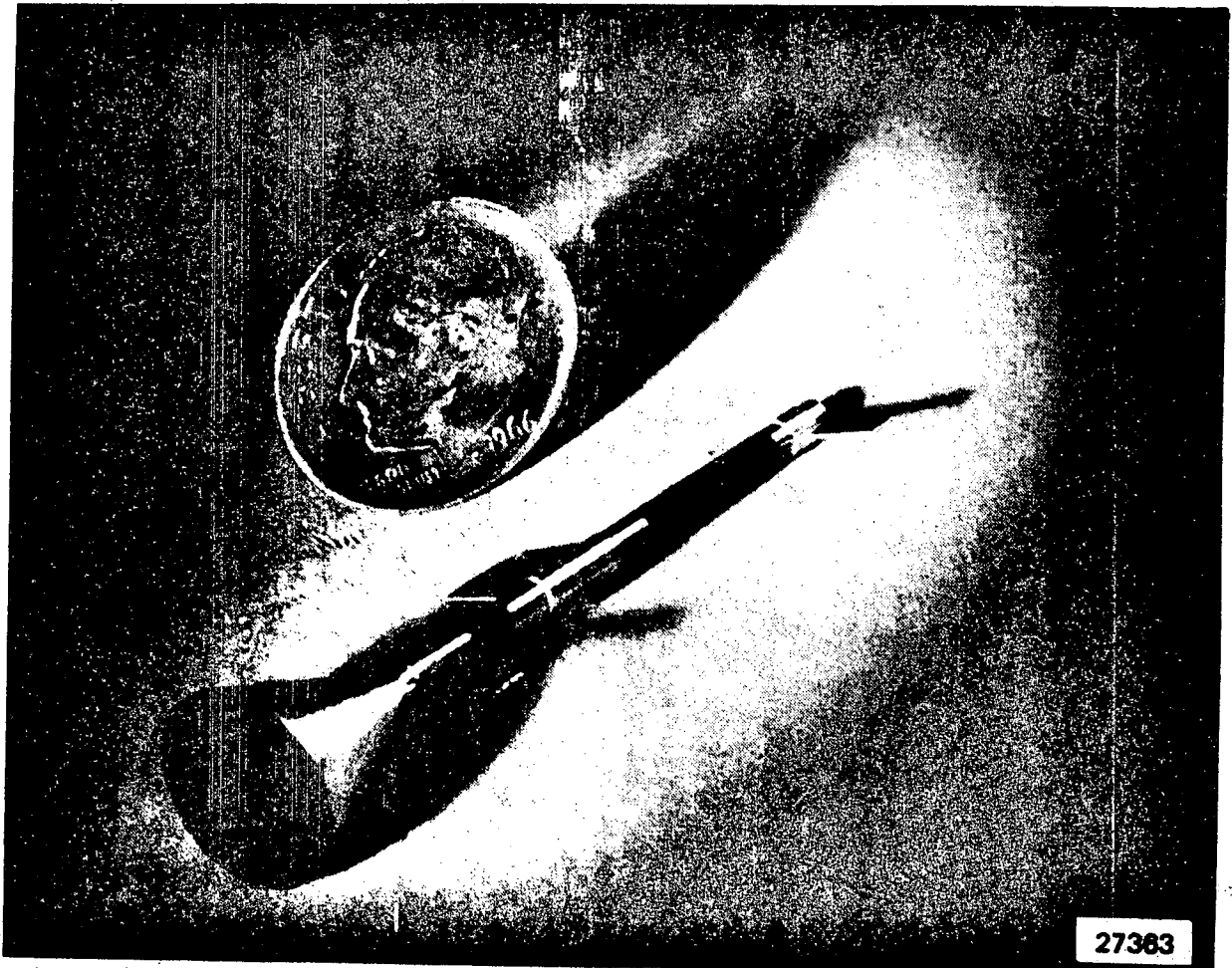


Figure 27. Photograph of a Spiraltron electron multiplier.

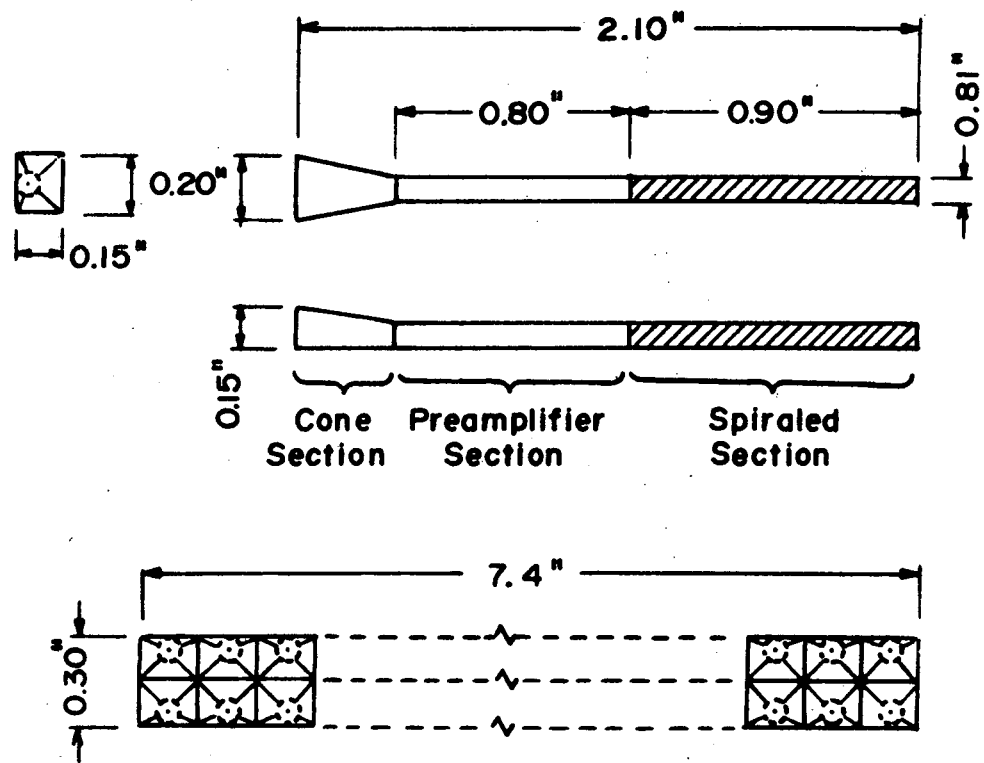


Figure 28. Preamplified Spiraltron Array.

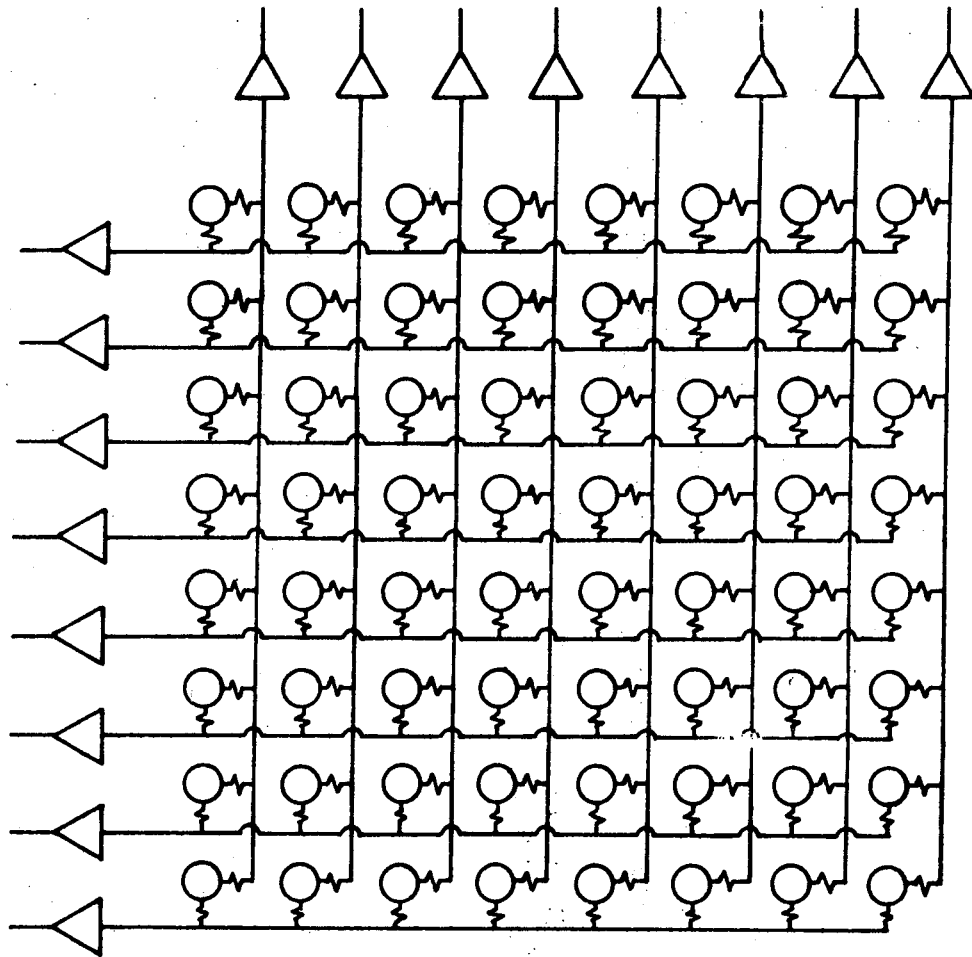


Figure 29. Spiraltron Array Preamplifier Connections.

"OR" gate to determine a "Non-Zero" condition in that address buffer. The "Non-Zero" conditions of each buffer are then routed to an "OR" gate which is allowed to freeze a time encoder. The time encoder is sampled and reset to zero at the rate of 512 samples per second, the time encoder can count up to 31 of the 16,384 pulses in the 2 milli-seconds between samples.

Every 1/512th of a second (2 milli-seconds), the spacecraft system samples and resets the horizontal and vertical address buffers and the time encoder. A total event scaler is used to count the total events which is determined by the number of signals the time encoder receives from the "OR" gate. The total event scaler responds to each signal while the time encoder stays frozen until its contents are read out, at which time it resumes counting until it receives another event signal.

Imaging Proportional Counter Detector

A multi-anode imaging proportional counter is used as a detector for the high-resolution spectrometer.

The coordinates of each event are located by sensing the anode wire involved and the division of charge between the low impedance charge sensitive preamplifiers at either end of the highly resistive anode wire. If Q_L is the charge collected at the left end of the anode and Q_R is the charge collected at the right end of the anode, the position (d) of

the X-ray induced ionization along a wire of length (l) from the left end is

$$d = \frac{Q_R}{Q_L + Q_R}$$

The sum of Q_L and Q_R form the total charge which may be pulse height analyzed to determine the intensity of the ionization. The actual electronic block diagram is shown in Figure 31.

Eight amplifiers are connected to every four consecutive anodes on the left end of the anodes, while on the right end eight additional amplifiers suffice whereas 64 amplifiers are required if two amplifiers were used for each anode.

The collective anode is identified by the particular combination of a "left" amplifier and a "right" amplifier collecting the charge for a given X-ray event. For example, if a charge is sensed by Q_{LA} and Q_{RC} of Figure A, the collecting anode is identified as anode number 3 and decoding is more easily visualized as two matrices as shown in Figure 32.

Figure 33 is the complete block diagram for the curved crystal imaging proportional counter and shows that the outputs of the 16 threshold discriminators. The outputs of the discriminators are inputs to an anode identification coder which can be interrogated by either the spacecraft telemetry system or by an on-board data processor. Additionally, the outputs of the four "left" amplifiers of a matrix are summed together as are the four "right" amplifier outputs for that matrix. The outputs of the summing amplifiers for each matrix are

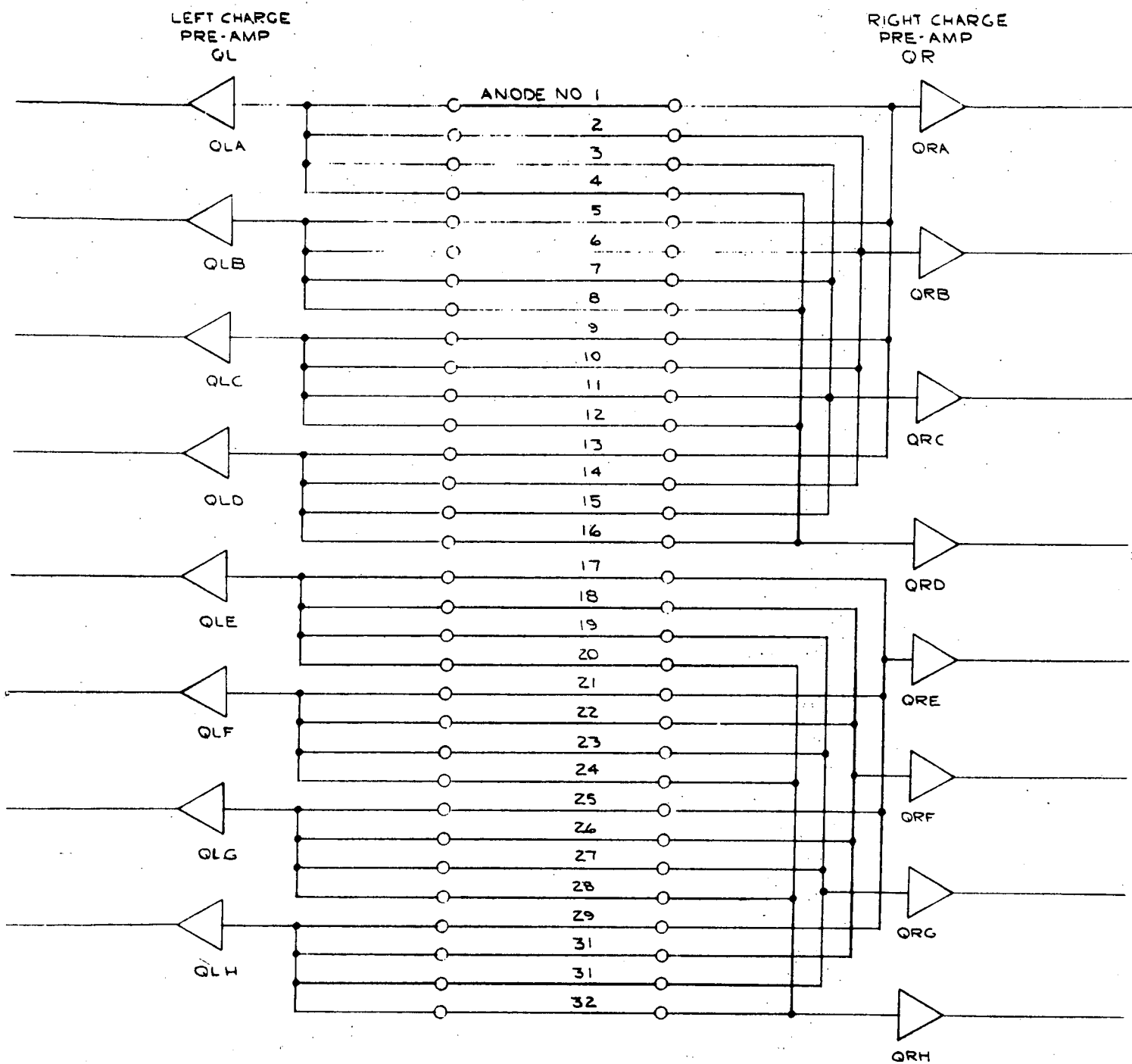


Figure 31. Position sensitive proportional counter anode wiring diagram.

<u>MATRIX A</u>				
	QRA	QRB	QRC	QRD
QLA	1	2	3	4
QLB	5	6	7	8
QLC	9	10	11	12
QLD	13	14	15	16

<u>MATRIX B</u>				
	QRE	QRF	QRG	QRH
QLE	17	18	19	20
QLF	21	22	23	24
QLG	25	26	27	28
QLH	29	30	31	32

Figure 32. Position sensitive proportional counter anode decoding logic.

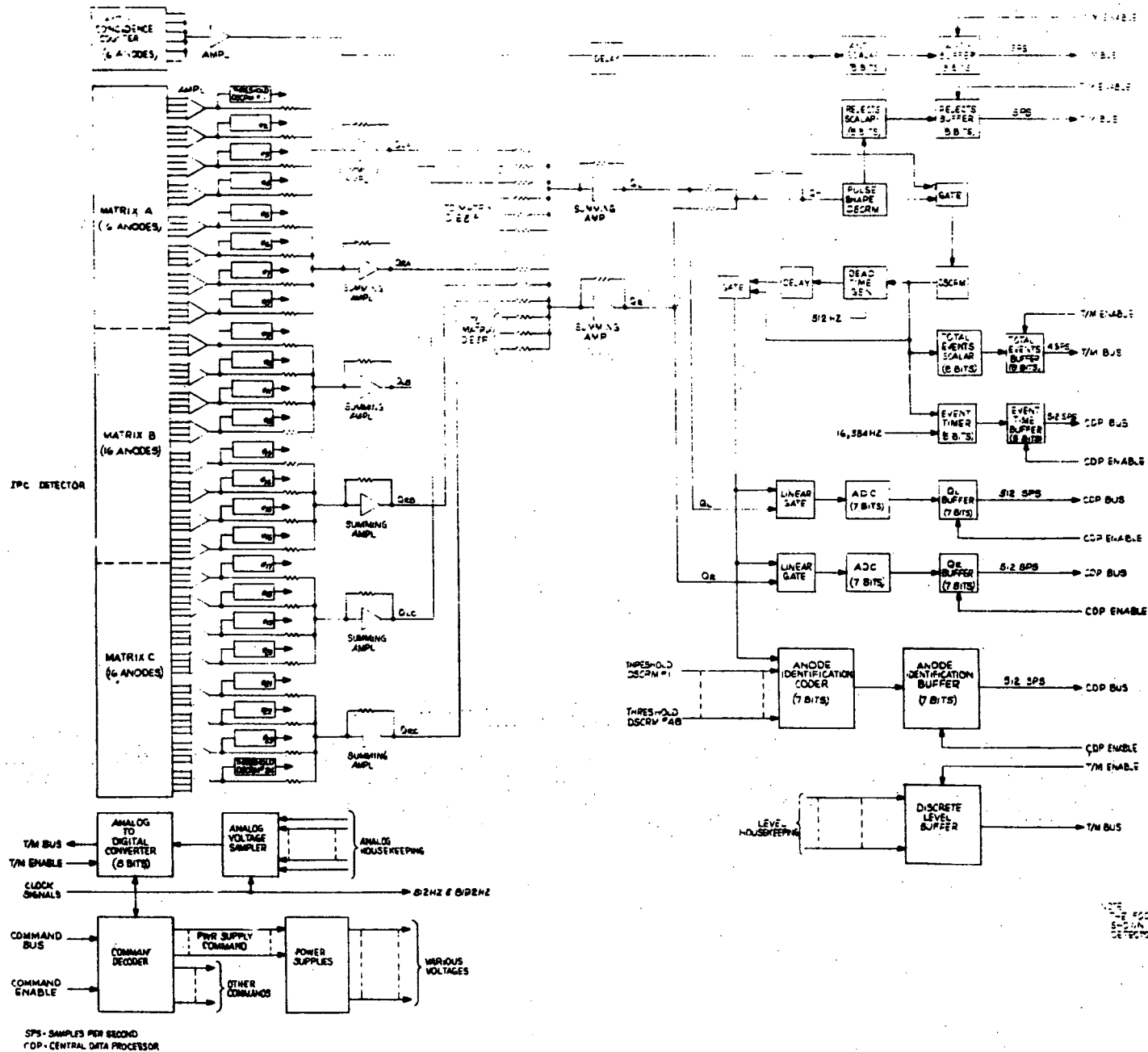


Figure 33. Focal Plane spectrometer position sensitive proportional counter electronics block diagram.

similarly summed on a corresponding "left" and "right" amplifier basis. Therefore, for a given event there exists a "left" and "right" signal that originates in the charge collected off each end of the collecting anode. The "left" and "right" signals are summed to form the total charge signal. The total charge signal is then subjected to pulse shape discrimination and anti-coincidence discrimination. An acceptable event causes the generation of an event marker which in turn controls the other process involving the "left" and "right" signals. The event marker enables the "left" and "right" signals to pass through a gate to 128 level analog-to-digital converters. The outputs of the two converters are stored in buffers for subsequent readout by the spacecraft data processing system. The time of the event is also recorded in this particular case.

TABLE 5 - FOCAL PLANE SPECTROMETER

<u>Weight</u>	<u>Pounds</u>
Spectrometer Assembly	278
IPC Electronics	68.5
Crystal Rotation Servo System	18.5
Spiraltron Detector Array	32
TOTAL	397.0

Power Requirement (Watts)

	<u>Element</u>	<u>Highest Power Config.</u>	<u>Peak</u>
Imaging Prop Counter Detector	15	15	15
Spiraltron Array	13.5	--	--
Crystal Translation Posi- tron Servo	6	--	--
Crystal Angular Positron Servo	6	6	--
Detection Translational Positron Servo	6	--	--
Detector Select Servo	6	--	--
TOTAL		21 Average	21 Peak

Data Processing Requirements

	<u>Channels</u>	<u>bits/sample</u>	<u>Samples/sec</u>	<u>Total</u>
I.P.C.				
QL	1	7	512	3584
QR	1	7	512	3584
A mode ID	1	6	512	3072
				10,240
Spiraltron Array (to TM)				
	1	6	512	3072

TM Requirements (IPC only)

	<u>Channels</u>	<u>Bits/sample</u>	<u>Samples/sec</u>	<u>Total</u>
Positron (Anode)	1	6	512	3072
Positron (Along wire)	1	6	512	3072
Charge	1	3	512	1536
Total Event	1	8	4	32
Crystal Angle	1	15	1	15
Crystal Translation	1	10	1	10
Detector Translation	1	10	1	10
Housekeeping (Analog)	1	8	1	8
Housekeeping (Digital)	1	8	1	8
			TOTAL	7763

Command summary (bits)

24

Pointing Requirements

Accuracy \pm 1 arc minute

Stability \pm 1 arc sec/sec or equivalent

2. Flat Crystal Spectrometers

There will be two similar experiments which will be mounted in a common housing and use identical collimation systems. The basic items of each system are:

- a. Collimator
- b. Rotating Crystal
- c. Stepping Motor
- d. Shaft Encoder
- e. Proportional Counter
- f. Electronics

The collimator will be 15 inches long and is composed of 1/8" hex cells. The effective angular collimation is 1° full width. The cell network itself will be supported in a stiff structural framework and mounted to the optical bench to preserve its linearity and alignment. The frontal area of each collimator will be 500 cm² in the form of a truncated triangle about 18" high with a 9.5" base.

The crystal arrays will be mounted on a rigid plate having integral bearing posts which have been machined such that their center of rotation is in line with the first surface of the crystal and is at its center of inertial balance. This may be accomplished by balance weights, since the crystal assembly will be asymmetric along its long axis to match the geometry of the collimator. The crystal assembly will in all probability be composed of several small pieces of crystal which may or may not be of uniform thickness. In this case,

coplanarity of the crystal face may be accomplished by casting a suitable thickness of low expansion RTV (.005"-.010") between the crystal elements and the back plate while the crystal is being held against an optically flat surface by a vacuum. In this way the different thicknesses will be accommodated.

The two types of crystal elements which will be used are: Quartz (S_iO_2) which will be oriented at 34° to the horizontal plane of the optical bench, and lithium fluoride (LiF) which will be oriented at 25.5° to the same plane.

The crystal assembly will be mounted to a mechanical drive system which will rotate it through a 10° arc by means of a magnetic detent gear head stepping motor. A 14-bit shaft encoder with an integral speed increaser will monitor its angular displacement with a resolution of 10 arc sec.

The proportional counter detectors for each crystal will again be very similar in construction but will vary only because of the decreased width necessary for the counter associated with the S_iO_2 crystal. In this case, the counter will have a 2" wide active area. For the LiF crystal, the counter will have a 5" wide active area. The main counting wires will run the long dimension and be confined by a system of anti-coincidence wires. The counter will have a sealed window of 2 mil beryllium. The gas will be a mixture of 90% Argon and 10% CO_2 at 1 atmosphere of pressure.

The block diagram of the proportional counter and its electronics is illustrated in Figure 34.

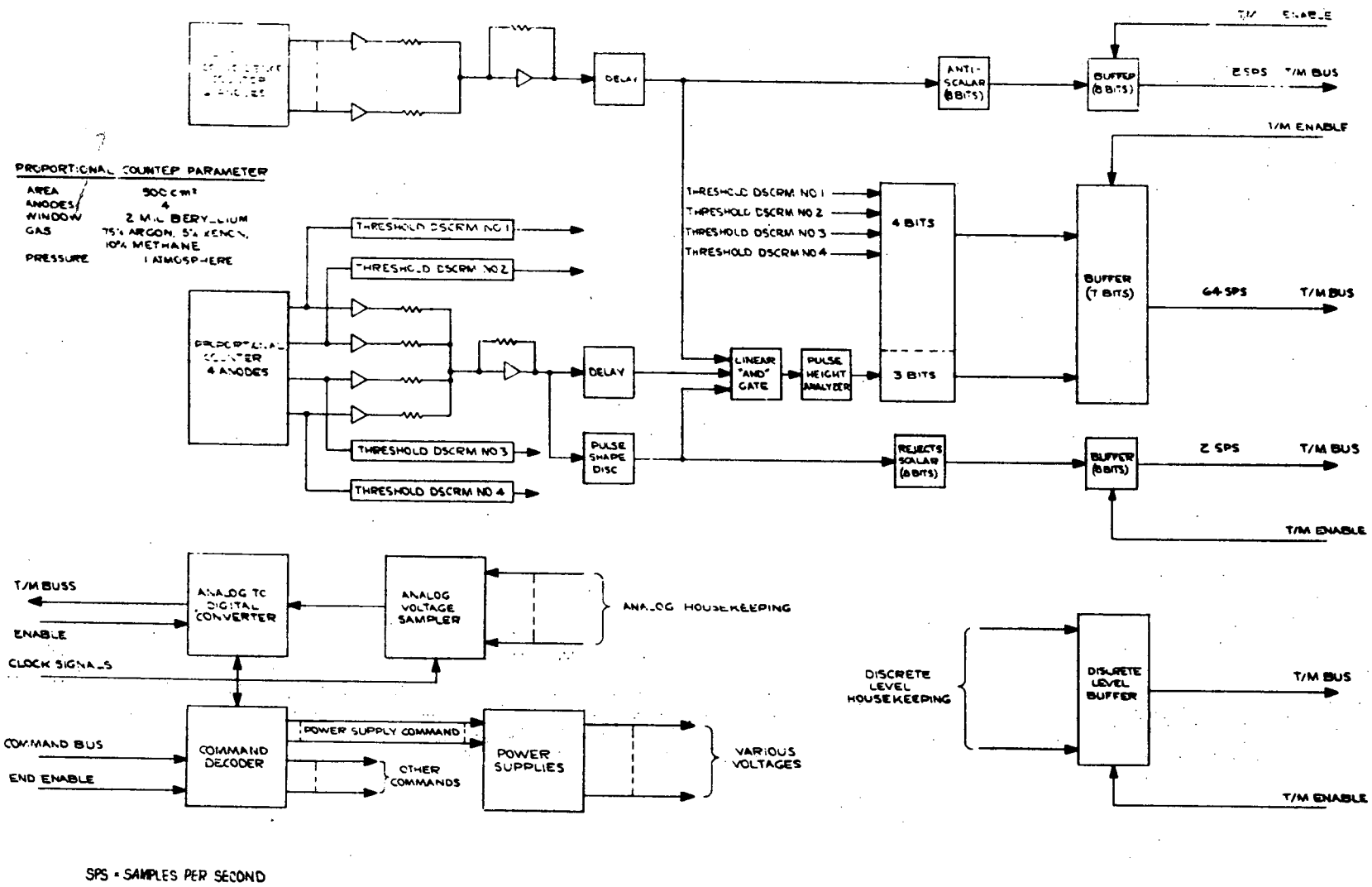


Figure 34. Iron Line Spectrometer Electronics Block Diagram.

Each of the four anodes is served by a pre-amplifier and a threshold discriminator. The four pre-amplifiers input to a common summing amplifier which inputs to a delay circuit and a pulse shape discriminator. The pulse shape discriminator distinguishes between pulses caused by X-rays, gamma-rays, and charged particles. The pulse shape discriminator output is used to permit passage of the delayed X-ray pulse through the linear gate. An anti-coincidence counter is used to inhibit the passage of the data pulse through the linear gate. Both the anti-coincidence pulses and the pulse shape discriminator reject pulses are counted and stored for telemetry sampling.

The acceptable X-ray events are pulse height analyzed by an 8-level system. The event discription, which consists of 3 amplitude and 4 anode identification bits, is then stored in a buffer until it is sampled by the data processing system. The extra anode identification could be eliminated, but the standard telemetry interface system planned for this experiment has extra bits available in this case.

TABLE 6 - ENGINEERING SUMMARY FLAT CRYSTAL SPECTROMETER

Weight

Detector Assembly	55
Electronics	<u>26</u>
TOTAL	81 (per unit)

Power (per unit) Watts

	<u>Element</u>	<u>Average</u>	<u>Peak</u>
Electronics	5.0	5.0	5.0
L. V. Power Supply Losses	1.5	1.5	1.5
H. N. Power Supplies	2.0	2.0	2.0
Scanning Servo	<u>6</u>	--	<u>6</u>
		8.5	14.5

<u>TM Requirements</u>	<u>No. of Channels</u>	<u>Bits/ Sample</u>	<u>Sample/ Sec</u>	<u>Total</u>
Anticoinc.	1	8	1	8
PSD Rejects	1	8	1	8
PHA	1	8	1	64
Shaft Position	1	12	1	12
Housekeeping	2	8	1	<u>16</u>
			TOTAL	108
				Unit

Command bits required 21

Pointing Requirements

Accuracy ± 1 arc minute
 Stability ± 1/4 arc minute/sec

Section II

A New High-Resolution, High Sensitivity
Flat Crystal Spectrometer

Although curved crystal spectroscopy can be very useful in the lab, a number of difficulties appear when applying this concept to space applications. These problems, such as the low efficiency factor, the limited choice of bendable crystals in the wavelength range of interest, the need for a high spatial resolution multi-channel two-dimensional detector, the high pointing and aspect accuracy needed, and the effects of the telescope image distribution and double reflection efficiency, as well as the general mechanical and electrical complexity of the system, led us to search for a simpler, more efficient device designed around the explicit needs of X-ray spectroscopy and compatible with present spacecraft systems and capabilities. The new device consists of a simple one-dimensional Baez concentrator, a flat crystal, and a proportional counter with several anodes. A diagram of the geometry of this device is shown in Figures 35 and 36.

The crystal is placed in front of the concentrator focus so that the Bragg reflected X-rays focus to a line at the spectrometer focus, although for the highest sensitivity it can be positioned at the focus. Because the plane of dispersion is normal to the plane of concentration, a ray with a vertical divergence ϕ_n differs from the Bragg angle setting θ_B by an amount Δ , where

$$\Delta \approx \phi_n^2 / 2 \tan \theta_B$$

Since ϕ_n is small, almost the entire crystal contributes to reflecting a single resolution element of radiation.

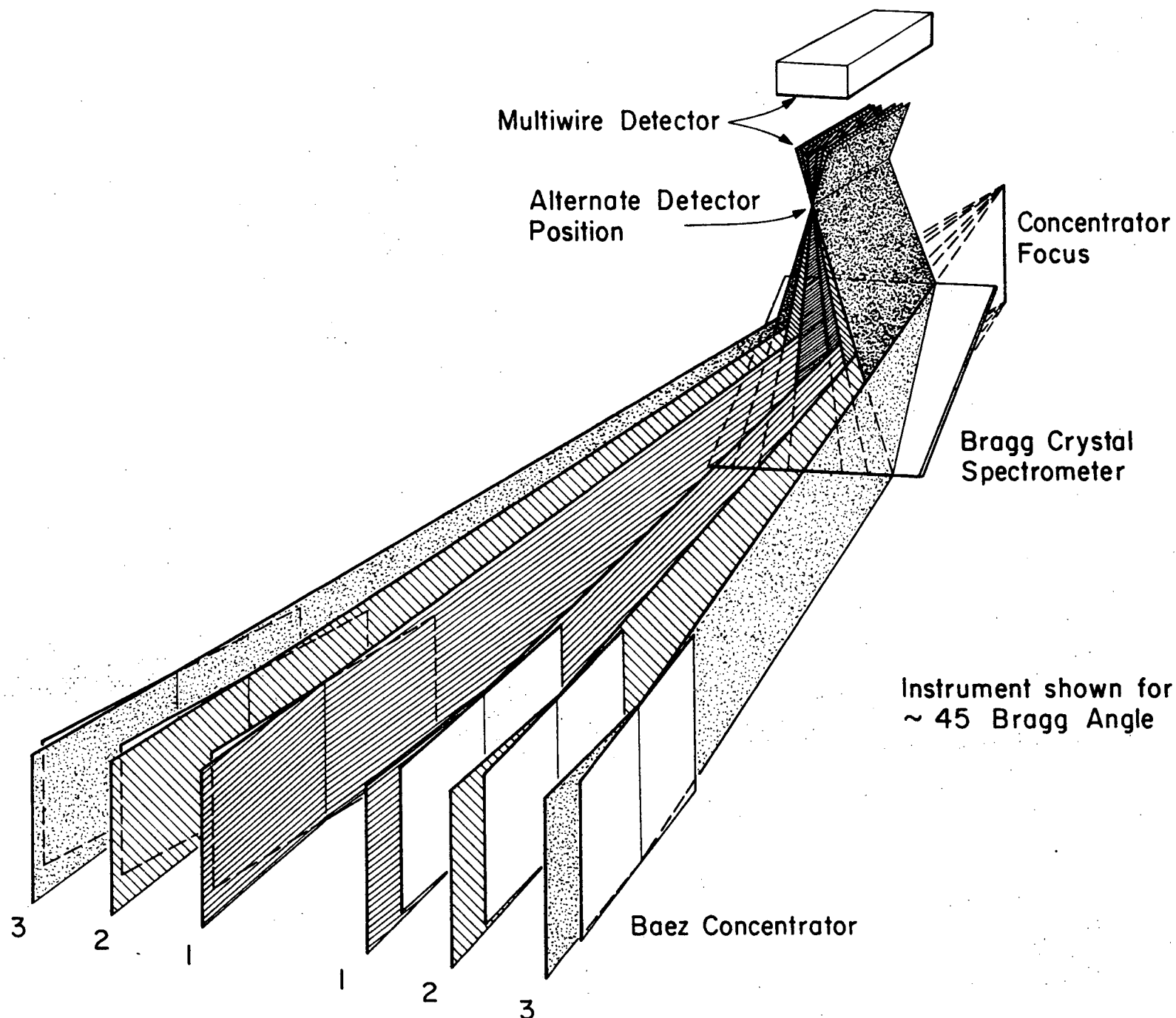


Figure 35. A diagram of the geometry of the new spectrometer.

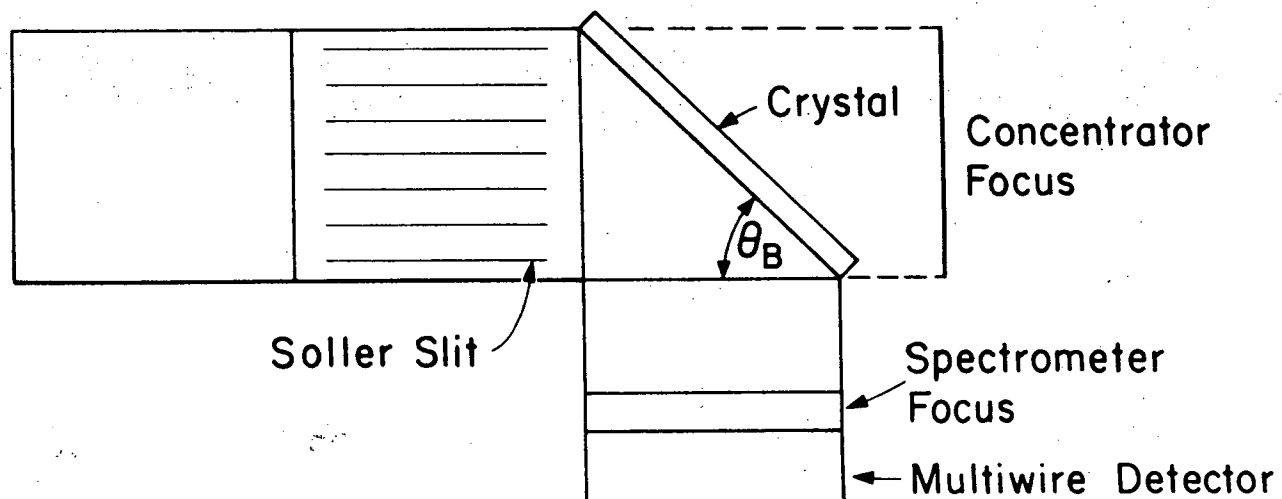
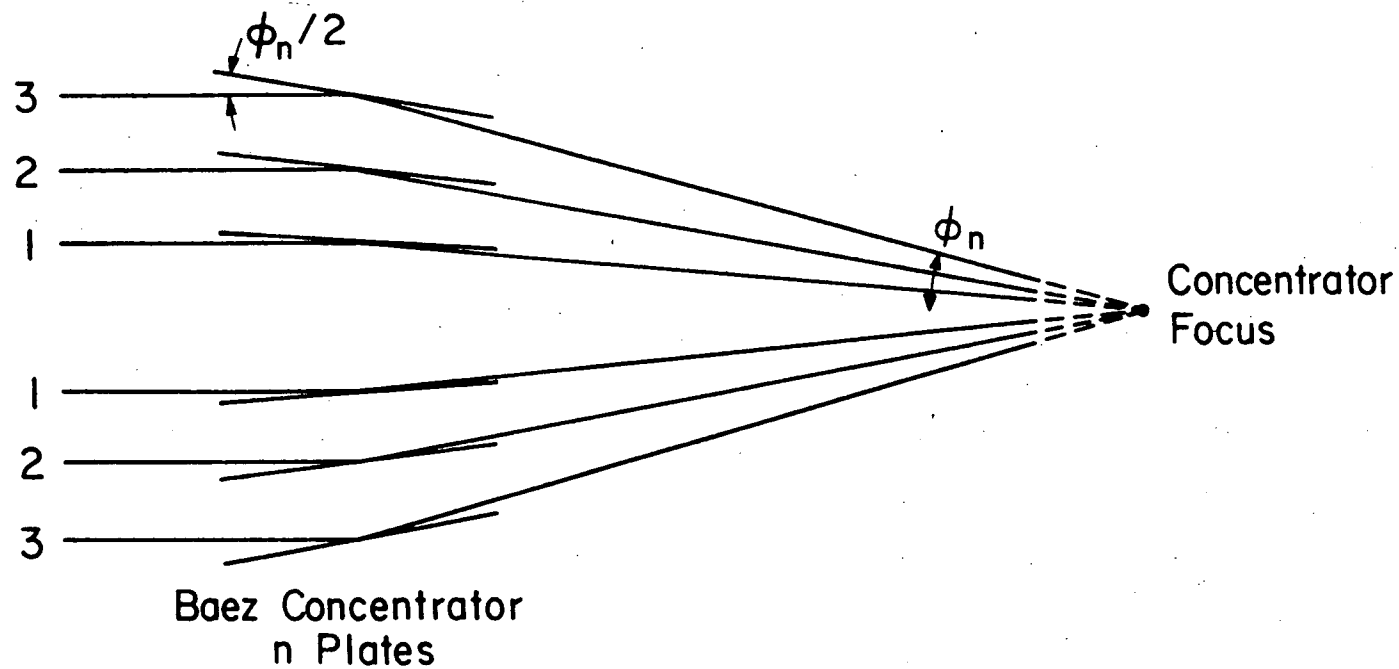


Figure 36. A diagram of the geometry of the new spectrometer.

In order to compute the sensitivity of this instrument, we have chosen a modest 30 x 30 cm concentrator with a 400 cm focal length and a total effective geometrical area of 430 cm². It was assumed that the plates were Kanigen coated, and the grazing incidence efficiency of nickel was used. We define the spectrometer efficiency factor F as the ratio of the number of Bragg-reflected to incident X-rays assuming a peak crystal reflectivity of 100%. F is calculated from the expression for Δ and the ratio of the line and crystal resolutions r_L and r_C respectively. This efficiency and the total effective area of this device with an EDDT crystal are given in Figure 37. Two calculations are shown, one with and the other without the grazing incidence efficiency of the nickel coating. Even for the case of a highly resolving crystal and a narrow line ($r_{CL} = r_C = 3000$) the effective area of the spectrometer is 130 cm², as opposed to 100 cm² for a curved crystal spectrometer with a 1 m diameter high resolution telescope (see Figure 11).

In order to obtain the lowest minimum detectable signal the detector will be placed near the focus. Because the crystal reflects only a small range of Bragg angles, the detector need only have a few channels. The symmetry of the concentration permits corresponding proportional counter wires on either side of the central axis to be connected in parallel. Thus a six-wire proportional counter with three independent data channels will provide an equivalent detector resolution of about 7000, which is sufficient even when very highly

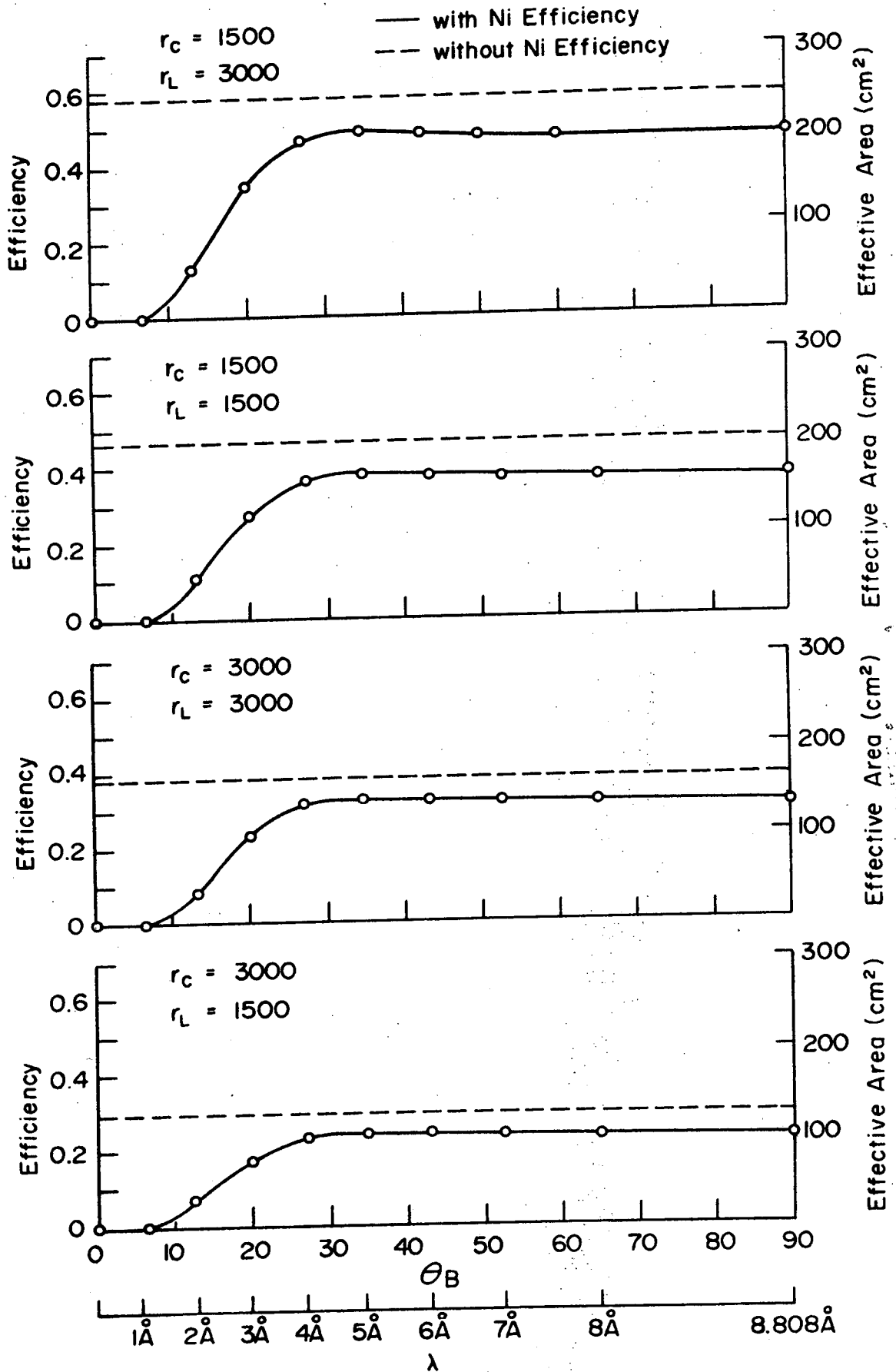


Figure 37.

FLAT CRYSTAL SPECTROMETER EFFICIENCY

resolving crystals are used. For the highest sensitivity, and for lower resolving crystals, the proportional counter can be moved to the focus, where only a single anode is needed, with a corresponding detector resolution of about 3500. If we assume a wire separation of 1 mm, these detector configurations correspond to effective detector areas of 3 cm² and 18 cm², and minimum sensitivities equal to or better than those of the curved crystal spectrometer. Furthermore, this device still retains some sensitivity in the Fe K α region, and because of the one-dimensional concentration, it has a sensitivity at Fe K α comparable with the flat crystal iron line detector discussed in Section I, part 3.

References

1. Schnopper, H. W. and Kalata, K., App. Phys. Lett. 15, 134 (1969).
2. Tucker, W., Ap. J., 148, 745 (1967).
3. Underwood, J. H., Science, 159, 383.
4. Pounds, K. A., private communication.
5. Argo, H. V., Bergey, J. A., and Evans, W. D., Ap. J., 160, 283 (1970).
6. Liefeld, R. J., private communication.
7. Henke, B. L., X-ray Fluorescence Analysis for Sodium, Fluorine, Oxygen, Nitrogen, Carbon, and Boron, Advances in X-Ray Analysis Vol. 7, 460 (1964).
8. LOXT Technical Proposal for the HEAO, May 1970.
9. Lukirskii, A. P., Savinor, E. P., Brytov, I. A. and Shepeler, Yu. F., Bull Acad. Sci. USSR, 28, 774 (1964).
10. Smith, D. G. and Pounds, K. A., IEEE Transactions on Nuclear Science, NS-15, 3 (1968).
11. Somer, T.A. and Graves, P. W., IEEE Transactions on Nuclear Science, NS-16, 1 (1969).
12. Wolber, W. B., private communication.
13. Ehlert, R. C. and Mattson, R. A., Advances in X-ray Analysis, Vol. 10, 390 (1967).
14. Bell, K. L. and Kingston, R. A., Mon. Not. R. Astr. Soc. 136, 241 (1967).
15. Brown, R. L. and Gould, R. J., Bull. Am. Astron. Soc. 2, 184 (1970).

Published Results of This Program

1. New High-Resolution, High-Dispersion X-Ray Spectrometer, H. W. Schnopper and K. Kalata, App. Phys. Lett. 15, 134 (1969).
2. Polarimeter for Cosmic X-Rays, H. W. Schnopper and K. Kalata, Astron. J. 74, 854 (1969).
3. A High-Dispersion, High-Resolution X-Ray Spectrometer Having Means for Detecting a Two-Dimensional Spectral Pattern Patent Number 3,628,040, issued December 14, 1971.

4.0 Further Theoretical and Experimental Studies of Curved Crystal Spectrometers

This section describes work carried out during the last phase of the study under the direction of Professor Clark. The scientific personnel engaged in these studies were:

Dr. G. Clark	Professor
Dr. C. Canizares	Staff Scientist
Mr. D. Bardas	Research Assistant

List of Figures

- 4.1.1 Coordinates for ray tracing studies of spectrometer optics
- 4.1.2 Distribution of rays on the crystal face
- 4.1.3 Distribution of rays at the crystal focus
- 4.1.4 Distribution of rays on a plane located 5.4 cm from the focus toward the crystal
- 4.1.5 Distribution of rays on a plane located 13.6 cm from the focus toward the crystal
- 4.1.6 Variation of the θ_B with the vertical position on the crystal face
- 4.1.7 Variation of θ_B with the horizontal position at the spectrometer focus
- 4.1.8 Variation of θ_B with the vertical position on a plane 8.16 cm from the crystal toward the focus
- 4.1.9 Variation of θ_B with the horizontal position and plane 8.16 cm from the crystal toward the focus
- 4.1.10 Distribution of rays at the crystal focus for images located + 0.18, 0.0 and 0.18 cm from the nominal position in the telescope focal plane
- 4.1.11 Variation of θ_B with vertical position at the spectrometer focus for images located 0.18, 0.0 and -0.18 cm from the nominal position in the telescope focal plane
- 4.1.12 Optical simulation showing the images for off-axis point sources
- 4.2.1 Rowland circle radius/crystal resolution and detector resolution versus θ_B
- 4.3.1 Overall view of breadboard curved crystal spectrometer mounted in the 24" vacuum chamber
- 4.3.2-4 Various views of breadboard curved crystal spectrometer
- 4.4.1 Lead stearate multilayer preparation facility
- 4.5.1 Reflected intensity versus grazing angle of incidence for carbon K X-rays reflected from a 100-layer lead stearate crystal deposited on a flat glass substrate

- 4.5.2 Reflection of 44 \AA from an uncoated flat glass substrate
- 4.6.1 Reflected intensity versus grazing angle of incidence for the central ray of Copper L X-rays on a spherically bent mica crystal
- 4.7.1 Channeltron pulse height spectrum

4.1 Spectrometer Geometrical Optics

A Monte Carlo ray tracing program has been developed to study the spectrometer geometry. In order to obtain realistic results and to allow further sophistication for comprehensive resolution studies, the true LOXT high resolution telescope parameters were incorporated into the program. Thus the image in the focal plane was taken to have a nominal blur circle radius of $.001^\circ$ and to diverge in five concentric cones with half angles of 4.25 , 3.97 , 3.70 , 3.50 and 3.27° . Rays were randomly tossed within this envelope, reflected from the "crystal" surface and intercepted at several potential detector locations. The coordinate system is shown in Figure 4.1.1.

The results of a typical run for a spherical crystal are displayed in Figures 4.1.2-12. The parameters for this run are listed in Table 4.1.1. The Figures are scatter plots which indicate the location of each of the 10,000 tossed rays. All linear dimensions are in cm.

Figure 4.1.2 shows the distribution of rays around a ring on the crystal face. The distribution of rays at the spectrometer focus is shown in Figure 4.1.3. The focussing properties are clearly illustrated by the narrowness of the envelope in the y direction, that is, in the Rowland circle plane. It is also apparent that the spherical crystal reduces the divergence perpendicular to the plane, allowing the use

of a smaller detector area (0.06 cm^2 in the example shown). Figures 4.1.4 and 4.1.5 display the images at detectors separated from the crystal by 0.8 and 0.5 times the nominal crystal-focus distance. The annular cross section of the ray bundle is again evident as is the considerably larger detector area required.

The second-order variation of Bragg angle across the crystal face is shown in Figure 4.1.6. Here we have plotted the location of the ray at the crystal projected onto the axis perpendicular to the spectrometer plane (XXTAL) vs. the Bragg angle which would be met by the ray. For this example the full width of the Bragg angle distribution is 0.1° , which, if no attempt were made to further subdivide the angular interval, would yield a resolution of $\rho = \frac{\Delta\lambda}{\lambda} \approx 1500$. Figures 4.1.7 and 4.1.8 show that while the entire interval is focussed in the spectrometer plane, it is possible to subdivide the data by using a one-dimensional position-sensitive detector to determine the perpendicular (x) coordinate. This is due to the fact that the annular distribution of rays at the crystal face serves to couple x and y and, since $y \propto \alpha$, the angular divergence in the spectrometer plane, and α is related to the deviation from nominal Bragg angle (see Section 2, Part III and Equation 4.2.1), then x is related to the Bragg angle θ_B . In this example, 1 mm detector resolution would yield $\Delta\theta \approx .05^\circ$ or a maximum $\rho \approx 2000$.

Figures 4.1.9 and 4.1.10 show similar plots for the case with the detector moved to within 8.2 cm of the crystal. The narrower Y vs. θ crescent clearly indicates the further increase in resolution obtainable by making position determinations forward of the Rowland circle focus.

The pointing requirement for LOXT is ± 1 arc minute with ultimate 1 arc second resolution obtained by subsequent analysis of the aspect system. Thus the image of a point source at the telescope focal plane will wander by approximately $\pm .18$ cm. Motion of the image perpendicular to the Rowland circle plane does not affect the focussing properties of the spherical optics, but deviations in the spectrometer plane contribute directly to deviations in Bragg angle. As mentioned in Section 2, page 17, this could complicate the spectrometer operation. We now feel, however, that the image jitter can be used to advantage.

Rather than attempt to follow the image motion in real time, this jitter can be used in an effective spectrum-scanning technique. Figure 4.1.11 shows the ray envelopes at the spectrometer focus for source deviations of $-.18$, $0.$, and $+.18$ cm from the spectrometer plane. The variation of Bragg angle with source position is evident in Figure 4.1.12, which shows the relation between θ_B and the vertical position at the focus. In this case the range of Bragg angles is 0.8 degrees which gives a spectrum scan of width $\Delta\lambda = \lambda/150$.

For point sources, the ex post facto aspect determination

would allow one to distinguish between Bragg angle regions while the X coordinate determination of a one-dimensional detector would further subdivide the θ_B interval as discussed above.

The mapping of diffuse sources could be accomplished by using the two-dimensional detection capabilities of the multiwire counter or the Chevron channel electron multiplier array. The detector would simultaneously record X-rays of different wavelengths from different portions of the source, with each count received labelled by θ_B and one spatial coordinate in the source. The use of an aperture in the shape of a vertical slit, a horizontal slit or a small diameter circle would increase respectively the angular resolution, the position sensitivity, or both.

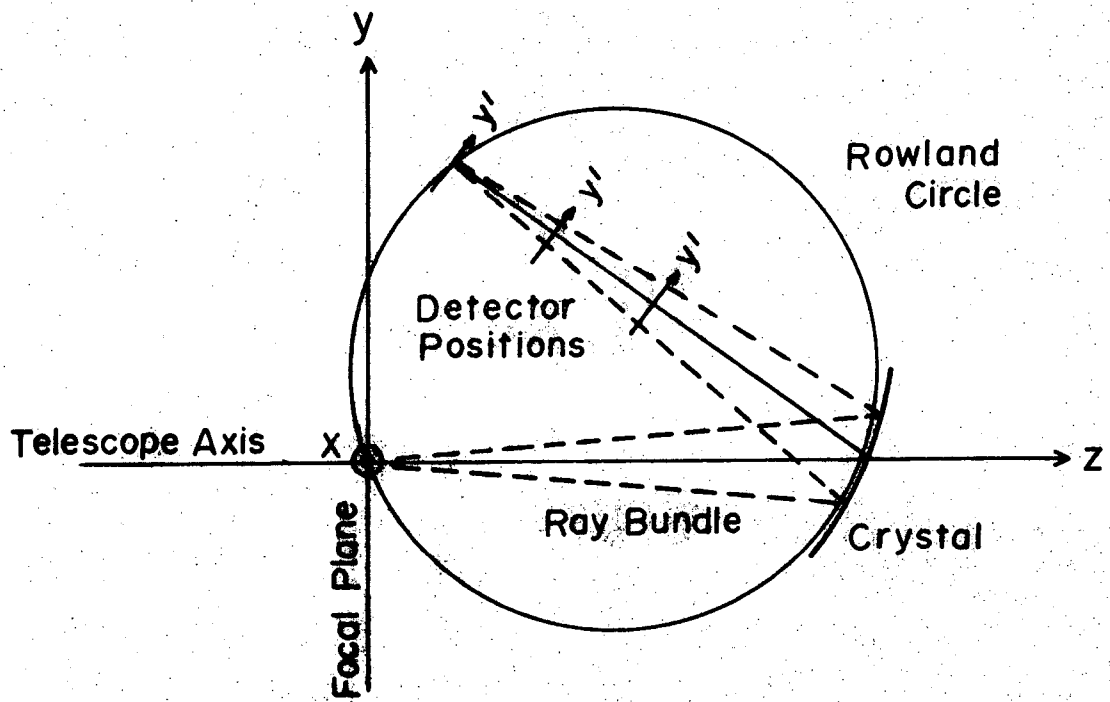
The effect of large-scale motions of the source in the telescope focal plane have been studied optically. Figure 4.1.13 shows the images at the Rowland circle focus for a range of source deviations from the central axis. This photograph was made using a point light source and a spherical mirror.

Table 4.1.1

Parameter for Ray Tracing Program

Cone half angles	4.25, 3.97, 3.70, 3.50, 3.27 degrees
Crystal Radius	30 m
Blurr circle	0.001°
Bragg Angle	65°
Detector to crystal distances	27.2, 21.75, 13.59, 8.16 cm
Jitter	<u>±</u> 0.18cm (1.0 arc min)

5 A

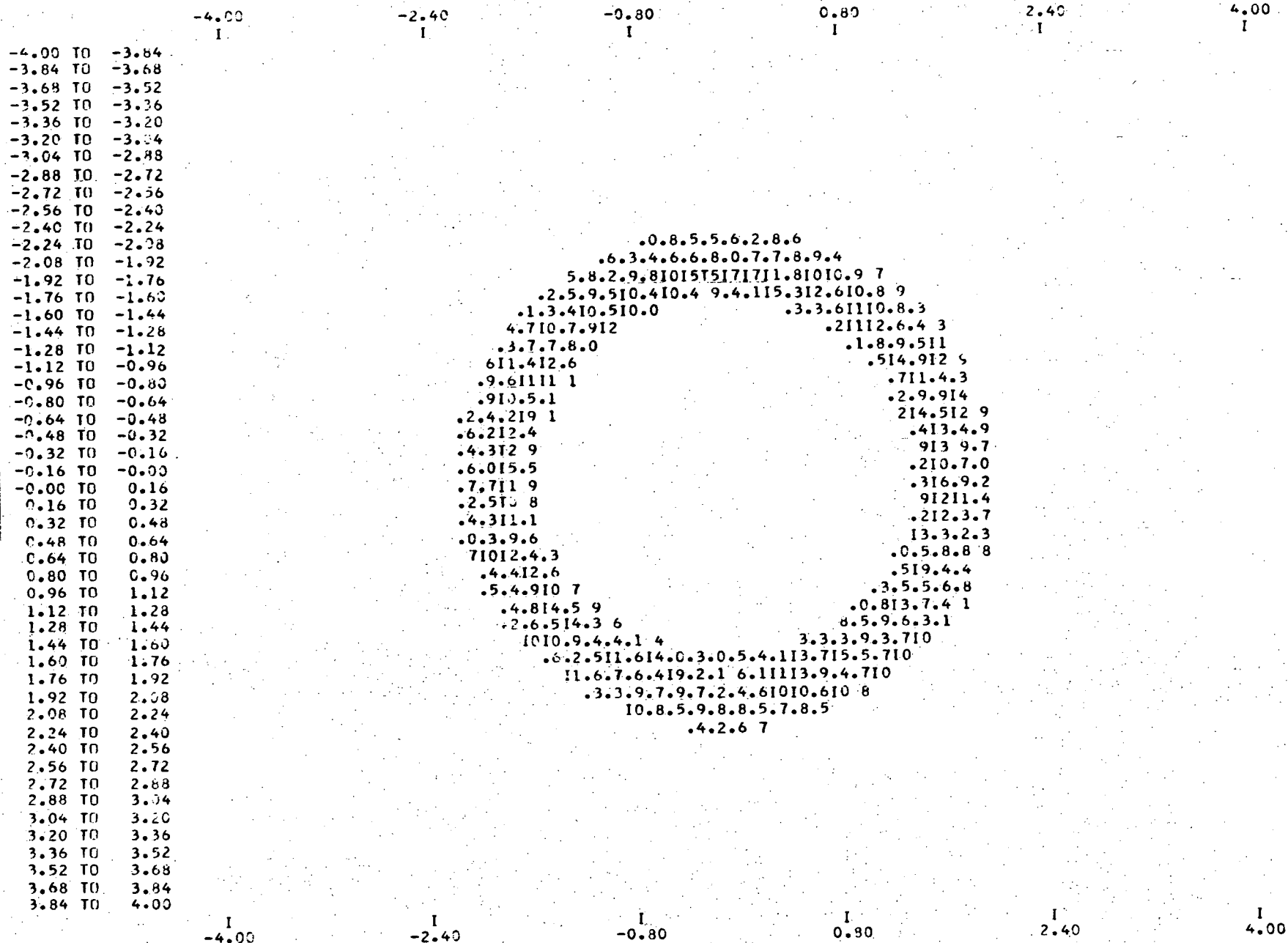


5B

Fig. 4.1.1

XTLRAD=30 CM, ORIGIN= 0., 0., THETA=65. BLUR=.001

YXTL(VERTICAL) VS. XXTL(HORIZONTAL)



XMEAN = 0.01 YMEAN = 0.03 SCALE FACTOR = 2

XTLRAD=30 CM, ORIGIN= 0., 0., THETA=65. BLUR=.001

D2_Y(VERTICAL) VS. D2_X(HORIZONTAL)

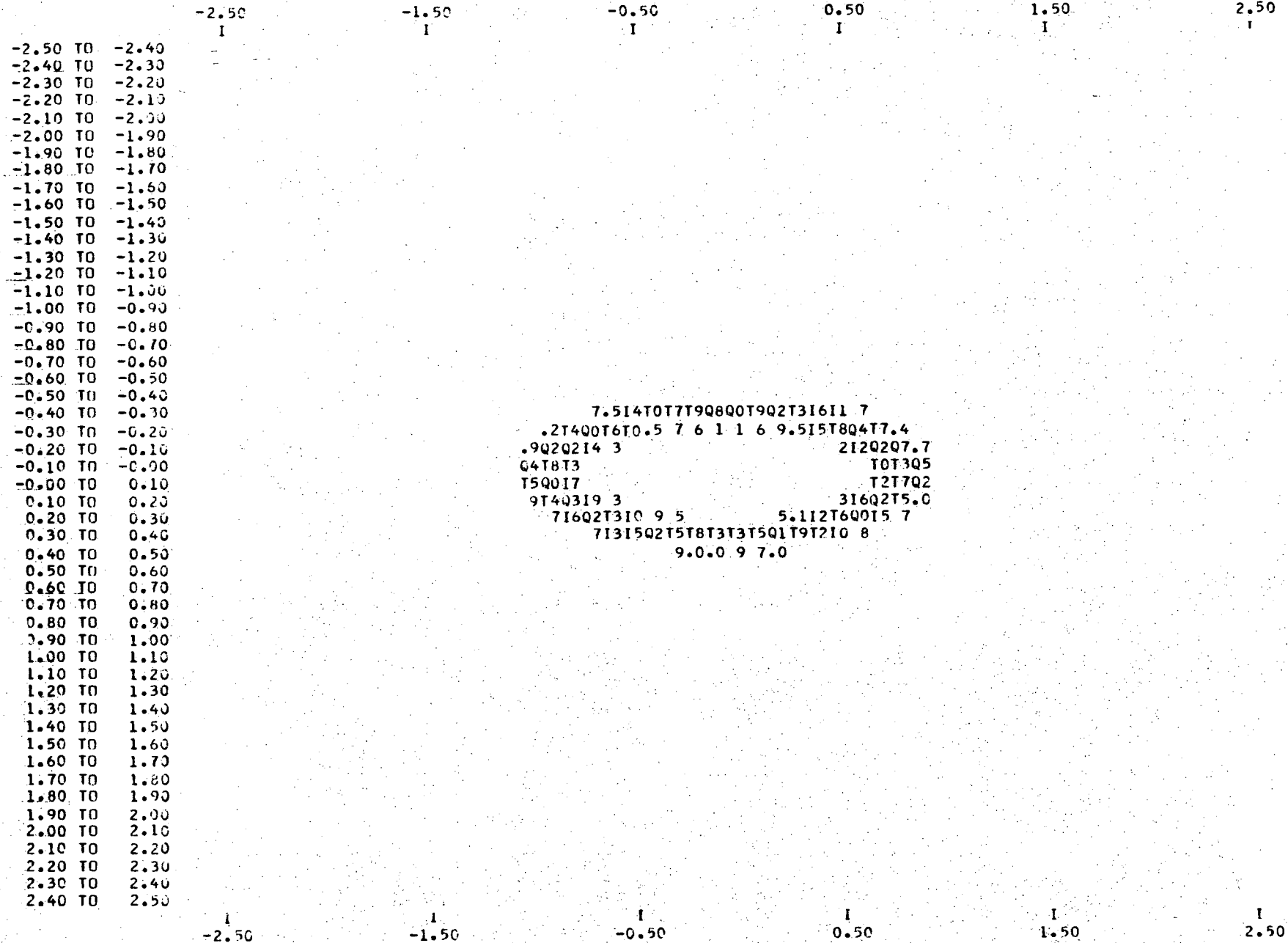


FIG. 4.1.4

5 B

7.514T0T7T9Q8Q0T9Q2T3I6I1 7
 .2T4Q0T6T0.5 7 6 1 1 6 9.5I5T8Q4T7.4
 .9Q2Q2I4 3 2I2Q2Q7.7
 Q4T8T3 TOT3Q5
 T5Q0I7 T2T7Q2
 9T4Q3I9 3 3I6Q2T5.0
 7I6Q2T3I0 9 5 5.1I2T6Q0I5 7
 7I3I5Q2T5T8T3T3T5Q1T9T2I0 8
 9.0.0 9 7.0

XMEAN = 0.01 YMEAN = -0.00 SCALE FACTOR = 4

XLTRAD=30 CM, ORIGIN= C., O., THETA=65. BLUR=.001

03 Y(VERTICAL) VS. 03 X(HORIZONTAL)

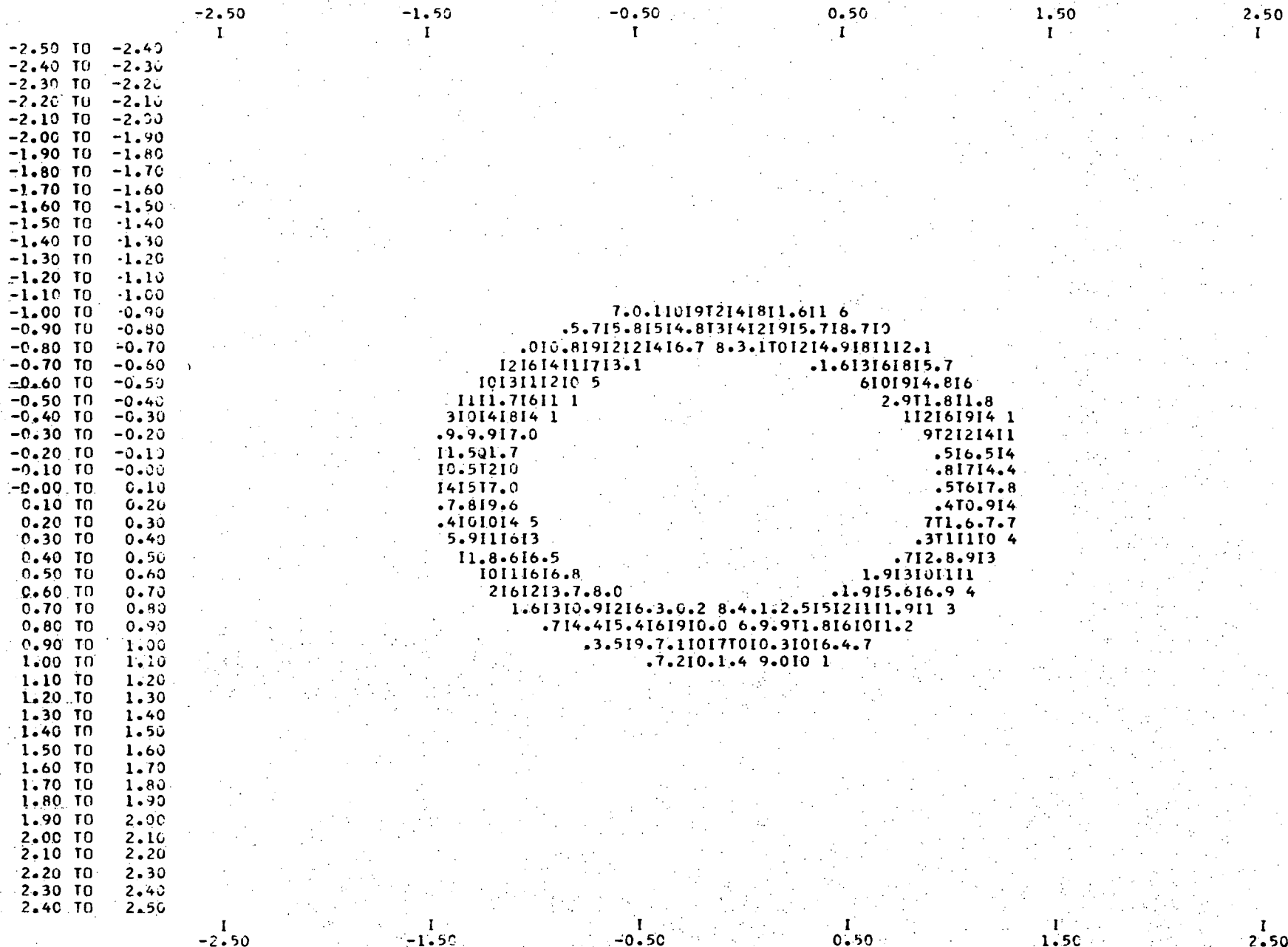


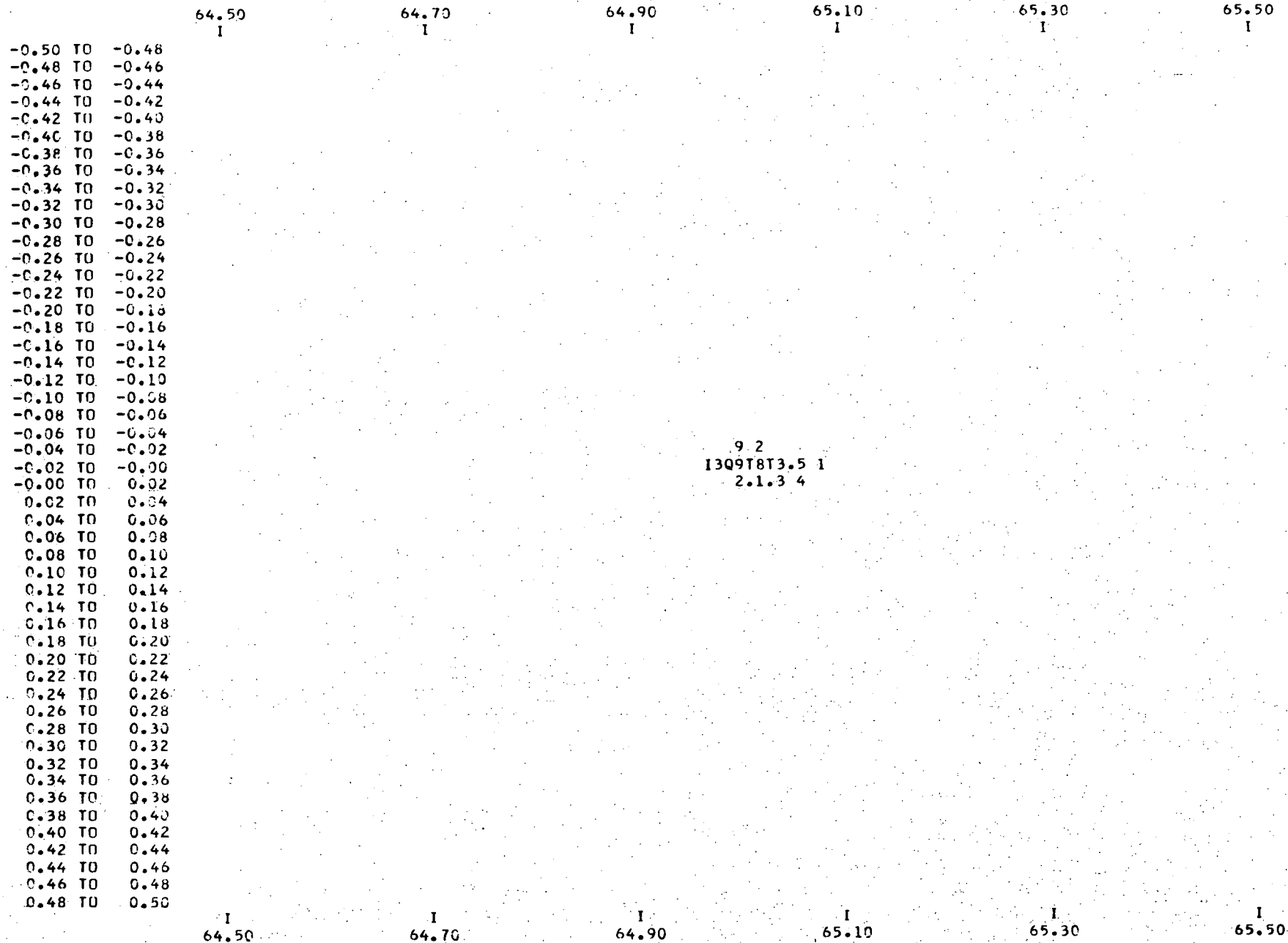
Fig 4.1.5

5 P

XMEAN = 0.01 YMEAN = 0.01 SCALE FACTOR = 2

XTLRAD=30 CM, ORIGIN= G., C., THETA=65. BLUR=.001

D1 Y(VERTICAL) VS. THET(HOPIZONTAL)



XMEAN = 65.00 YMEAN = -0.01 SCALE FACTOR = 48

XTLRAD=30 CM, ORIGIN= 0., 0., THETA=65. BLUR=.001

DI X(VERTICAL) VS. THET(HORIZONTAL)

	64.50 I	64.70 I	64.90 I	65.10 I	65.30 I	65.50 I
-2.50 TO	-2.40					
-2.40 TO	-2.30					
-2.30 TO	-2.20					
-2.20 TO	-2.10					
-2.10 TO	-2.00					
-2.00 TO	-1.90					
-1.90 TO	-1.80					
-1.80 TO	-1.70					
-1.70 TO	-1.60					
-1.60 TO	-1.50					
-1.50 TO	-1.40					
-1.40 TO	-1.30					
-1.30 TO	-1.20					
-1.20 TO	-1.10					
-1.10 TO	-1.00					
-1.00 TO	-0.90					
-0.90 TO	-0.80					
-0.80 TO	-0.70					
-0.70 TO	-0.60					
-0.60 TO	-0.50					
-0.50 TO	-0.40					
-0.40 TO	-0.30					
-0.30 TO	-0.20					
-0.20 TO	-0.10					
-0.10 TO	0.00					
0.00 TO	0.10					
0.10 TO	0.20					
0.20 TO	0.30					
0.30 TO	0.40					
0.40 TO	0.50					
0.50 TO	0.60					
0.60 TO	0.70					
0.70 TO	0.80					
0.80 TO	0.90					
0.90 TO	1.00					
1.00 TO	1.10					
1.10 TO	1.20					
1.20 TO	1.30					
1.30 TO	1.40					
1.40 TO	1.50					
1.50 TO	1.60					
1.60 TO	1.70					
1.70 TO	1.80					
1.80 TO	1.90					
1.90 TO	2.00					
2.00 TO	2.10					
2.10 TO	2.20					
2.20 TO	2.30					
2.30 TO	2.40					
2.40 TO	2.50					

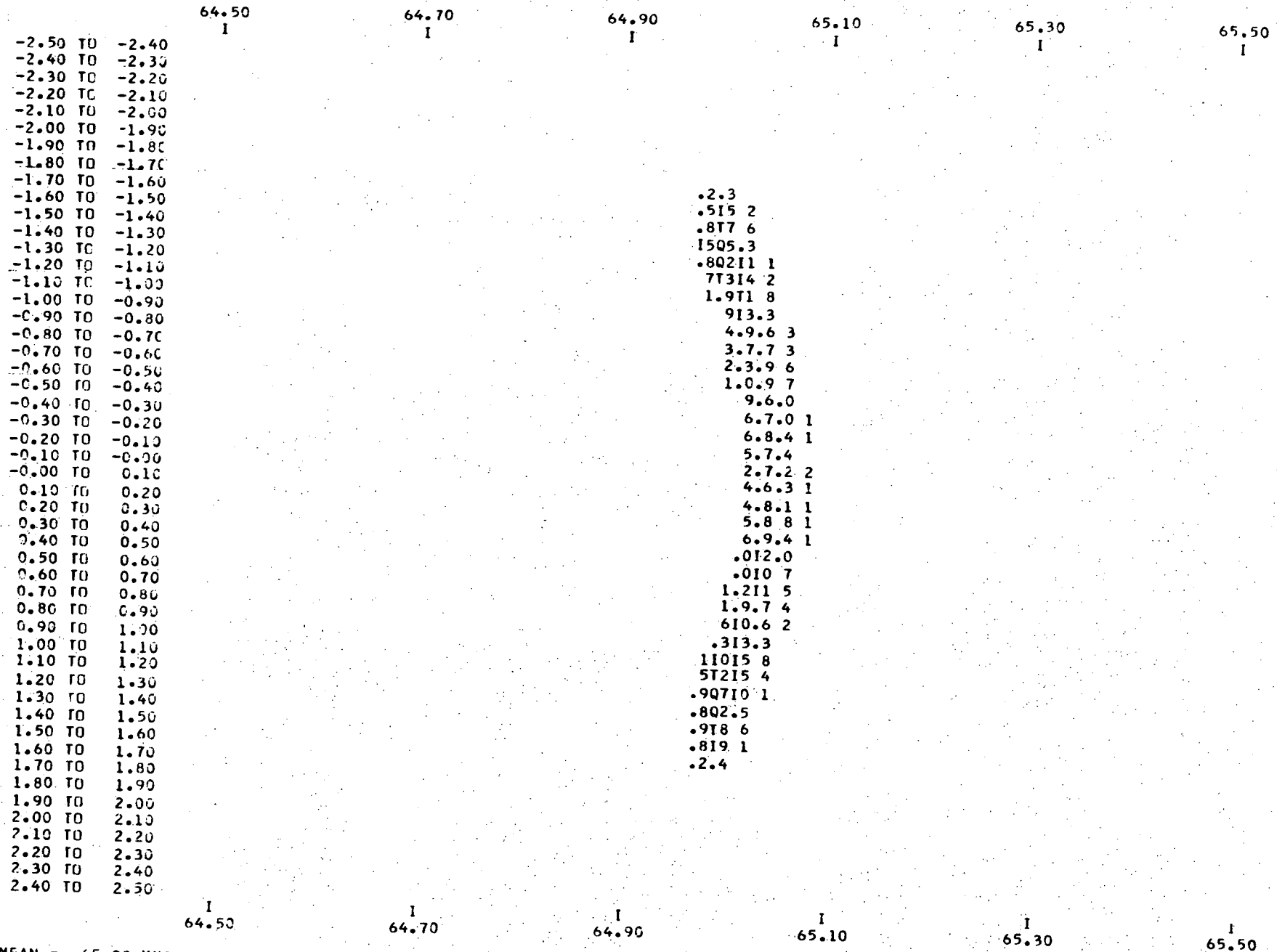
7 8
1078 6
100713 1
1.870.0
410.9 3
1.210 8
8.9.3 1
410.6 1
4.9.3 1
812.3 1
.312 7
512.9 4
11018.0
.90714 2
1001 6
7 8

Fig 418

XMEAN = 65.00 YMEAN = 0.00 SCALE FACTOR = 12

XTLRAD=30 CM, ORIGIN= 0., 0., THETA=65. BLUR=.001

D4 X(VERTICAL) VS. THET(HORIZONTAL)



XMEAN = 65.00 YMEAN = 0.01 SCALE FACTOR =

XTLRAD=30 CM, ORIGIN= 0., 0., THETA=65. BLUR=.001

D4 Y(VERTICAL) VS. THET(HORIZONTAL)

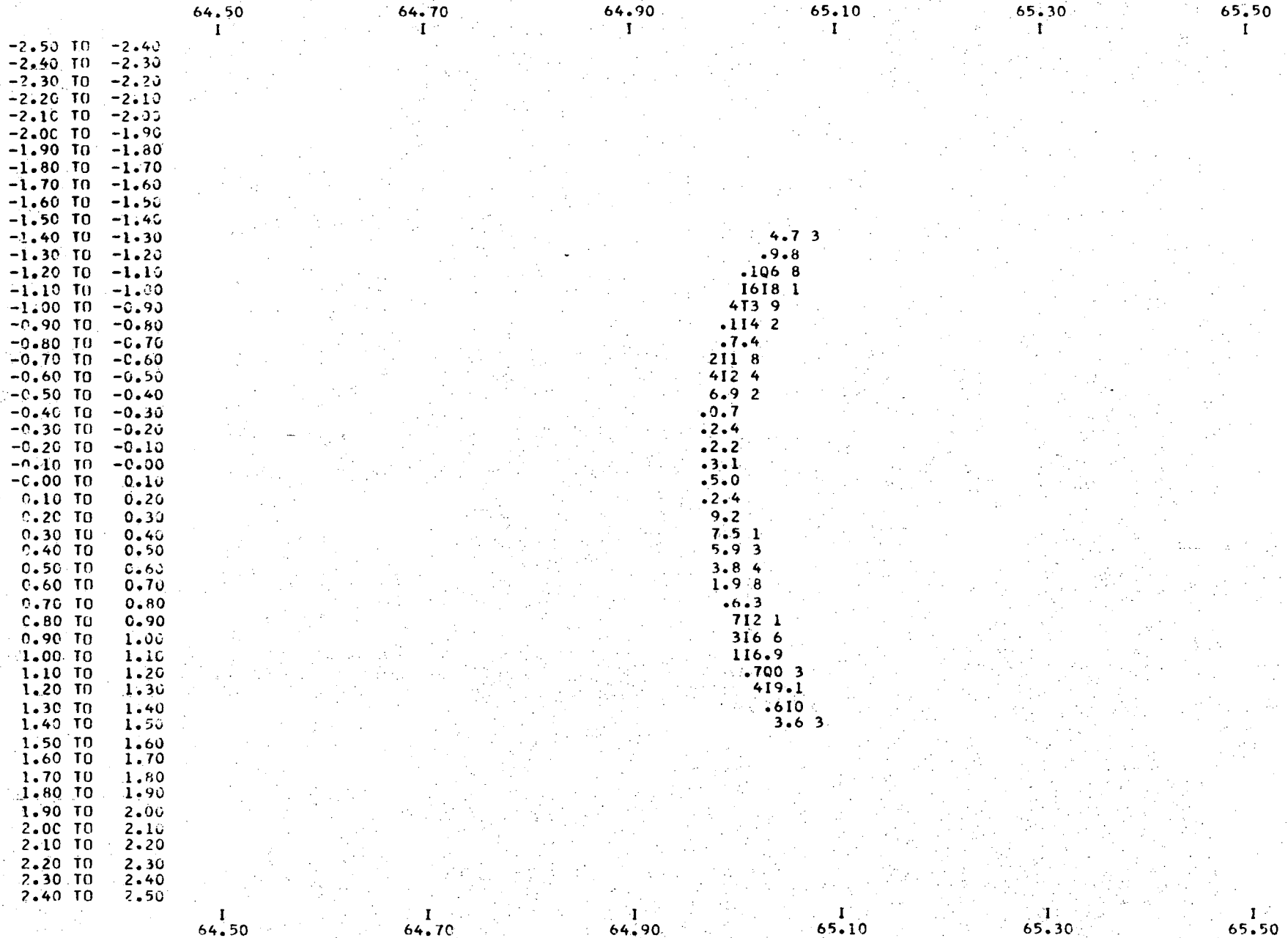


FIG. 4.1.10

5K

XMEAN = 65.00 YMEAN = 0.02 SCALE FACTOR = 10

XTLRAD=30 CM,

THETA=65. BLUR=.001

D1 Y(VERTICAL) VS. D1 X(HORIZONTAL)

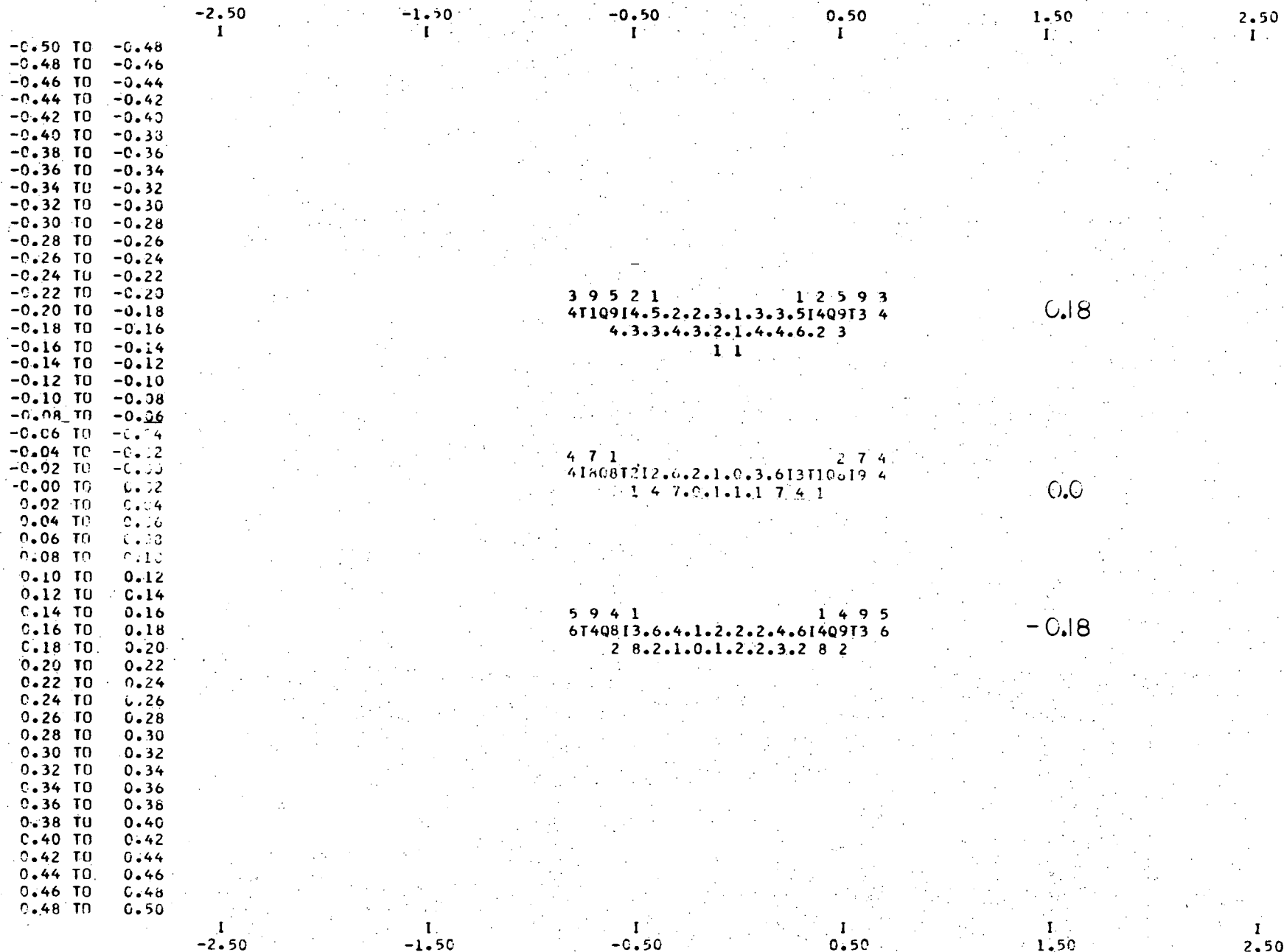


Fig. 4.1.11

5L

XMEAN = 0.00 YMEAN = 0.17 SCALE FACTOR = 20

XTLRAD=30 CM,

THETA=65. BLUR=.001

DI X (VERTICAL) VS. THET (HORIZONTAL)

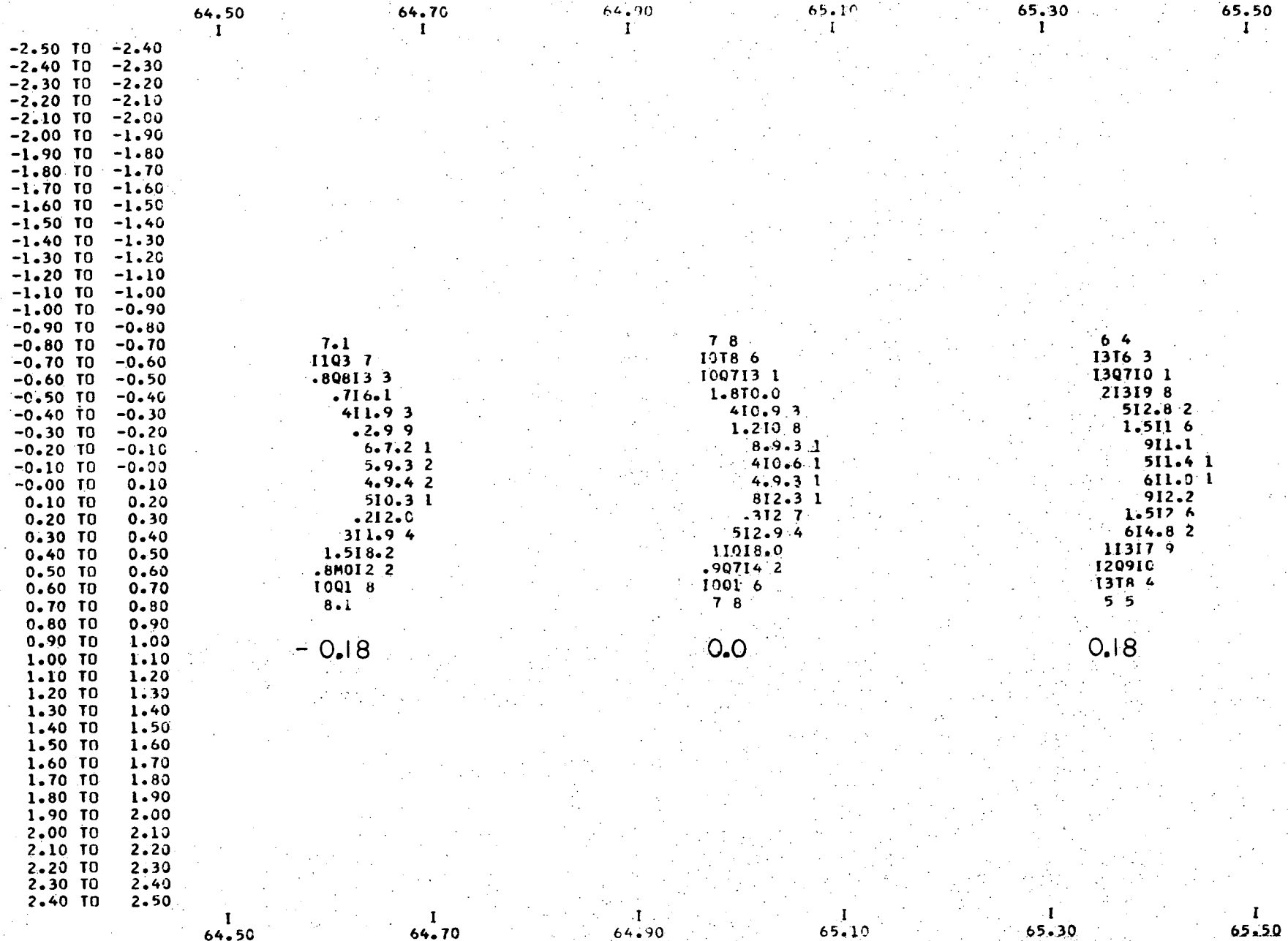
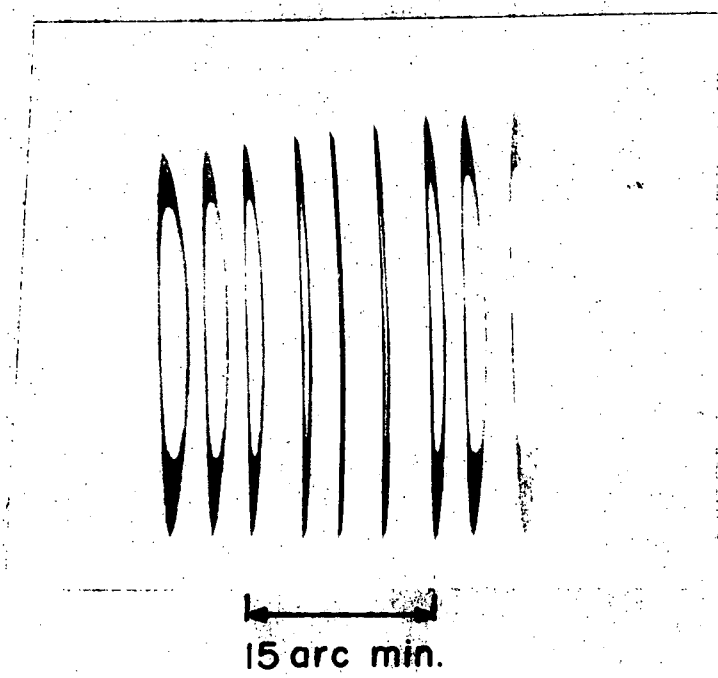


Fig. 4.1.12

5 M

XMEAN = 64.62 YMEAN = 0.00 SCALE FACTOR = 12



SPECTROMETER IMAGE FOR OFF AXIS SOURCE

Fig. 4.1.13

5 N

4.2 Detector Resolution Requirements

The finite size of the high-resolution telescope image has the effect of smearing somewhat the range of Bragg angles accepted. This contribution to the degradation of the spectrometer resolution can be minimized by using larger Rowland circle radii - that is, by reducing the angle subtended by the image as seen from the crystal. On the other hand, larger Rowland circle radii require larger crystals and larger detectors, if the detector is to be moved forward of the spectrometer focus. For crystals with poor inherent resolution such as lead stearate multilayers, the optimum Rowland circle radius can be chosen considerably smaller than for, say, KAP. It is for this reason that the LOXT breadboard spectrometer described in Section 4.3 was designed to give the flexibility of adjustable Rowland circle radius.

A reasonable limit on the radius can be found by requiring that the image angular size,

$$\frac{h}{R} = \Delta\theta_i,$$

be smaller than the inherent crystal resolution,

$$\frac{1}{\rho} \tan \theta_B = \Delta\theta_C.$$

Here h is the image size, R the crystal radius, ρ the

crystal resolution and θ_B the nominal Bragg angle. This gives

$$R/\rho > \frac{1}{\tan\theta_B} \times 10^{-2} \text{ inches,}$$

for 10 arc sec telescope resolution. The ratio R/ρ is plotted in Figure 4.2.1a.

The Bragg angle interval can be subdivided by a position-sensitive detector using the relation for second-order deviation of Bragg angle across the crystal face. For spherical optics,

$$|\theta_B - \theta_B^0| \approx \frac{1}{2} \alpha^2 \cot \theta_B^0 \quad (4.2.1)$$

where θ_B^0 is the Bragg angle at the center of the crystal and α is the angular divergence in the spectrometer plane. For a detector near the crystal face, the requirement that the spatial resolution effects be smaller than the inherent crystal resolution gives

$$\Delta y < 3 \sin\theta_0 \tan\theta_0,$$

where y is the detector resolution in mm. This relation is shown in Figure 4.2.1b. These results, which are being checked carefully by the Monte Carlo program described in Section 4.1, show that the spatial resolution required for a position-sensitive detector is modest and well within the capabilities of the instruments discussed in Section 4.3.

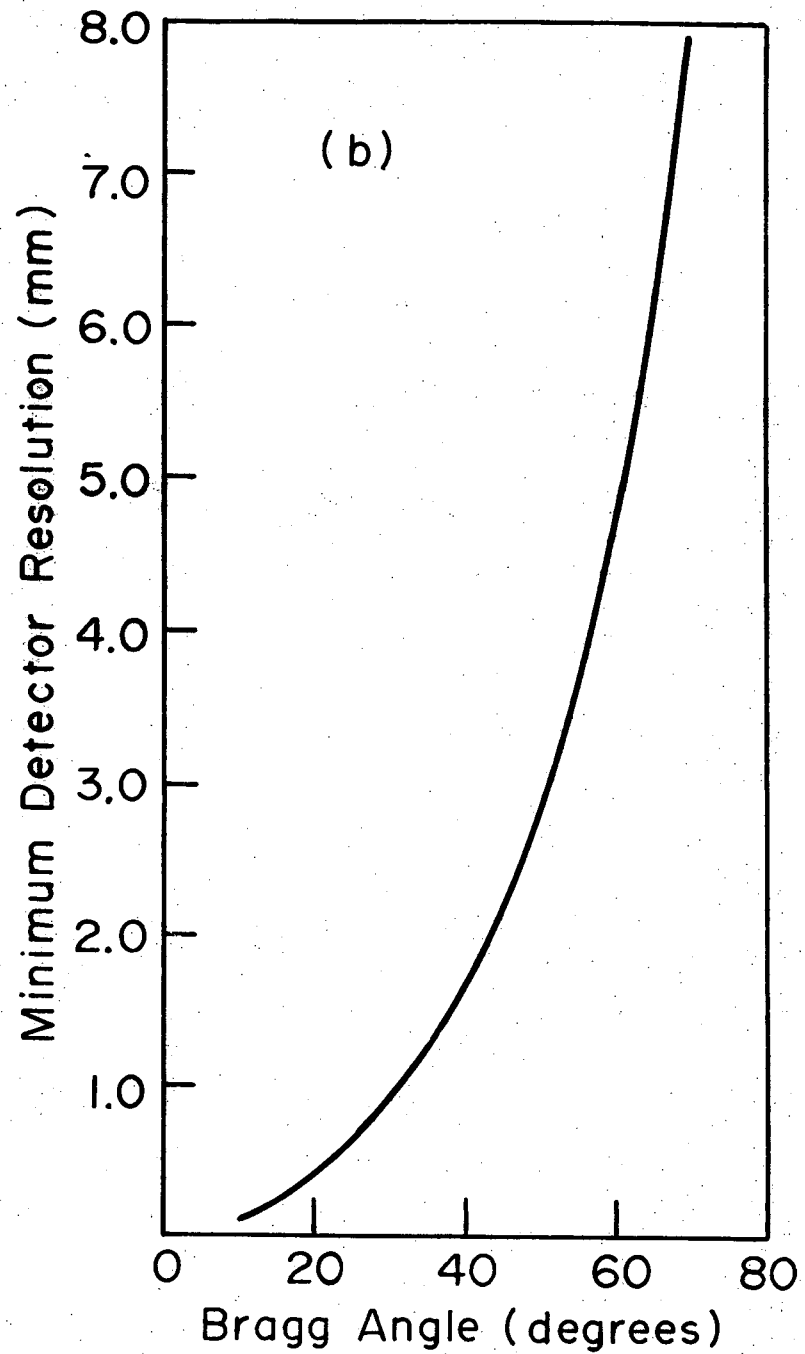
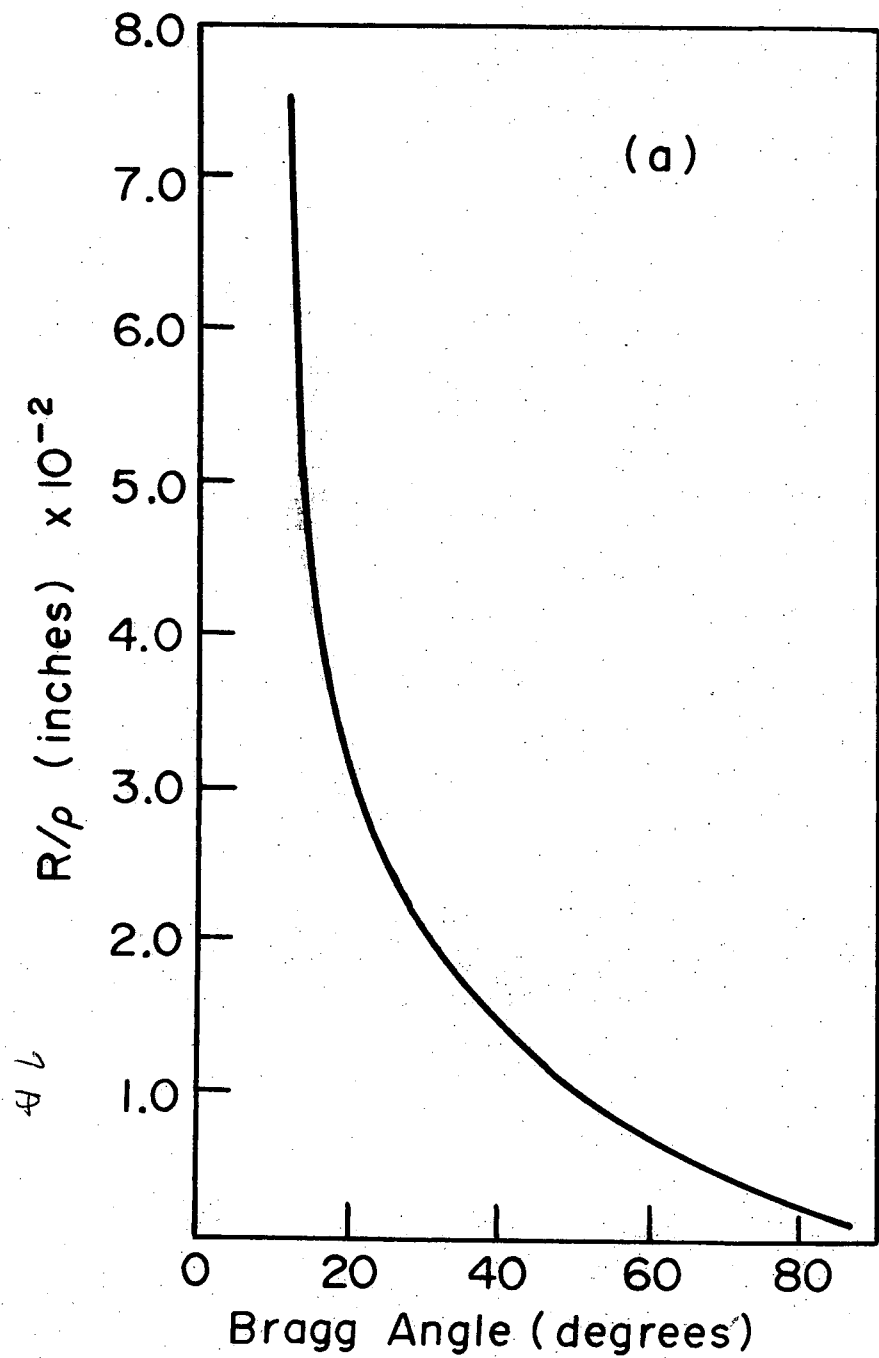


Fig. 4.2.1

4.3 Breadboard System Design and Construction

4.3.1 Curved-Crystal Spectrometer

One of the central objectives of Phase A was the construction of a breadboard, curved-crystal spectrometer capable of fully exploring all aspects of the proposed system. The primary considerations were (i) to allow complete flexibility of operating modes and (ii) to approximate as many of the final design characteristics as possible. These were met within the Phase A budget constraints and the limitations of the 24" vacuum chamber which houses the unit.

The flexibility of the system was achieved by maintaining independent motions for each of the spectrometer elements. Four stepping motors are used to control the crystal position, crystal angle, detector position and detector angle, respectively. The step sizes are 8.1 arc sec for the angular positions, 0.0002" for the crystal and 0.00014" for the detector linear positions. Angular fiducials are accurate to 30 arc sec. In Figures 4.3.1-.4, the spectrometer is shown mounted vertically in the vacuum chamber. A single wire proportional counter and associated preamplifier are mounted on the detector arm.

In order to operate the spectrometer through a wide range of Rowland circle radii despite the spatial limitations of the vacuum chamber, two X-ray sources have been included in the system. One is fixed in position as an appendage

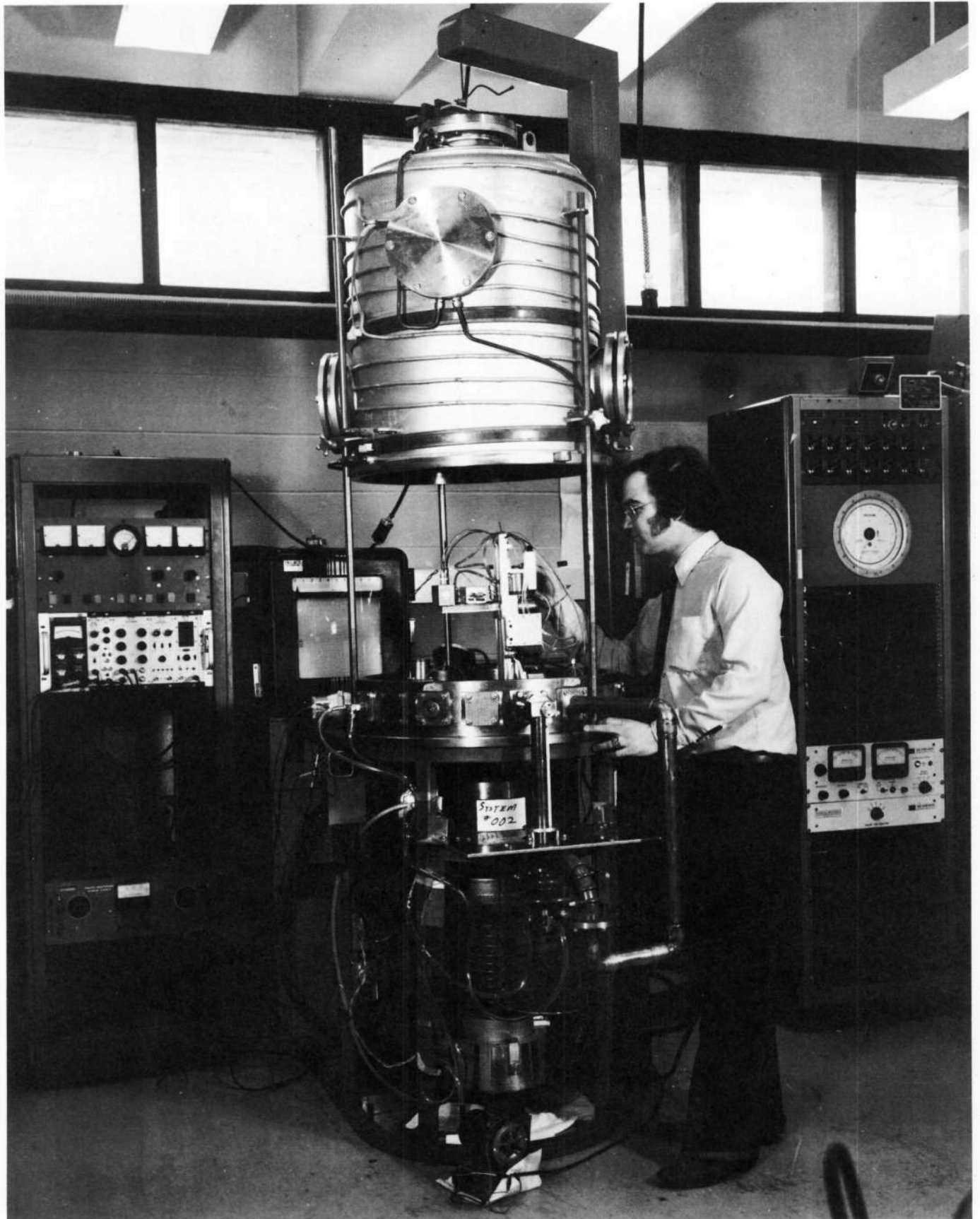
outside the vacuum chamber wall, and the second is mounted on a stepping-motor-controlled slide inside the chamber. The fixed source can be used for source-crystal distances of from 8" to 24", and thus serves to study crystals with radii of curvature from about 14" to 24". The movable source can be placed from 0" to 14" from the crystal to explore the same crystals at small Bragg angles or to investigate crystals with radii of curvature of 3" to 14". This complete flexibility in Rowland circle diameter allows one to choose the optimum radius for each reflector depending on its resolution (see Section 4.2).

Both X-ray guns are essentially similar in design. The external source consists of an X-ray tube with interchangeable targets and an electron gun. The entire assembly is mounted on one of the feedthrough ports of the vacuum system. The travelling source is small (2 ½" x 1 ½" x 2") and is constructed from stainless steel with a Keleff shroud for the anode. Oil cooling is used for both sources to allow operation at working intensities. Both are windowless, although the external gun can be differentially pumped to insure a clean spectral line. Both fixed and variable focus electron guns can be used and the resultant X-ray beam diverges in a 5½ half-angle cone similar in size to that of the high resolution telescope. The two guns are indicated in Figure 4.3.3.

Figure 4.3.1

Overall view of breadboard curved crystal spectrometer mounted in the 24" vacuum chamber. The external X-ray gun is at the top of the vertical pipe in the foreground. The right-hand relay rack contains the vacuum controls and ion gauge supply. The proportional counter measurement chain is mounted in the left-hand rack. The pannel at the top of the rack houses the X-ray tube power supply controls and interlocks.

9A



9B

Figure 4.3.2

The breadboard curved crystal spectrometer. The left-hand track, seen from behind, controls the moveable X-ray gun seen on the lower right-hand side of the picture. Its stepping motor is mounted vertically at the far end of the track. The detector arm and the crystal move along the other track attached to the vacuum chamber floor. In the crystal mount is a spherically bent mica crystal. The detector arm crawls along the large gear and the detector itself moves along the arm. The narrow proportional counter body is here seen edge-on with the preamplifier mounted behind it. The tubing at the rear of the chamber supplies gas to the proportional counter. The tubes in the foreground circulate cooling oil through the X-ray gun to a heat-exchanger outside the chamber. The multipin feedthrough supplies power and pulses to the stepping motors.

9c

9D

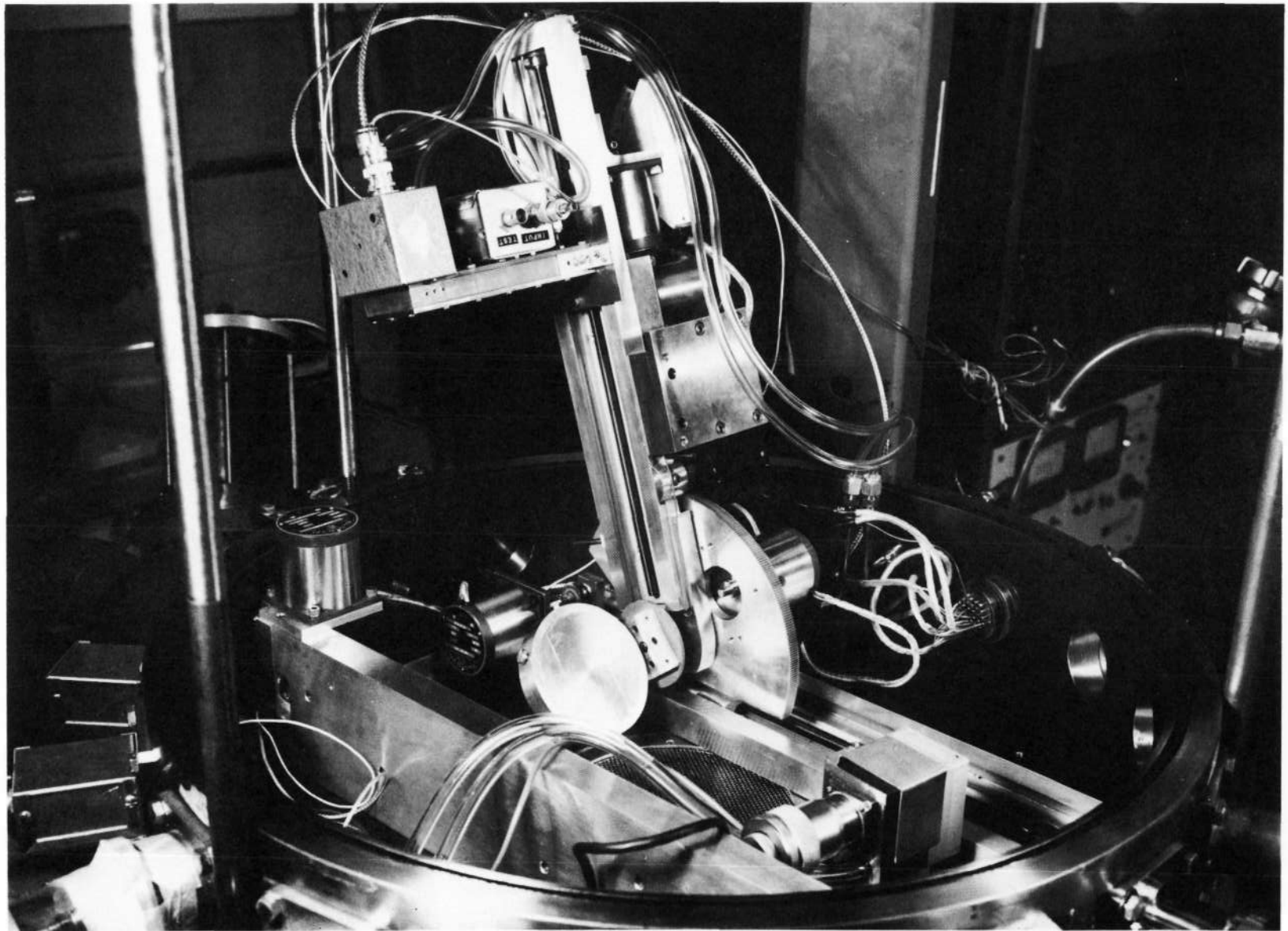


Figure 4.3.3

Breadboard curved crystal spectrometer. The external X-ray source is on the left-hand side of the picture. The moveable X-ray gun with its Keleff high voltage insulating shroud is shown attached to its track. The stepping motor attached to the large gear controls the crystal angle which can be read on the partially obscured vernier scales. A bubble level accurate to less than 30 arc sec is also mounted on the crystal drive. Another pair of levels (only one of which is visible here) are attached near the top of the detector arm. These serve as fiducials for absolute calibration of the stepping motor pulse counting system.

9E

9 F

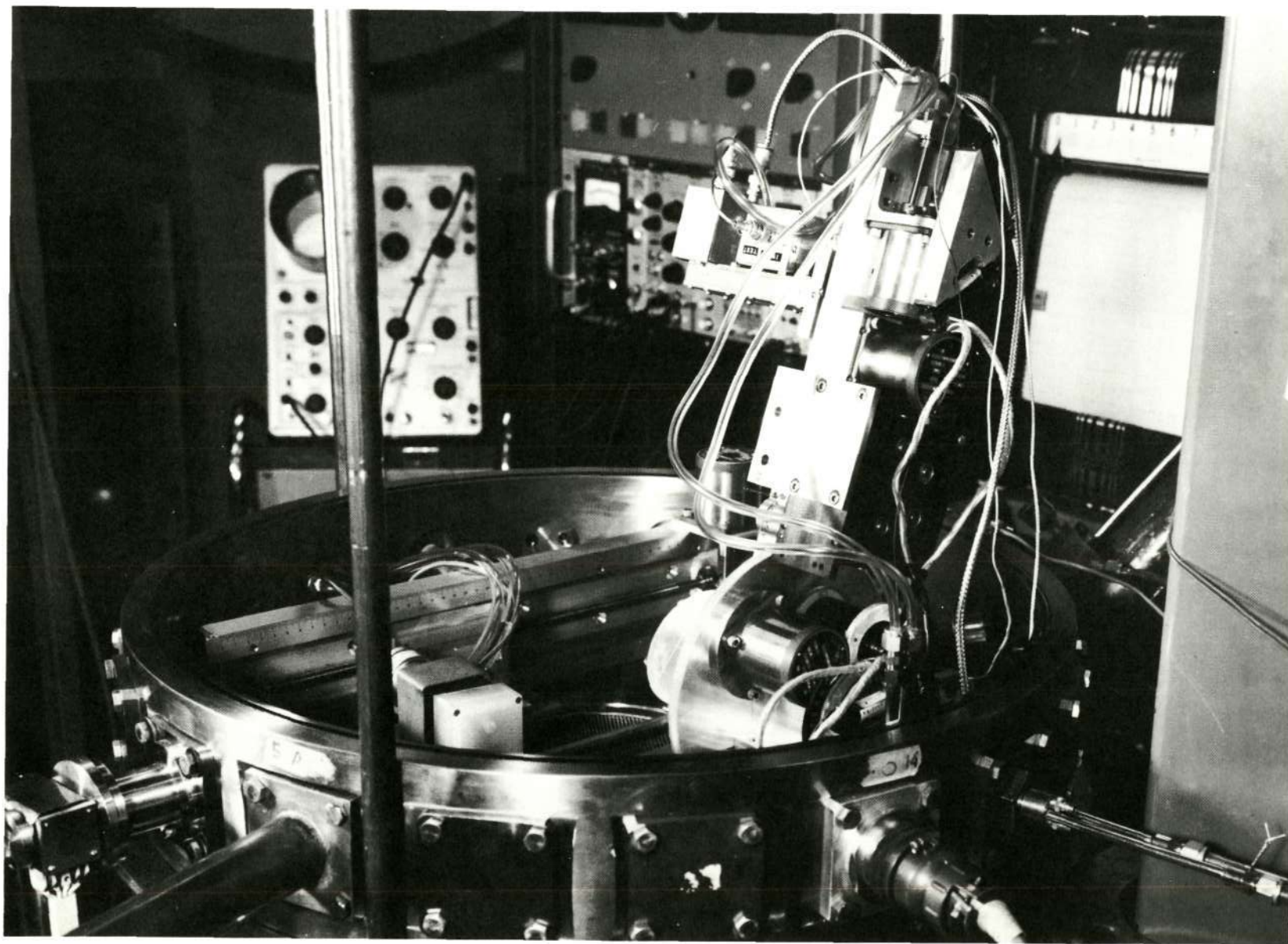
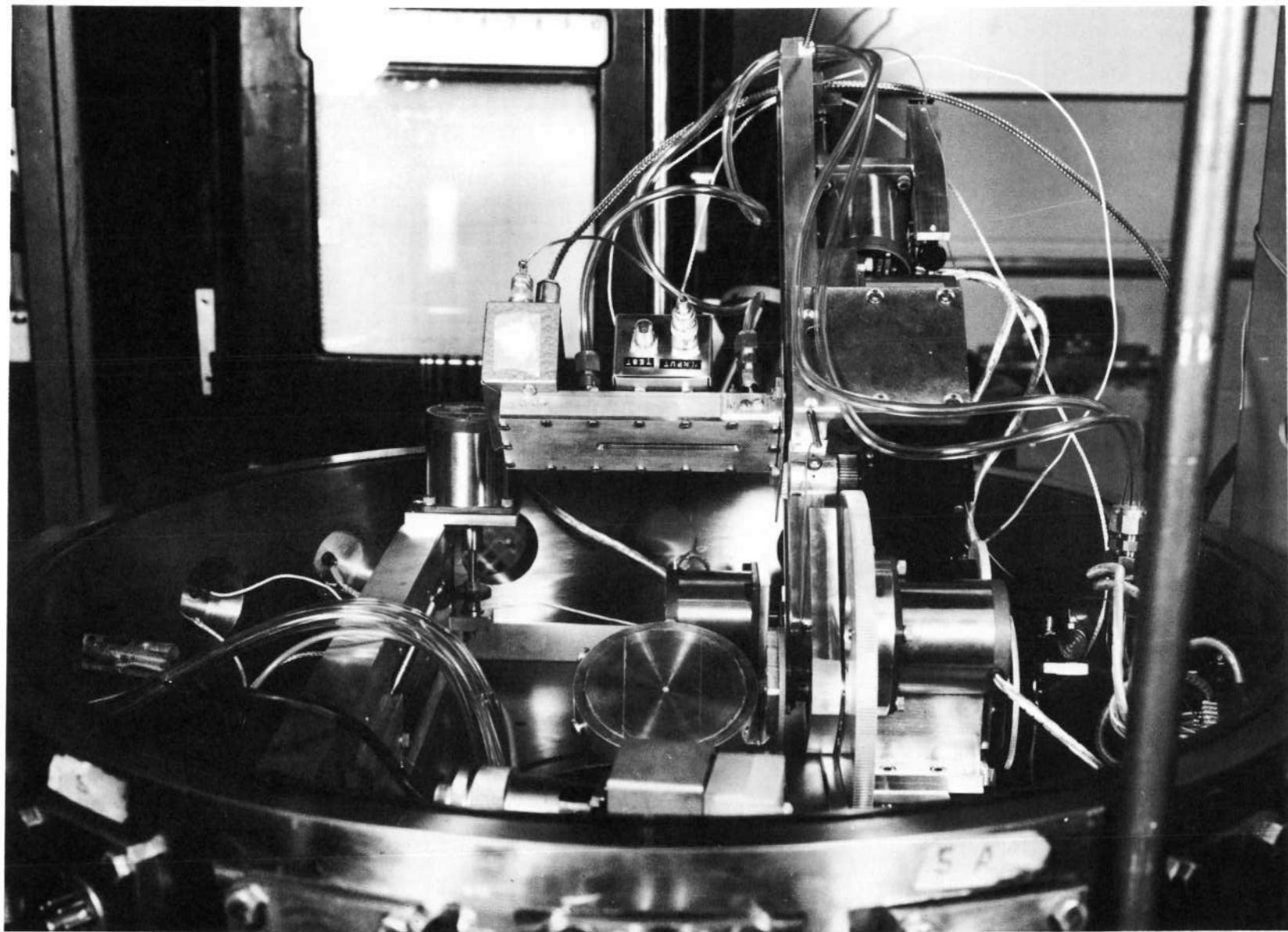


Figure 4.3.4

Breadboard curved crystal spectrometer. This view shows the X-ray gun in the foreground, the curved mica crystal and the slit window proportional counter. The gas feed-throughs and the preamplifier are attached to the back of the counter. This configuration shows the detector moved forward to scan the crystal face.

4-6



4.3.2 Spectrometer Vacuum System

The breadboard spectrometer is housed in a vacuum system acquired at low cost. Several months of reconditioning were required to make the station operational.

The chamber is of stainless steel construction with a 24" diameter, 30" high bell jar. Twenty feedthrough ports allow easy access to components inside the chamber. A six-inch diffusion pump, large roughing pump, small fore pump, and liquid nitrogen cold trap can achieve pressures of down to about 5×10^{-7} Torr.

The chamber, with the bell jar raised to expose the breadboard spectrometer, is shown in Figure 4.3.1 .

4.3.3 Control and Data Acquisition System

Both control of the breadboard spectrometer motions and data acquisition from the position-sensitive detectors will be accomplished by means of a Data General Nova 1220 computer with 8K memory. The unit has arrived and software and hardware systems are being developed.

The spectrometer control will be achieved by counting pulses as they are sent to each of the five stepping motors located within the vacuum chamber. This method has the advantages of obviating the need for accurate, absolute-position encoders and of allowing preprogrammed θ - 2θ

motion of the crystal and detector, crystal scanning, etc. The interfacing required for such a system is straightforward and is already underway. (Previously pulses were counted by several electronic-electromechanical scalars.)

The Nova will simultaneously be used as a complete data acquisition system capable of performing one and two-dimensional analysis of the multiwire proportional counter, spiraltron array and chevron channel plate detectors. Both analog (charge division) and digital modes will be accommodated, the former by means of external analog/digital converters. This A/D facility will also be used to determine pulse height spectra for the proportional counter allowing a high non-spectral line background rejection.

4.3.4 Proportional Counter

The breadboard spectrometer is now being operated with a single wire proportional counter which incorporates several design features to be used in the multi-wire detector. Figure 4.3.2 shows this counter mounted in position on the spectrometer.

The counter body is 2" x 6" and 1" thick and is constructed from magnesium. Both front and rear faces are demountable allowing easy access to the anode. The 3" x 3/32" slit window is covered by a thin, stretched polypropylene film supported by a 70 lines/inch nickel wire mesh. This window, which is commonly used for soft X-ray detection,

has a thickness of $100 \mu\text{g}/\text{cm}^2$. An additional $50 \mu\text{g}/\text{cm}^2$ coat of graphite was applied to the inside of the window to provide electrical contact with the counter body and thus prevent static charge accumulation.

The anode is a 0.0008" gold-plated molybdenum wire. It is strung on a G-10 bonded fiberglass frame which is screwed to the rear face plate of the counter. This frame construction has been widely used in large multi-wire charged particle detectors. It allows the convenience of winding a multi-wire grid and of servicing readily the entire unit even after initial assembly. The frame supports the wire about 2.5 mm below the window.

High voltage is brought into the counter via a small Stupekoff seal. The signal is decoupled from the anode by a large blocking capacitor mounted inside the counter body. This method was used to test the feasibility of such a system, which would remove the risk of using a large number of high-voltage feedthroughs on a multi-wire counter. Other methods, such as insulating an entire wall of the counter, are also under consideration.

Because of gas diffusion through the thin window, the counter is operated in a continuous flow mode. Using 90% argon, 10% methane gas, a 25% pulse height resolution has been obtained for the $\sim 6 \text{ keV Fe}^{55}$ line. A miniature five-transistor preamplifier of local design is mounted on the back of the counter to drive the long signal cable. Standard

amplification techniques have been used.

A large multiwire counter is now under construction.

4.4 Lead Stearate Crystal Preparation Facility

For the longer wavelength end of our region of interest ($44 \text{ \AA} - \sim 100 \text{ \AA}$), one of the crystals which should prove most effective is the Lead Stearate Multilayer crystal. Such crystals are formed through building up the crystal layer by deposition on a clean glass substrate. Following the method of B. Henke of the University of Hawaii, we have developed a facility to produce these lead stearate multilayers. Since the deposition method is essentially identical for a variety of multilayered crystals including Lead, Barium, or Calcium-Stearate, we now have the capability to produce any of these. Because of its slightly better reflection coefficient, we are concentrating on producing Lead Stearate multilayers at the present time.

Figure 2.4.1 shows the apparatus. The Lead Stearate is produced as a monolayer. This is accomplished by depositing a few drops of Stearic acid dissolved in n-hexane on the surface of a bath solution containing free lead ions. The n-hexane evaporates quickly and the lead ions combine with the stearic acid to form the lead stearate chain molecule. These molecules float vertically and form a film which spreads out and covers the surface of the liquid. A calculation involving the concentrations of our solutions and

the area to be covered sets the number of drops at about 6 for our purpose. The apparatus shown in Figure 2.4.1 consists of a shallow tank ($\frac{1}{2}$ " deep) with a 4" deep trough at one end to allow the glass substrate to be completely immersed. The tank is 7" wide and 36" long and its top edge is $\frac{1}{2}$ " wide. This edge was machined flat. All surfaces touched by the liquid are coated with Teflon for cleanliness and the top edges treated with parafin to make them hydrophobic. The tank is levelled by means of four adjustable legs and filled with the bath solution containing the lead ions. Because of the hydrophobic property of the edges, the top of the liquid can be made to rise as much as $\frac{3}{16}$ " above the top of the tank. This effect can clearly be seen in Figure 2.4.1 at the top left-hand side of the tank. At the right of the tank, one can see the pH electrode which monitors the pH at all times. The glass substrate can be seen in the out position on the left side of the tank and is lowered and raised into and out of the liquid with a cycle time of 1 minute, 56 seconds. At each end of the motion, micro switches are activated which automatically reverse the direction. The substrate is attached to a rod, long enough so that the angle of entry into the surface of the liquid is approximately 90° throughout each dip. As the dipping proceeds and the film is used up, the monolayer is kept pressed against the glass substrate by a delicate, Teflon-covered ($\frac{1}{4}$ mil Teflon), balsawood float which is

pulled from underneath the tank with a force sufficient to exert about 30 dynes/cm pressure on the film. Thus, although the film cannot be seen, the number of layers deposited can be counted by monitoring the movement of the float. Because the float sits 3/16" above the edge of the tank, it is essentially frictionless. Approximately 10 layers are deposited from each monolayer film, at which point the surface is swept clean, the pH adjusted, and a fresh monolayer applied. Continuing for many hours in this fashion, multilayer crystals of 100 reflecting layers or more can be easily produced. The glass plate can be cut into section after completing the dipping process and tested in our spectrometer.

Curved crystals are produced by mounting a spherically curved substrate in the flat glass plate and dipping in the same manner. A substrate polished to $\lambda/40$ has been procured from Perkin & Elmer, since surface smoothness has been found to be essential to proper multilayer production.

A flat crystal has been compared with a similar multilayer produced by Professor Henke at his laboratory. The peak reflectivity of our crystal was ~20% greater than the comparison standard and within 20% of that of the best multilayers he has produced. More accurate efficiency measurements are underway. Section 4.5 discusses tests of another flat crystal using the breadboard spectrometer.

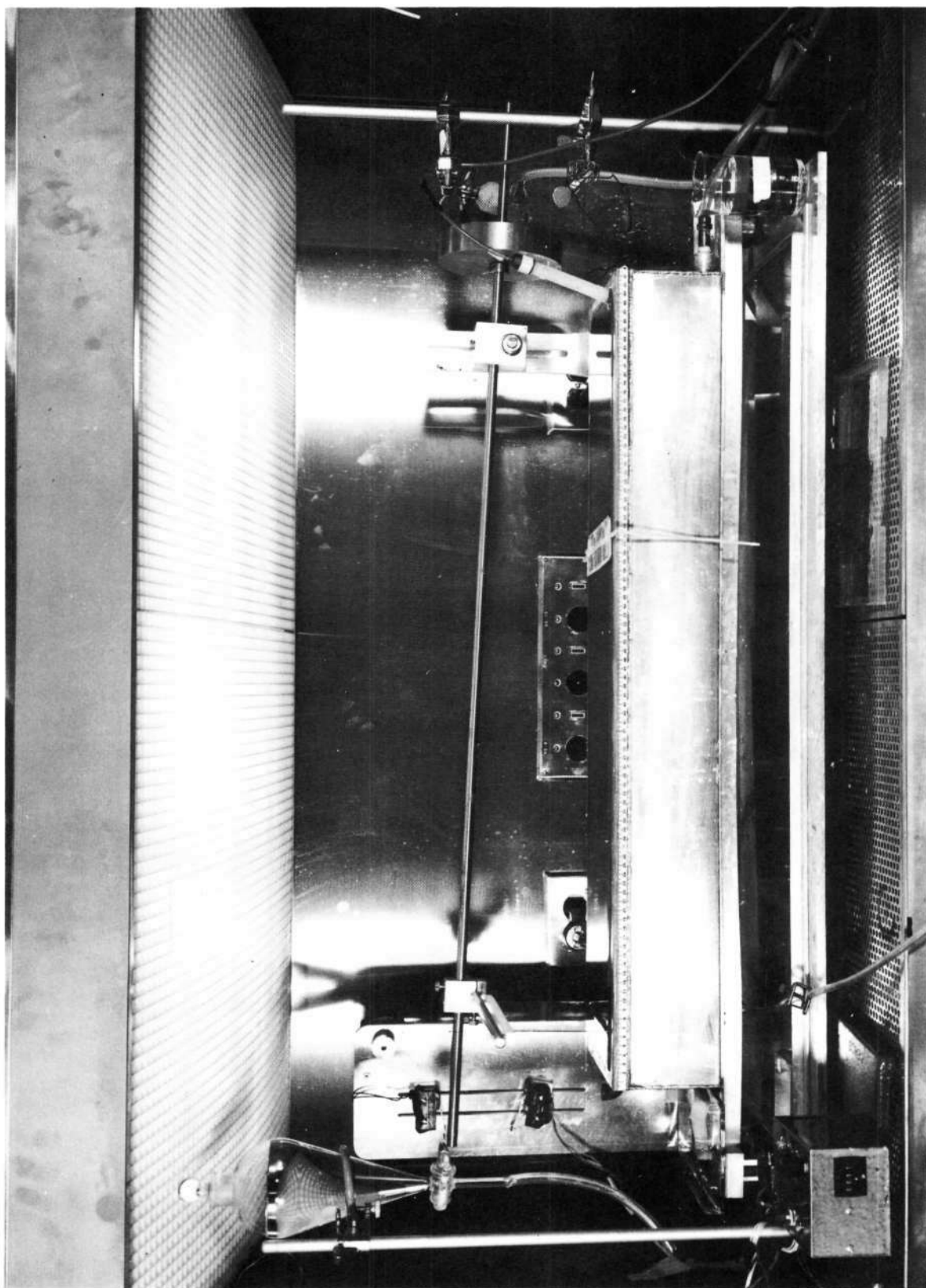
Beacuse of this success, we now feel that production

of X-ray diffractors for the long wavelength region poses no serious problems and that these diffractors can be made to take advantage of the benefits of spherical Rowland geometry.

Figure 4.4.1

Lead stearate multilayer apparatus. This shows the teflon-coated dip tank with the water level standing above the tank edge. The arm pivots about its support on the right-hand side of the tank, travelling between the two micro switches located on the left. Each dip deposits a monolayer on the glass sheet with the balsa float maintaining the proper pressure. The pH meter probe on the right monitors the solution.

16A



4.5 Measurement of Bragg Reflection of 44 \AA Carbon K_{α} X-Rays by Lead Stearate Multilayer with the Breadboard Spectrometer

A 100-layer lead stearate crystal on a flat glass substrate prepared with the apparatus described in Section 4.4, was mounted in the crystal holder of the breadboard spectrometer. A carbon target was placed in the travelling X-ray tube. A proportional counter with a $\sim 100\mu$ stretched polypropylene window was mounted on the detector arm. The system was closed and evacuated. The X-ray tube was then turned on and operated under steady conditions during a series of measurements with the crystal and detector in the θ - 2θ position, i.e., with equal angles of incidence and reflection for rays striking the center of the crystal.

Figure 4.5.1 is a plot of the results which shows the specular reflection of the 44 \AA carbon K_{α} X-rays from the lead stearate coated glass falling off rapidly, as expected, at angles beyond the critical angle for total external reflection, with a strong peak around 26° which is the Bragg angle for reflection of 44 \AA X-rays from a crystal with the $2d = 100 \text{ \AA}$ spacing of lead stearate. Figure 4.5.2 shows the results of similar measurements performed with plane glass plate with no lead stearate deposition. A similar specular reflection is observed, but without the peak at 26° .

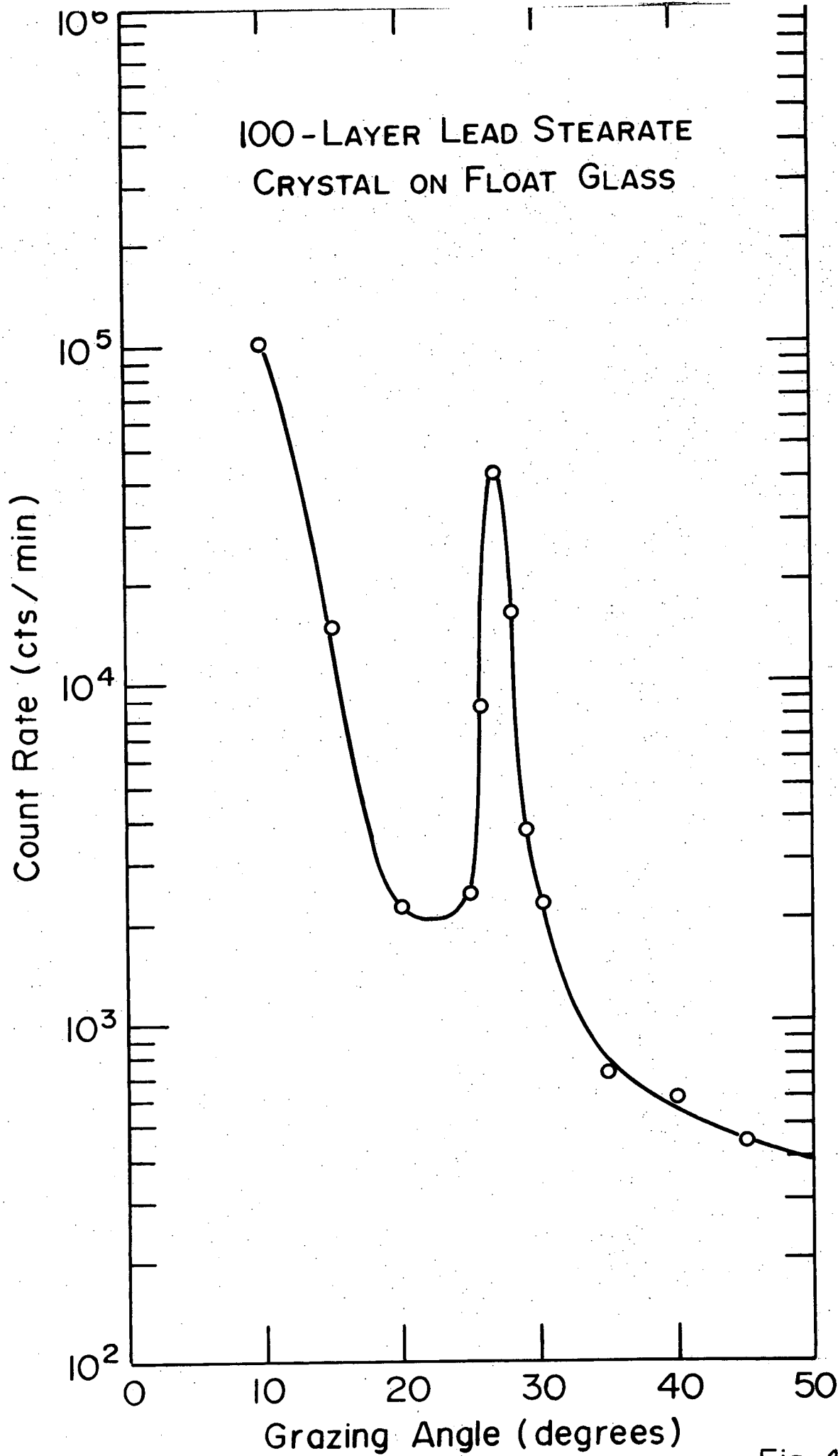
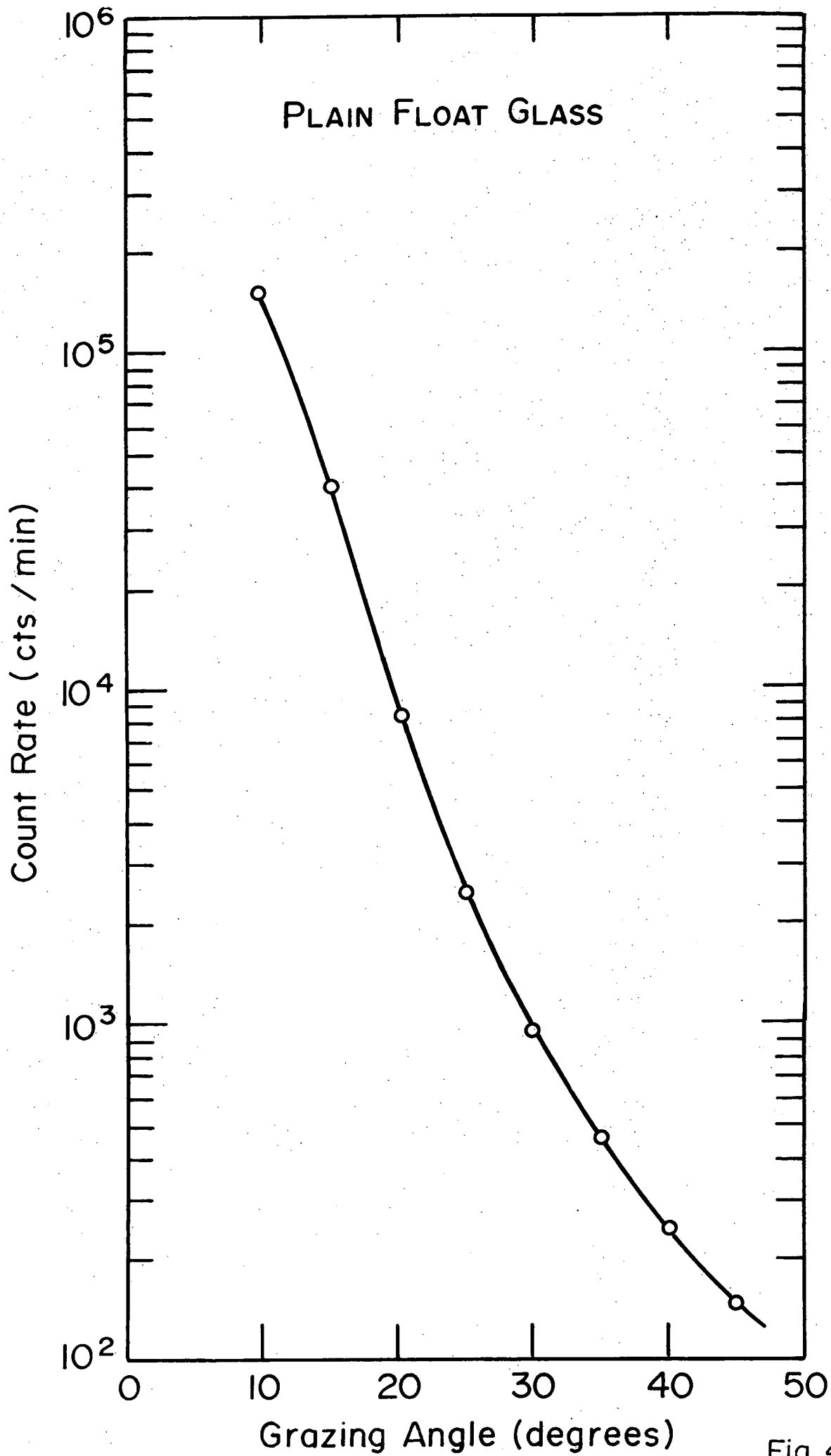


Fig. 4.5.1



17-B

Fig. 4.5.2

4.6 Test of Bragg Reflection from a Spherically Curved Mica Crystal

A preliminary test was made of the feasibility of bending mica to achieve a useful approximation to the spherical configuration described on page 11 of Section 3. A spherically bent mica crystal was purchased. It consisted of a thin mica sheet pressed and glued to conform to a spherical mold with a radius of curvature of 14".

The performance of the spherically bent mica crystal as a diffractor in the Rowland geometry was tested with the breadboard spectrometer using Copper L radiation of wavelength $\lambda \sim 13.9 \text{ \AA}$. The source, crystal and detector were positioned to conform to the Rowland condition when the central ray was incident on the crystal at the Bragg angle. The crystal mount was then rotated about an axis perpendicular to the scattering plane and the counting rate was measured as a function of the angle of rotation. The result shown in Figure 4.6.1 illustrates that the range of rotation angle within which the Bragg condition is satisfied somewhere on the crystal is very narrow as expected. The results indicate that this first crude spherical diffractor would provide a spectral resolution of approximately $\lambda/\Delta\lambda \approx 500$ if used as is. Efforts will be made during Phase B to produce improved spherical mica diffractors. In addition, the fabrication of similar spherical diffractors will be attempted with clinocllore, a mica-like crystal with $2d = 28 \text{ \AA}$.

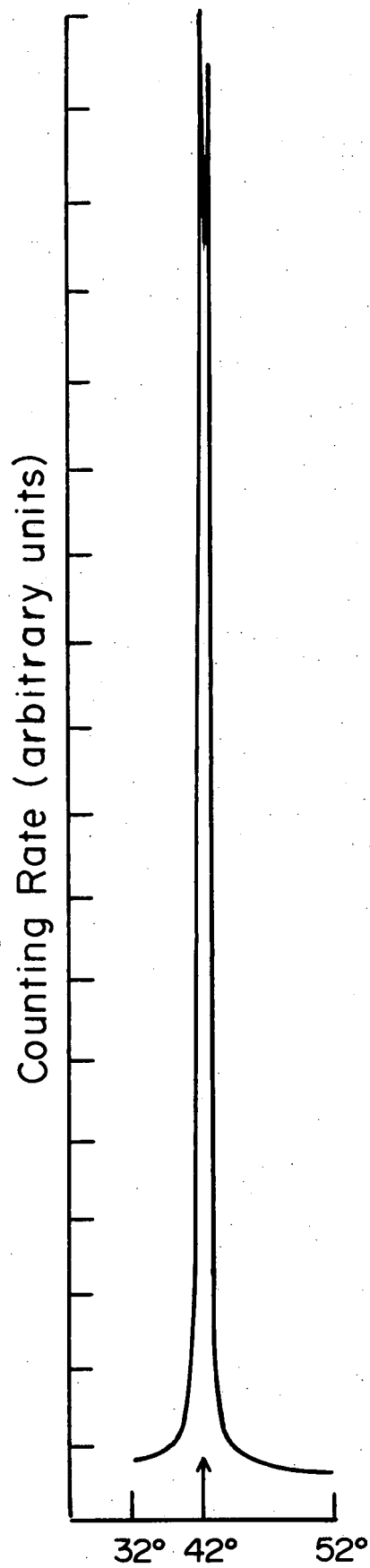


Fig. 4.6.1

18 A

Since mica and certain other crystals can be cylindrically bent with good precision, an alternative scheme for achieving the benefits of the spherical configuration appears to be worth a careful evaluation. This scheme will employ narrow cylindrically bent facets glued to individual metal supports that are mounted with adjusting screws on a supporting back. Once the facets are tilted and aligned to conform approximately to the ideal spherical surface, their supports will be epoxied in place.

4.7 4.7 Tests of Windowless Photoelectric Detectors

Since X-rays with wavelengths above the Carbon K edge are not efficiently detected by the proportional counter, windowless detectors such as the chevron channel electron multiplier are being studied. Several measurements of channeltron efficiencies in the soft X-ray region have been made.¹ We have performed preliminary tests of a Bendix Channeltron using the parallel beam, soft X-ray facility of the Center for Space Research.

X-rays produced by fluorescence using a Copper primary target. The X-ray gun high-voltage supply is 4 KV. The primary target is located in a clean vac-ion

¹D. G. Smith, K. A. Pounds, IEEE Trans. on Nuc. Sci. NS15 541 (1968); W. Parkes, R. Gott, K. A. Pounds, IEEE Trans. on Nuc. Sci NS17, 360 (1970).

pumped system while the rest of the station is diffusion-pumped. The secondary targets include Boron (0.183 keV), Carbon (0.277 keV), Magnesium (1.25 keV), Aluminum (1.48 keV), Vanadium (0.51 keV), Chromium (0.57 keV) and Iron (0.70 keV). The fluoresced X-rays pass down a 25 ft. evacuated pipe to the experimental bell jar.

The Channeltron and a standard proportional counter were mounted side by side in the beam. The proportional counter was fitted with a stretched polypropylene window $100 \mu\text{g}/\text{cm}^2$ thick, backed by a 70 lines/inch nickel mesh support. The window was coated with $50 \mu\text{g}/\text{cm}^2$ carbon to provide electrical contact. P10 (90% argon - 10% methane) gas was flowed through the counter. Standard pulse counting electronics were used.

The Channeltron was mounted in a mini-box and operated with a collecting cap in the pulse counting mode. The pre-amplifier was as described in Bendix Technical Applications Note 9803. Most tests were run with 2800 VDC applied to the Channeltron, although tests were also made at 2600 VDC. A pulse height spectrum for the Channeltron in this configuration is shown in Figure 4.7.1.

In order to compensate for the proportional counter window, most data were collected with an additional window placed in front of both counters or in front of the Channeltron alone. Several runs were made using various

targets. The results are summarized below. All measurements were made with the beam near normal incidence.

Only the results for Aluminum (8.4 \AA) and Magnesium (9.9 \AA) are quoted here since for these two elements we were able to produce a clean monochromatic line.

Wavelength	Quantum Efficiency
8.4 \AA	$1.09\% \pm .12\%$
9.9 \AA	$1.12\% \pm .12\%$

These were calculated after subtracting background counts from the raw data. Background for Channeltron at 2800 V was 58 counts in 100 secs. At 2600 V background was 27 counts in 100 secs, and at this voltage the Channeltron was 95% and 91% as efficient as at 2800 Volts for 8.4 \AA and 9.9 \AA respectively.

We have acquired a Bendix chevron channel electron multiplier array and are currently constructing a one-dimensional multiwire readout. Such a detector system is already under study by American Science and Engineering for use as the LOXT, high-resolution imaging detector. They performed preliminary position detection measurements with this detector in the parallel-beam, soft X-ray facility discussed above. The experiment was performed using a slit in front of the chevron to define a narrow width X-ray beam. The one-dimensional imaging was performed with an array of wires to collect the electron burst from the rear of the

chevron. A capacitor charge dividing network similar to that devised by Gott, Parks and Pounds¹ gave resolutions better than the wire spacing.

¹R. Gott, W. Parkes, K. A. Pounds, IEEE Trans. on Nuc. Sci. NS17, 376 (1970), and Nuclear Instr. Meth. 81, 152 (1970).

Figure 4.7.1

A pulse height spectrum for the Channeltron electron multiplier. This was obtained using a voltage of 2500 VDC and aluminum K X-rays. Since the Channeltron is being used in the quantum counting mode, lower level discrimination is used on this signal.

